

①

NAVAL POSTGRADUATE SCHOOL MONTEREY, CALIFORNIA

AD-A284 032



THESIS

DTIC
ELECTE
SEP 09 1994

S

G

D

SHORT TERM TELECONNECTIONS ASSOCIATED WITH
WESTERN PACIFIC TROPICAL CYCLONES

BY

CORY A. SPRINGER

JUNE 1994

Thesis Advisor:

Tom Murphree

Approved for public release; distribution is unlimited.

1519

94-29293



DTIC QUALITY ASSURANCE

9 0 0 2 4

REPORT DOCUMENTATION PAGEForm Approved
OMB No. 0704-0188

Public reporting burden for this collection of information is estimated to average 1 hour per response, including the time for reviewing instruction, searching existing data sources, gathering and maintaining the data needed, and completing and reviewing the collection of information. Send comments regarding this burden estimate or any other aspect of this collection of information, including suggestions for reducing this burden, to Washington headquarters Services, Directorate for Information Operations and Reports, 1215 Jefferson Davis Highway, Suite 1204, Arlington, VA 22202-4302, and to the Office of Management and Budget, Paperwork Reduction Project (0704-0188) Washington DC 20503.

1. AGENCY USE ONLY (Leave blank)		2. REPORT DATE *June 1994	3. REPORT TYPE AND DATES COVERED Master's Thesis
4. TITLE AND SUBTITLE *SHORT TERM TELECONNECTIONS ASSOCIATED WITH WESTERN PACIFIC TROPICAL CYCLONES			5. FUNDING NUMBERS
6. AUTHOR(S) *Cory A. Springer			
7. PERFORMING ORGANIZATION NAME(S) AND ADDRESS(ES) Naval Postgraduate School Monterey CA 93943-5000			8. PERFORMING ORGANIZATION REPORT NUMBER
9. SPONSORING/MONITORING AGENCY NAME(S) AND ADDRESS(ES)			10. SPONSORING/MONITORING AGENCY REPORT NUMBER
11. SUPPLEMENTARY NOTES The views expressed in this thesis are those of the author and do not reflect the official policy or position of the Department of Defense or the U.S. Government.			
12a. DISTRIBUTION/AVAILABILITY STATEMENT Approved for public release; distribution is unlimited.			12b. DISTRIBUTION CODE *A
13. ABSTRACT (maximum 200 words) * The short term teleconnections arising from an individual tropical cyclone in the western Pacific were examined using a global operational data assimilation system and forecast model. In the data assimilation, the tropical cyclone was modified using a tropical cyclone bogusing procedure that either maintained the storm in, or eliminated the storm from, the model's initial conditions. These different initial conditions were used as the initial fields for several 20 day runs of the forecast model. These runs were used to simulate the global atmosphere with and without the tropical cyclone. The differences between these simulations were used to infer the global teleconnection response to the tropical cyclone. This response was dominated by a strong, quasi-stationary Rossby wave train that extended from east Asia across the North Pacific into North America. This wave train was initiated when an anticyclonic circulation formed near Japan as the tropical cyclone approached the east Asian jet. The anticyclone formation was primarily the result of the absolute vorticity advection by the divergent wind and vortex stretching (i.e., the Rossby wave source) associated with the tropical cyclone. The wave response continued to develop after this wave source, and the tropical cyclone itself, dissipated. This development was clearly seen in the growth and eastward propagation of Rossby wave energy across the midlatitude North Pacific and North America. The growth tended to be greater near areas of potential barotropic instability along the North Pacific jet, while the propagation tended to occur parallel to the jet. The net effect of the tropical cyclone was especially evident in the North Pacific-North American region, where the model atmosphere with the tropical cyclone showed a midlatitude jet and storm track that were markedly different from the jet and storm track seen in the model atmosphere without the tropical cyclone. The two tropical cyclones investigated in this study were super typhoon Yuri (November-December 1991) and typhoon Robyn (August 1993).			
14. SUBJECT TERMS *Teleconnections; Tropical Cyclones; Tropical Cyclone Bogusing; Rossby Wave Source, Rossby wave train, Extended-Range Forecasting			15. NUMBER OF PAGES *151
			16. PRICE CODE
17. SECURITY CLASSIFICATION OF REPORT Unclassified	18. SECURITY CLASSIFICATION OF THIS PAGE Unclassified	19. SECURITY CLASSIFICATION OF ABSTRACT Unclassified	20. LIMITATION OF ABSTRACT UL

NSN 7540-01-280-5500

Standard Form 298 (Rev. 2-89)
Prescribed by ANSI Std. Z39-18
298-102

Approved for public release; distribution is unlimited

Short Term Teleconnections
Associated with
Western Pacific Tropical Cyclones

by
Cory A. Springer
Lieutenant, United States Navy
B.S., United States Naval Academy, 1985

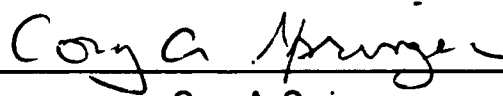
Submitted in partial fulfillment
of the requirements for the degree of

MASTER OF SCIENCE IN METEOROLOGY AND PHYSICAL OCEANOGRAPHY

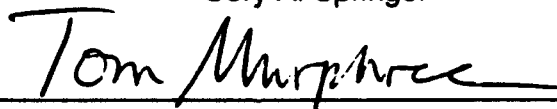
from the

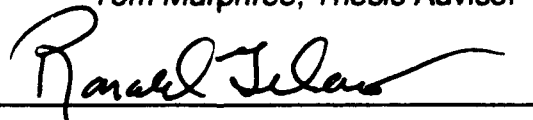
NAVAL POSTGRADUATE SCHOOL
June 1994

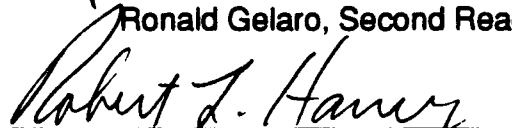
Author:


Cory A. Springer

Approved by:


Tom Murphree, Thesis Advisor


Ronald Gelaro, Second Reader


Robert L. Haney, Chairman
Department of Meteorology

ABSTRACT

The short term teleconnections arising from an individual tropical cyclone in the western Pacific were examined using a global operational data assimilation system and forecast model. In the data assimilation, the tropical cyclone was modified using a tropical cyclone bogusing procedure that either maintained the storm in, or eliminated the storm from, the model's initial conditions. These different initial conditions were used as the initial fields for several 20 day runs of the forecast model. These runs were used to simulate the global atmosphere with and without the tropical cyclone. The differences between these simulations were used to infer the global teleconnection response to the tropical cyclone.

This response was dominated by a strong, quasi-stationary Rossby wave train that extended from east Asia across the North Pacific into North America. This wave train was initiated when an anticyclonic circulation formed near Japan as the tropical cyclone approached the east Asian jet. The anticyclone formation was primarily the result of the absolute vorticity advection by the divergent wind and vortex stretching (i.e., the Rossby wave source) associated with the tropical cyclone.

The wave response continued to develop after this wave source, and the tropical cyclone itself, dissipated. This development was clearly seen in the growth and eastward propagation of Rossby wave energy across the midlatitude North Pacific and North America. The growth tended to be greater near areas of potential barotropic instability along the North Pacific jet, while the propagation tended to occur parallel to the jet. The net effect of the tropical cyclone was especially evident in the North Pacific - North American region,

where the model atmosphere *with* the tropical cyclone showed a midlatitude jet and storm track that were markedly different from the jet and storm track seen in the model atmosphere *without* the tropical cyclone.

The two tropical cyclones investigated in this study were super typhoon Yuri (November-December 1991) and typhoon Robyn (August 1993).

Accession For	
NTIS CRA&I	<input checked="" type="checkbox"/>
DTIC TAB	<input checked="" type="checkbox"/>
Unannounced	<input type="checkbox"/>
Justification	
By	
Distribution /	
Availability Codes	
Dist	Avail and/or Special
A-1	

TABLE OF CONTENTS

I. INTRODUCTION	1
A. MOTIVATION FOR THIS STUDY	1
B. BACKGROUND	1
1. ATMOSPHERIC INTERACTION OVER LONG DISTANCES	1
2. MODELING TELECONNECTIONS	2
3. INTERANNUAL TELECONNECTIONS	2
4. INTRASEASONAL TELECONNECTIONS	4
5. SHORT-TERM TELECONNECTIONS	7
C. DESIGN OF THIS STUDY	7
II. DATA AND PROCEDURES	10
A. TROPICAL CYCLONE SELECTION	10
B. ATMOSPHERIC MODEL DESCRIPTION	11
C. MODEL OUTPUT FIELDS	12
1. SEA LEVEL PRESSURE	12
2. ATMOSPHERIC HEATING	12
3. 200 MB GEOPOTENTIAL HEIGHT	12
4. 200 MB WIND	13
5. 200 MB VELOCITY POTENTIAL	13
6. 200 MB RELATIVE VORTICITY	13
D. TROPICAL CYCLONE BOGUSING PROCEDURES	13
E. MODEL RUNS AND ANALYSES	15

F. WAVE AND INSTABILITY CALCULATIONS	17
1. QUASI-GEOSTROPHIC WAVE ACTIVITY FLUX VECTORS ..	17
2. 200 MB POTENTIAL BAROTROPIC INSTABILITY	17
G. ROSSBY WAVE SOURCE CALCULATION	18
1. MOTIVATION FOR CALCULATION	18
2. FORMULATION OF THE ROSSBY WAVE SOURCE	19

III. RESULTS

A. OVERVIEW	21
B. PREREQUISITE 1 – BOGUSING AND THE INITIAL CONDITIONS	22
1. SLP INITIAL CONDITIONS	22
2. CONCLUSION FOR PREREQUISITE 1	23
C. PREREQUISITE 2 – TYPHOON TRACK AND INTENSITY	24
1. TYPHOON TRACK	24
2. TYPHOON INTENSITY	25
3. CONCLUSION FOR PREREQUISITE 2	26
D. PREREQUISITE 3 – COMPARISONS WITH CLIMATOLOGY	26
1. 200 MB GEOPOTENTIAL HEIGHTS	26
2. ATMOSPHERIC HEATING	27
3. CONCLUSION FOR PREREQUISITE 3	28
E. PREREQUISITE 4 – EFFECTS OF ENSEMBLE AVERAGING	28
1. 200 MB GEOPOTENTIAL HEIGHTS	28
a. RESULTS OF THE POSITIVE FORECASTS	29
b. RESULTS OF THE NEGATIVE FORECASTS	31
2. ATMOSPHERIC HEATING	32

a. RESULTS OF THE POSITIVE FORECASTS	32
b. RESULTS OF THE NEGATIVE FORECASTS	33
3. CONCLUSIONS FOR PREREQUISITE 4	34
F. HYPOTHESIS 1 – TELECONNECTIONS ASSOCIATED WITH TYPHOON ROBYN	34
1. ENSEMBLE AVERAGE DIFFERENCES IN ATMOSPHERIC HEATING AND 200 MB GEOPOTENTIAL HEIGHTS	35
2. CONCLUSION FOR HYPOTHESIS 1	37
G. HYPOTHESIS 2 – THE JET’S ROLE IN TELECONNECTIONS ..	38
1. 200 MB HEIGHT DIFFERENCES AND THE JETS	39
2. THE JETS AND THE WAVE RESPONSE	41
3. BAROTROPIC INSTABILITY	44
4. CONCLUSION FOR HYPOTHESIS 2	45
H. HYPOTHESIS 3 – THE ROLE OF ROSSBY WAVE SOURCES IN TELECONNECTIONS	45
1. THE ROSSBY WAVE SOURCE	46
2. THE ROSSBY WAVE SOURCE COMPONENTS	47
3. THE RELATIVE VORTICITY AND DIVERGENT WINDS ASSOCIATED WITH THE ROSSBY WAVE SOURCE	48
4. THE RELATIVE IMPORTANCE OF THE ROSSBY WAVE SOURCE IN THE VORTICITY EQUATION	49
5. COMPARISON OF THE ROSSBY WAVE SOURCES FOR YURI AND ROBYN	50
6. CONCLUSION FOR HYPOTHESIS 3	53
I. COMPARISON OF MODEL AND ANALYZED HEIGHT FIELDS	53

IV. CONCLUSIONS	56
A. SUMMARY	56
B. THE UPPER-LEVEL HEIGHT PATTERNS ASSOCIATED WITH OTHER RECURVING TYPHOONS DURING 1993	57
C. IMPLICATIONS FOR EXTENDED-RANGE FORECASTING	59
D. RECOMMENDATIONS FOR FUTURE WORK	59
1. ADDITIONAL CASE STUDIES	60
2. FURTHER STUDY OF TELECONNECTIONS MECHANISMS	60
APPENDIX A – TABLES	63
APPENDIX B – FIGURES	65
INITIAL DISTRIBUTION LIST	136

LIST OF ACRONYMS AND SYMBOLS

ADVDIV	advection of absolute vorticity by the divergent part of the wind
ADVROT	advection of absolute vorticity by the rotational part of the wind
β	total derivative of the Coriolis parameter, $\frac{df}{dy}$
BTI	barotropic instability
χ	velocity potential
EA	ensemble average
ECMWF	European Center for Medium-range Weather Forecasting
Forecast 1	20 day NOGAPS model run started from 12Z, 05 August 1993 initial conditions for typhoon Robyn; or 15 day NOGAPS model run started from 00Z, 26 November 1991 initial conditions for super typhoon Yuri
Forecast 2	20 day NOGAPS model run started from 00Z, 07 August 1993 initial conditions for typhoon Robyn; or 15 day NOGAPS model run started from 12Z, 27 November 1991 initial conditions for super typhoon Yuri
Forecast 3	20 day NOGAPS model run started from 12Z, 08 August 1993 initial conditions for typhoon Robyn; or 15 day NOGAPS model run started from 00Z, 29 November 1991 initial conditions for super typhoon Yuri
FNMOCC	Fleet Numerical Meteorology and Oceanography Center
GCM	general circulation model
gpm	geopotential meter
H1	first major positive 200 mb height response to Robyn
H2	second major positive 200 mb height response to Robyn
H3	third major positive 200 mb height response to Robyn

H4	fourth major positive 200 mb height response to Robyn
IDEA Lab	Interactive Digital Environmental Analysis Laboratory
JTWC	Joint Typhoon Warning Center
L1	first major negative 200 mb height response to Robyn
L2	second major negative 200 mb height response to Robyn
L3	third major negative 200 mb height response to Robyn
m	meter
mb	millibar
NCAR	National Center for Atmospheric Research
NEGATIVE	synthetic tropical cyclone data assimilation (bogusing) procedure applied to the NOGAPS initial conditions that has the affect of removing the storm from the model's initial conditions
NMC	National Meteorological Center
NO	data assimilation (bogusing) procedure that has no special treatment of tropical cyclones in the NOGAPS initial conditions
NOGAPS	Navy Operational Global Atmospheric Prediction System
NP-NA	North Pacific-North America
NRL	Naval Research Laboratory
OLR	outgoing long wave radiation
POSITIVE	the standard synthetic tropical cyclone data assimilation (bogusing) procedure applied to the NOGAPS initial conditions that has the affect of improving the atmospheric circulation around the cyclone in the model's initial conditions
Q	atmospheric Heating
QG	quasi-geostrophic
S	Rossby wave source

s	second
SO	Southern Oscillation
SLP	sea level pressure
T79	triangular 79 wave truncation
u	zonal component of the wind
u_x	zonal component of the divergent wind
u_v	zonal component of the rotational wind
v	meridional component of the total wind
V	horizontal wind vector
V_x	divergent horizontal wind vector
V_v	rotational horizontal wind vector
v_x	meridional component of the divergent wind
v_v	meridional component of the rotational wind
ζ	200 mb relative vorticity
Z	Zulu time (Greenwich Mean Time)

ACKNOWLEDGMENTS

I gratefully acknowledge Professor Tom Murphree and Dr. Ron Gelaro for their counsel and guidance. Their instruction was invaluable in bringing this study to a successful conclusion. Dr. Gelaro and his colleagues, Dr. Jim Goerss and Mr. Robin Brody, at the Naval Research Laboratory in Monterey, provided crucial scientific and technical collaboration, especially in performing the data assimilation and model runs. Without this collaboration, this project could not have happened. I also appreciate the help from Professor Pat Harr in interpreting his observational work on tropical cyclones. And thanks to Lt. Steve Woll for answering all of my computer questions. Most importantly, I would like to thank my wife, Teddy for her diligent editing and support, and my son Jacob. Both of them gave me a great reason to smile every day.

I. INTRODUCTION

A. MOTIVATION FOR THIS STUDY

Throughout history, climate changes of both long and short duration have critically affected human societies, often causing significant social and economic disruptions. Unfortunately, climate changes, especially longer term changes, are very difficult to accurately predict. However, considerable progress has been made in the last 20 years in understanding short term climate changes and making extended range (weekly to monthly) predictions. In this study, we examine how, in the extended range, the global atmosphere is affected by tropical cyclones. In particular, we explore how *individual* typhoons may affect the extratropical atmosphere over periods of one to three weeks. By improving our understanding of such effects, we hope to contribute to the development of more accurate extended range forecasts of weather and climate.

B. BACKGROUND

1. ATMOSPHERIC INTERACTIONS OVER LONG DISTANCES

The impacts of a disturbance in one part of the atmosphere on another distant part of the atmosphere, such as the impacts of a typhoon in the western tropical Pacific on the atmosphere over North America, are described by the term *teleconnections*. Teleconnections are interactions between phenomena occurring in widely separated parts of the atmosphere. Some of the earliest studies of teleconnections were correlation studies intended to find statistically significant relationships that could be used in making statistical forecasts (e.g., the Indian monsoon rainfall studies by Walker (1924) and Walker and Bliss

(1932)).

2. MODELING TELECONNECTIONS

Modeling studies of teleconnections have been very important in developing our understanding of teleconnection dynamics. Observational studies have contributed much to our understanding, but they have many limitations. These limitations arise from sparse data coverage, especially in the tropics and Southern Hemisphere, and a limited ability to test specific hypotheses, especially cause and effect hypotheses. Today's atmospheric general circulation models (GCMs) can overcome many of these problems. A GCM can provide high temporal and spatial resolution, global coverage, long or numerous integration periods, and the ability to extensively alter initial and boundary conditions.

But in order to be useful in a teleconnection study, the model must realistically simulate the large-scale background environment in which the teleconnection occurs, as well as the specific atmospheric processes that produce the teleconnection. Therefore, any model used for a teleconnection study must first pass several simulation tests. Once the model sufficiently demonstrates its performance, it can be used to evaluate specific hypotheses.

3. INTERANNUAL TELECONNECTIONS

Interannual teleconnections tend to be global in scale and of low frequency. The first person to identify and document interannual teleconnections was Sir Gilbert Walker (Walker 1924, Walker and Bliss 1932). He is credited with detecting and describing the Southern Oscillation (SO). This low frequency atmospheric fluctuation appears as a see-saw shift of sea level pressure (i.e., a mass exchange) between Indonesia and the eastern Pacific.

In addition to discovering the SO, Walker described correlations between the SO and other meteorological parameters, including extratropical parameters. For example, he described significant correlations between the SO and: (1) rainfall over the Hawaiian Islands; (2) sea level pressure over the southeastern United States; and (3) temperatures over western Canada.

Walker's work was given little notice until Bjerknes (1966, 1969, 1972) proposed a mechanism that linked the negative phase of the SO (when sea level pressure is anomalously high in the western Pacific and low in the eastern Pacific) to El Niño. El Niño is an event characterized by the appearance of anomalously warm water in the central and eastern Pacific. Bjerknes (1966, 1969, 1972) showed from several case studies that during the Northern Hemisphere winter in which an El Niño event is occurring, the tropical Pacific SST anomalies were associated with a stronger Hadley circulation and stronger midlatitude westerlies over the northeastern Pacific, a stronger and deeper low in the Gulf of Alaska, and a weakened Icelandic Low which contributed to weather anomalies in Europe. Bjerknes proposed in this work that the changes in tropical Pacific SST affected the midlatitude circulation by altering the strength and intensity of the tropical Pacific portion of the Hadley circulation.

In studying the global atmosphere during several major El Niño events, Horel and Wallace (1981) found clear evidence for teleconnections in the strong correlations between various tropical Pacific parameters and atmospheric parameters elsewhere in the world. For example, they found that SST anomalies in the central and eastern tropical Pacific were well correlated with 700 mb height anomalies over the North Pacific and North America. They found

that these and similar correlations were strongest during the northern winter and weakest during the northern summer.

Hoskins and Karoly (1981) concluded from the results of a modeling study that the propagation of Rossby wave energy from the tropics to the extratropics may explain the patterns of correlations seen by Horel and Wallace (1981) and others. Hoskins and Karoly (1981) concluded that this propagation, and its associated teleconnections, is likely to occur only when westerly flow extends from the midlatitudes into the tropical heating region.

Tribbia (1991) used a simple model with no background flow to study the response to tropical forcing. He found that Rossby wave packets propagated northeastward and southeastward from the source region. As these wave trains moved poleward, they turned more eastward and eventually turned equatorward. However, when a realistic background flow was included in the model, the Rossby waves were absorbed by the tropical easterlies. Tribbia (1991) concluded that the Northern Hemisphere teleconnection response to tropical heating tends to be larger in the northern winter, when the Northern Hemisphere tropical easterlies are confined to a relatively narrow latitudinal band.

4. INTRASEASONAL TELECONNECTIONS

Nitta (1987) studied observed summertime convective activities in the western Pacific and their effects on Northern Hemisphere circulations. He found that Northern Hemisphere summer heating anomalies in the tropical western Pacific were correlated with 500 mb height anomalies extending from China to North America. These height anomalies appeared as an alternating series of highs and lows across the Pacific. Nitta speculated that these height

anomalies represented Rossby waves that were being generated by the anomalous heating. He concluded that for this wave train to develop, the anomalous heating probably needed to be located in the northern tropics in or near the midlatitude westerlies.

Kurihara and Tsuyuki (1987) conducted an observational and modeling study of the subtropical high pressure area near Japan during August 1984. As in Nitta (1987), they discovered a 500 mb height anomaly pattern across the Pacific, in apparent response to enhanced convection near the Philippine Islands. They were successful in modeling the height anomaly using a linear, barotropic vorticity model with August 1984 mean zonal winds excited by a vorticity source at 20°N. They concluded that intensified convection around the Philippines was important for initiating barotropic Rossby waves that propagated across the Pacific.

Hoskins and Karoly (1981) used a linear, steady-state, five-layer baroclinic model to study the response of a spherical atmosphere to thermal forcing. They found that an equivalent barotropic structure with the largest amplitudes in the upper troposphere developed far from the forcing area. Hoskins and Karoly also found that the long wave length responses propagated strongly poleward and eastward, roughly along a great circle path. Conversely, the shorter waves appeared to be trapped equatorward of the poleward flank of the jet. They also found that a midlatitude or high latitude height anomaly was easier to force with a heating source located in the subtropics rather than centered at higher latitudes.

Murphree (1994) used a global shallow water model of the atmosphere to simulate the tropical forcing of teleconnections over North America. He applied

the quasi-stationary wave activity flux vector (Plumb 1985) to track the propagation of wave activity in the model fields. He found that the wave energy from the tropics tended to propagate eastward along the midlatitude jets, and hypothesized that the jet acted as a barrier and a wave guide that focused energy dispersing from the tropics. He also found that large wave energy sources were associated with barotropically unstable areas on the jet flanks. Thus, he hypothesized that both guiding and amplification of the wave response along the extratropical jets may be important in producing North American teleconnections.

To test this hypothesis, Gelaro and Murphree (1994) examined GCM responses in the midlatitudes to tropical heating anomalies in the tropical Pacific. They found strong intraseasonal variations in the midlatitude responses, and clear relationships between these responses and the variations of the east Asian-North Pacific jet. The strongest teleconnection responses usually occurred near the jet exit, in association with regions of potential barotropic instability. Gelaro and Murphree (1994) concluded that forcing by the midlatitude background flow is important in producing intraseasonal variations in North Pacific-North American (NP-NA) teleconnections, and that waveguiding and amplification by the east Asian-North Pacific jet may be the primary mechanisms for this forcing.

Neith (1992) investigated the relationships between tropical heating and Northern Hemisphere midlatitude jets using the northern summer results from a GCM. He discovered a 30- to 60-day variation in the jets that was well correlated with heating anomalies in specific tropical locations. For example, Neith (1992) showed that the North Pacific jet was strong during and for several

days after periods of: (a) positive heating anomalies over the tropical western and central Pacific, and (b) negative anomalies over the Indian Ocean.

5. SHORT-TERM TELECONNECTIONS

Harr and Elsberry (1991) found in an observational study that western Pacific tropical cyclones may be associated with distinct large scale flow anomalies across the midlatitude North Pacific region. For example, they found that recurving tropical cyclones were associated with a wave train-like pattern of cyclonic and anticyclonic anomalies in the 700 mb flow that stretched eastward from east Asia to western North America (Figure 1). Periods during which there were few or no tropical cyclones had a distinctly weaker flow anomaly pattern (Figure 2). These results suggest that short term tropical disturbances, such as tropical cyclones, may influence the remote large-scale atmospheric circulation.

Miller (1993) and Woll (1993) investigated the global response to a single tropical cyclone using a GCM. They found, for the case of super typhoon Yuri in November 1991, a strong global scale response to the storm that was located far from the storm and persisted long after the storm had dissipated. Woll (1993) demonstrated that the model's response could be described by the propagation of Rossby wave energy from the region just east of Japan through which Yuri had passed. This energy was subsequently guided and, apparently, amplified by barotropic instabilities along the jet.

C. DESIGN OF THIS STUDY

In this study, we used a tropical cyclone bogusing procedure to modify an individual tropical cyclone in the initial conditions for a global forecast model. The modifications were done to maintain or to remove the storm in the model

initial conditions. We then ran the model out for several weeks, using initial conditions with and without the tropical cyclone, to simulate the global atmosphere when the storm is present and when it is absent. This was the basic procedure used by Miller (1993) and Woll (1993). However, for this study, we investigated further the mechanisms behind the response to Yuri and examined the response to another storm, typhoon Robyn during August 1993.

Three hypotheses were tested in this study. The first two were described by Woll (1993).

- Hypothesis 1: Individual tropical cyclones can produce strong teleconnections.
- Hypothesis 2: The development of the teleconnection is strongly influenced by the wave guiding and amplification effects of the midlatitude westerly jet.

The third hypothesis was motivated by: (1) Woll's (1993) results which showed that the response to Yuri was initiated as Yuri approached the midlatitude jet just east of Japan, and (2) the work of Sardeshmukh and Hoskins (1988), which showed that in the vicinity of a jet, absolute vorticity advection by the divergent wind may be an important mechanism for generating Rossby waves.

- Hypothesis 3: The flux of ambient absolute vorticity associated with the divergent outflow from a tropical cyclone located near a jet may be an important mechanism for initiating a teleconnection response to the tropical cyclone.

In this study we also compared the model's forecast fields to the corresponding analyzed fields. This was done to assess the applicability of the

model results to the real atmosphere.

The methods used in this study are described in Chapter II. The results are presented in Chapter III. Conclusions and recommendations for future work are given in Chapter IV.

II. DATA AND PROCEDURES

A. TROPICAL CYCLONE SELECTION

Previous studies of teleconnections due to tropical disturbances (e.g., Tribbia 1991) have indicated that the tropical disturbances may need to be located within or near a region of westerly winds, in order to have a large impact in the extratropics. Previous studies of the extratropical impacts of tropical cyclones (e.g., Harr and Elsberry 1991, Woll 1993) have indicated that tropical cyclones that recurve poleward toward the extratropical westerlies may have a clear impact on the extratropical circulation. Thus, we wanted in our choice of a typhoon for this study to select a typhoon that recurved. We also wanted to extend Woll's (1993) study of super typhoon Yuri, which occurred during the Northern Hemisphere late autumn (November - December 1991), by considering a typhoon that occurred during the northern summer. Based on these considerations, we examined the records of several recurving typhoons during the July - October periods of 1991, 1992, and 1993. From these we, selected for our study typhoon Robyn, which occurred in August 1993.

Robyn was selected because it:

- was strong, with wind speeds in excess of 58 m/s;
- was long-lasting, maintaining typhoon strength winds for five days;
- recurved well into the midlatitudes, reaching 36°N with wind speeds of 38 m/s, and 40°N with wind speeds of 30 m/s;
- occurred in relative isolation from other tropical cyclones; and
- was well forecast in the Navy's operational forecasts made during August 1993.

Figure 3 shows the maximum sustained winds at selected positions along the Joint typhoon Warning Center's (JTWC) best track for typhoon Robyn. The accuracy of the operational forecasts and the relative isolation of Robyn from other tropical cyclones was considered important because of Woll's (1993) experience in attempting to model the effects of typhoons Gay and Hunt which occurred simultaneously during November 1992. These storms were relatively poorly forecast in both the operational forecasts and in Woll's experiments. The forecasts confused the two storms and, effectively, forecast Hunt as Gay and Gay as Hunt.

In addition to studying Robyn, we also studied further the super typhoon Yuri model data used by Woll (1993). This Yuri data was used to test hypothesis 3 (see Chapter I, section C) which was developed after Woll completed his work.

B. ATMOSPHERIC MODEL DESCRIPTION

The GCM used in this study is the U.S. Navy Global Atmospheric Prediction System (NOGAPS) Version 3.2. NOGAPS is a full physics spectral model that is used operationally by the U.S. Navy for world-wide weather prediction and is run at the Fleet Numerical Meteorology and Oceanography Center (FNMOC) in Monterey, California. It uses a triangular 79 truncation (T79), which corresponds to a 1.5 degree latitude-longitude transform grid. It has 18 vertical levels and a time step of 30 minutes. NOGAPS uses the Arakawa-Schubert cumulus parameterization which includes the effects of downdrafts, latent heat of fusion, and evaporation of falling precipitation. Model equations are formulated in spherical coordinates and a hybrid vertical coordinate, η , is used – the same as in the European Center for Medium-range Weather Forecasting

(ECMWF) forecast model. An in-depth description of NOGAPS is contained in Hogan and Rosmond (1991).

The model runs for this study were performed by Dr. R. Gelaro at the Naval Research Laboratory (NRL) in Monterey, California. The computing facilities were at FNMOC. Postprocessing of the model output was done in the Interactive Digital Environmental Analysis (IDEA) Laboratory at the Naval Postgraduate School, Monterey, California.

C. MODEL OUTPUT FIELDS

Several standard NOGAPS fields were analyzed in this study. These global fields were provided by Dr. R. Gelaro of NRL on a 2.5 degree latitude – longitude grid. The temporal resolution was 12 hrs, with the model output being provided at the 00Z and 12Z model forecast times of each model day. Each of the model runs for Yuri lasted 15 days. For Robyn, the runs lasted 20 days. The following NOGAPS fields were investigated in this study.

1. SEA LEVEL PRESSURE

The sea level pressure (SLP), in millibars (mb), provided information on the initial conditions at the start of each model run and was used to represent the model's prediction of the tropical cyclone track.

2. ATMOSPHERIC HEATING

The atmospheric heating field (Q) in °C/day, is the vertical integral of the model's total heating. This heating is dominated by latent heat release in the vicinity of tropical cyclones or other large convective systems.

3. 200 MB GEOPOTENTIAL HEIGHT

200 mb geopotential height, in geopotential meters (gpm), represents the

structure of the upper troposphere. These heights were used to deduce upper tropospheric teleconnections and quasi-geostrophic wave dynamics.

4. 200 MB WIND

The 200 mb total horizontal wind field (V), in m/s, contains zonal (u) and meridional (v) components. This field describes the transfer of mass through the upper troposphere.

5. 200 MB VELOCITY POTENTIAL

The 200 mb velocity potential (χ) field, in m^2/s , was used to obtain the divergent horizontal wind (V_x) and rotational horizontal wind (V_v). The total horizontal wind is defined as the sum of these divergent and rotational winds ($V \equiv V_x + V_v$). The divergent horizontal wind was an important term in the Rossby wave source calculation (see Section G1). It also provided a good sense of the tropical cyclone's location, since there a strong upper level divergent horizontal wind emanated from the storm.

6. 200 MB RELATIVE VORTICITY

The 200 mb relative vorticity field (ζ), in m^2/s , represents the relative cyclonic or anticyclonic spin of the atmosphere. It was also an important term in the Rossby wave source calculation (see Section G2).

D. TROPICAL CYCLONE BOGUSING PROCEDURES

The spatial resolution of operational forecast models is too coarse to accurately depict the mesoscale characteristics of individual tropical cyclones. In order to overcome this obstacle, many operational forecast centers utilize a synthetic data assimilation procedure, or bogusing procedure, for tropical cyclones. The bogusing procedure used at FNMOC for NOGAPS forecasts puts

synthetic observations within a prescribed vortex structure into the model's initial conditions. This is done so that the model begins its computing with realistic environmental parameters in the vicinity of the tropical cyclone's current position. Bogusing is used in order to provide more accurate forecasts of the bogused storms' intensities and tracks, and of the surrounding circulation. Goerss and Jeffries (1994) described the operational NOGAPS bogusing procedure and evaluated its impacts on forecasts of western Pacific tropical cyclones. They showed that NOGAPS generally does quite well predicting storm intensity and track when the cyclone is at or above tropical storm strength.

This study used the tropical cyclone bogusing procedure as an experimental tool to selectively alter an individual tropical cyclone in the initial conditions for runs of the NOGAPS model. We used three types of bogusing for this study.

The first type is referred to as the POSITIVE bogus. This procedure calculated a set of initial conditions that were intended to give a relatively accurate depiction of the tropical cyclone. This POSITIVE bogus procedure was the same as the operational procedure described in Goerss and Jeffries (1994). We used the model runs that were started from the POSITIVE bogus initial conditions as our control representation of the atmosphere's development with the tropical cyclone included.

The second bogusing procedure, referred to as the NEGATIVE bogus, was used to remove the tropical cyclone from the NOGAPS initial conditions. We used the model runs that were started from the NEGATIVE bogus initial conditions to represent how the atmosphere might have evolved if the tropical cyclone had never occurred. The differences between the output from the model runs using the POSITIVE and NEGATIVE bogusing procedures allowed

us to infer what the impact of the tropical cyclone was on the atmosphere. These differences are referred to in this study as the model's *response* to the presence of the tropical cyclone.

A third type of bogus was also applied in this study, the NO bogus. The NO bogus was not actually a bogus, since no special treatment was given to Robyn or Yuri during the data assimilation. That is, in the NO bogus, no synthetic data assimilation was used in developing the initial conditions for Robyn or Yuri. Woll (1993) provides more details on the above bogusing procedures.

E. MODEL RUNS AND ANALYSES

We conducted a total of nine forecast runs for our studies of typhoon Robyn. These nine runs represent the three bogus types described above, plus three different initial times. For each initial time, three forecast runs were done: one using initial conditions from the POSITIVE bogus procedure, one using initial conditions from the NEGATIVE bogus procedure, and one using initial conditions from the NO bogus procedure. This gave a total of nine forecast runs.

The initial times were near the time at which Robyn reached its maximum intensity and were 36 hours apart. The three initial times were 12Z, 05 August 1993; 00Z, 07 August 1993; and 12Z, 08 August 1993.

The following naming convention was used to distinguish the runs:

- The three runs started at 12Z, 05 August 1993 were called the Forecast 1 runs.
- The three runs started at 00Z, 07 August 1993 were called the Forecast 2 runs.
- The three runs started at 12Z, 08 August 1993 were called the Forecast 3 runs.

Each of the nine model runs was identified by its initialization time and its bogusing procedure. For example, the run started at 12Z, 05 August 1993 from the initial conditions developed from the POSITIVE bogusing procedure was called the Forecast 1 POSITIVE run.

Note that the nine model runs differed only in their initial conditions. These initial condition differences represented three different start times and three different treatments of typhoon Robyn during the data assimilation. The same NOGAPS model was used for all nine runs.

Each of the nine forecasts was run out for 20 days, with model fields being output at 00Z and 12Z of each model day. Figure 4 shows a schematic of the data assimilation procedures and the nine model runs.

For many of the analyses of the model results, the model fields were first ensemble averaged. This procedure averaged together the results from runs that involved the same bogusing procedure but which had different initial times. This averaging was done only at corresponding forecast times and dates from the different runs. Figure 5 gives a schematic description of the ensemble averaging process.

The net effect of ensemble averaging was a relative enhancement of the features that were common in all the forecasts being averaged, and a relative reduction of the features that were different in the three forecast being averaged. Thus, for example, the global responses to typhoon Robyn that were found in all three of the POSITIVE runs were emphasized by the ensemble averaging. The ensemble averaging procedure is explained more fully in Woll (1993).

F. WAVE AND INSTABILITY CALCULATIONS

Hypothesis 2 proposes that the development of the teleconnection is strongly influenced by the waveguiding and amplification effects of the extratropical westerly jets (see Chapter I, Section C). In order to test this hypothesis and identify the mechanisms of the model's teleconnections, the following diagnostic quantities were calculated using the model's 200 mb height and wind fields.

1. QUASI-GEOSTROPHIC WAVE ACTIVITY FLUX VECTORS

Quasi-geostrophic wave activity flux vectors or Plumb fluxes, in m^2/s^2 , were used to track the quasi-geostrophic wave energy as it propagated through the model's upper troposphere (Plumb 1985).

These wave activity flux vectors were developed by Plumb (1985) from a conservation relation and are a phase independent quantity. The flux vectors are parallel to the wave energy propagation, and their magnitude is proportional to the amount of propagating energy. Converging flux vectors indicate a wave energy sink at the convergence center, while diverging vectors denote a wave energy source.

2. 200 MB POTENTIAL BAROTROPIC INSTABILITY

Barotropic instability has been suggested as a probable mechanism in tropical to midlatitude teleconnections (Woll 1993, Gelaro and Murphree 1994, Murphree 1994). Woll (1993) concluded that areas of potential barotropic instability contributed energy to the teleconnection response to super typhoon Yuri. In our study, as in the three previous studies mentioned, areas of potential barotropic instability in the model's circulation were identified using the

Rayleigh-Kuo criterion (Kuo 1949):

$$\beta - \frac{\partial^2 u}{\partial y^2} = 0. \quad (1)$$

Where β is the total derivative of the Coriolis parameter $\left(\frac{df}{dy}\right)$ and $\frac{\partial^2 u}{\partial y^2}$ is the second meridional derivative of the 200 mb zonal wind. In the current study, as in Woll (1993), all fields of $\beta - \frac{\partial^2 u}{\partial y^2}$ have been treated with a nine-point horizontal smoother before being plotted.

It is important to note that (1) is a necessary, but not a sufficient, condition to establish the presence of barotropic instability. Thus (1) denotes possible wave energy source areas, where barotropic instability mechanisms might provide energy to the waves, but it does not guarantee that these are actually wave energy source areas.

G. ROSSBY WAVE SOURCE CALCULATION

1. MOTIVATION FOR CALCULATION

A number of modeling and theoretical studies have indicated that it is very difficult, or impossible, for Rossby waves generated in the tropics to propagate through the tropical easterlies and impact the extratropics (e.g., Tribbia 1991). However, many studies have also indicated that tropical disturbances do have extratropical impacts that appear in the form of Rossby wave trains (e.g., Figure 6). One resolution of this paradox was offered by Sardeshmukh and Hoskins (1988) who noted that in many modeling and theoretical studies, the divergent portion of the horizontal wind (V_x) had been ignored. These studies assumed that V_x was insignificant in the teleconnection process because, on large scales, V_x usually is much smaller than V_y , the rotational portion of the

horizontal wind.

Sardeshmukh and Hoskins (1988) showed that, near an extratropical jet, the advection of absolute vorticity by the divergent component of the horizontal wind can be quite significant in generating Rossby waves. Thus, they defined a Rossby wave source in the absolute vorticity equation as the sum of two terms: the advection of absolute vorticity by the divergent horizontal wind and the stretching terms. They showed that the Rossby wave source caused by a localized tropical disturbance can extend well beyond the disturbance and into the region of the extratropical jet. Figure 7 shows an example of a Rossby wave source computed by Sardeshmukh and Hoskins (1988). Thus, they concluded that tropical disturbances may have an extratropical impact by indirectly generating Rossby waves at an extratropical jet, rather than by directly propagating Rossby waves out of the tropics

2. FORMULATION OF THE ROSSBY WAVE SOURCE

The Rossby wave source is contained in the absolute vorticity equation, shown below in isobaric coordinate form:

$$\left(\frac{\partial}{\partial t} + \mathbf{V}_w \cdot \nabla \right) (\zeta + f) = S \quad (2)$$

where $(\zeta + f)$ is absolute vorticity and S is the Rossby wave source, defined as:

$$S = -\nabla \cdot \{ \mathbf{V}_x (\zeta + f) \}. \quad (3)$$

Expanding (3) gives:

$$S = -\{ \mathbf{V}_x \cdot \nabla (\zeta + f) + (\zeta + f) \nabla \cdot \mathbf{V}_x \}. \quad (4)$$

Further expansion gives:

$$S = -\left\{ u_x \frac{\partial \zeta}{\partial x} + v_x \frac{\partial \zeta}{\partial y} + v_x \beta + (\zeta + f) \left(\frac{\partial u_x}{\partial x} + \frac{\partial v_x}{\partial y} \right) \right\}. \quad (5)$$

The first three terms on the right hand side of (5) represent the advection of absolute vorticity by the divergent horizontal wind (ADVDIV). The last term in

(5) is the vortex stretching (or divergence) term. Expanding (2) gives:

$$\frac{\partial \zeta}{\partial t} = -\mathbf{V}_v \cdot \nabla(\zeta + f) + S + \hat{\mathbf{k}} \cdot \left(\frac{\partial \mathbf{V}}{\partial p} \times \nabla \omega \right) - \omega \frac{\partial \zeta}{\partial p}. \quad (6)$$

The left hand term is the relative vorticity tendency; $-\mathbf{V}_v \cdot \nabla(\zeta + f)$ is the advection of absolute vorticity by the rotational part of the horizontal wind (ADVROT); S is the Rossby wave source; $\hat{\mathbf{k}} \cdot \left(\frac{\partial \mathbf{V}}{\partial p} \times \nabla \omega \right)$ is the twisting term; and $-\omega \frac{\partial \zeta}{\partial p}$ is the vertical advection term. In component form, ADVROT becomes:

$$u_v \frac{\partial \zeta}{\partial x} + v_v \frac{\partial \zeta}{\partial y} + v_v \beta. \quad (7)$$

Notice that this is similar in form to ADVDIV, except that the rotational horizontal wind is used in (7).

S and its individual components (see (5)) were calculated from the output fields from the Yuri and Robyn model runs. These calculations were made using finite difference approximations to the derivatives in (5). The tendency and ADVROT terms in (6) were also calculated in order to identify the relative importance of S with respect to these terms in the model's vorticity balance.

III. RESULTS

A. OVERVIEW

In order for the modeling strategy described in Chapter II to clearly describe the impacts of an individual tropical cyclone, certain prerequisites must be met. These prerequisites were described by Woll (1993) and shown by him to be satisfied in his modeling study of super typhoon Yuri. These prerequisites also apply in our study of typhoon Robyn.

- Prerequisite 1: The bogusing procedure used during the data assimilation must have a significant effect on the model's initial conditions only in the vicinity of the tropical cyclone.
- Prerequisite 2: The model runs that attempt to simulate the tropical cyclone (i.e., those for which the POSITIVE or NO bogus procedure was used) must give a relatively accurate simulation of the typhoon's track and strength. The model runs that attempt to remove the tropical cyclone from the model atmosphere (i.e., those for which the NEGATIVE bogus was used) must show, at most, only a very weak tropical cyclone.
- Prerequisite 3: All the model runs, regardless of the bogus procedure used, must provide a realistic representation of basic climatological features.
- Prerequisite 4: When ensemble averaging is done, the major features of the individual forecasts being averaged must be preserved in the average.

In the first part of this chapter, the ability of the typhoon Robyn runs to meet these prerequisites is determined. In the later sections, the first hypotheses concerning short-term teleconnections and individual tropical cyclones (see Chapter 1, section C) are examined by analyzing the typhoon Robyn modeling results. Finally, the third hypothesis, concerning the role of Rossby wave

sources in teleconnections, is investigated. Woll (1993) showed that the Yuri results supported the first two hypotheses, but he did not test the third hypothesis. So we tested the third hypothesis for both the Yuri and Robyn results.

In order to highlight the major features in the model results, many of the figures in this chapter show ensemble averages of the results. The results from Forecast 2 are shown when displaying the results from just one of the individual runs. The Forecast 2 results tended to be quite similar to those from Forecast 1 and Forecast 3.

B. PREREQUISITE 1 – BOGUSING AND THE INITIAL CONDITIONS

To test this prerequisite, the initial SLP fields were analyzed for each forecast. To highlight the impacts of the bogusing procedures on these initial conditions, several differences in these initial conditions were calculated: POSITIVE – NEGATIVE, NO – NEGATIVE, and POSITIVE – NO. Here, for example, POSITIVE – NEGATIVE refers to the difference between the results from runs using the POSITIVE bogusing and those from runs using NEGATIVE bogusing. Table 1 provides descriptions and explanations of these differences. This terminology is used throughout this study to refer to the difference fields. Table 1 provides descriptions and explanations of these differences.

1. SLP INITIAL CONDITIONS

The SLP initial conditions for the Forecast 2 POSITIVE, NEGATIVE, and NO bogus runs are shown in Figure 8. These three initial fields were very similar except in the tropical western Pacific, in the vicinity of Robyn. The POSITIVE bogus (Figure 8a) showed a strong pressure minimum at Robyn's position. The

NO bogus (figure 8b) showed a similar but weaker low pressure. The NEGATIVE bogus (Figure 8c) showed no signs of Robyn; only a broad monsoon trough was evident.

Figure 9 shows the Forecast 2 initial SLP difference fields. The effects of the bogusing are quite striking. The largest and most impressive differences appeared in the vicinity of typhoon Robyn, where expected. Some weaker differences also were evident in the southern hemisphere, quite distant from the bogused storm.

The SLP initial conditions and SLP initial condition differences for Forecast 1 and Forecast 3 were similar to those for Forecast 2. The only exception was in the Forecast 3 POSITIVE – NEGATIVE difference in which a small circular area of -4 mb occurred just southeast of Robyn, in the vicinity of tropical storm Steve.

2. CONCLUSION FOR PREREQUISITE 1

Ideally, the bogusing procedure would not have produced differences in the SLP initial conditions away from Robyn. However, those remote differences which did occur were relatively small compared to those near Robyn. Thus, we concluded that prerequisite 1 was met.

It is interesting to consider why these remote initial condition differences occurred. The differences near Steve may indicate that there was some coupling, at least in the data assimilation process, between Robyn and Steve. Thus, the changes in Robyn caused by the bogusing procedures may have inadvertently affected Steve.

The southern hemisphere differences were similar to those seen by Woll (1993). These differences may have arisen due to the finite wave number resolution (T79) used in the data assimilation and model. This limited

resolution meant that when the bogusing was applied to the shorter waves representing Robyn, there were small, but wide spread, impacts on the atmospheric structure. Those impacts which occurred in unstable areas were most likely to amplify during the data assimilation process. Such unstable areas were most likely along the strong wintertime jets of the Southern Hemisphere.

C. PREREQUISITE 2 – TYPHOON TRACK AND INTENSITY

The second prerequisite requires a good simulation of the typhoon in the POSITIVE runs. To a lesser extent, this prerequisite also requires a good simulation in the runs for which no bogusing was used, the NO forecasts. Conversely, this prerequisite requires that there be no typhoon in the NEGATIVE runs.

To test this prerequisite, the model tracks for Robyn were determined from the positions of the minimum SLP in the western Pacific at each model output time. These positions were then compared to the JTWC best track which we assumed to be the typhoon's actual track. The model intensities for Robyn were estimated from the strength of the SLP minima used to find the Robyn tracks. These model intensities were then compared to the JTWC estimates of Robyn's SLP minima.

1. TYPHOON TRACK

The positions of the SLP minima at selected times for the Forecast 2 POSITIVE, NO, and NEGATIVE runs are shown in Figures 10, 11, and 12, respectively. The SLP minima corresponding to Robyn from the POSITIVE and NO runs were well defined and showed clear recurving tracks (Figures

10b,c,d,e and 11b,c,d,e; cf. Figure 3). The NEGATIVE run did not show any organized area of low SLP corresponding to Robyn (Figure 12,b,c,d,e; cf. Figure 3). The NEGATIVE run did however show the slow development of a monsoon trough that extended southwest to northeast between the Philippines and southern Japan. The Forecast 1 and Forecast 3 results were similar (not shown).

Figure 13 shows the Forecast 2 POSITIVE, NO, and NEGATIVE model tracks (derived from the SLP minima shown in Figures 10-12) overlaid with the JTWC best track for typhoon Robyn (cf. Figure 3). The POSITIVE and NO model tracks were quite good early in the runs, but propagated Robyn too slowly once Robyn reached about 28°N . The higher latitude track from the Forecast 1 POSITIVE run was slightly less accurate than the track from the Forecast 2 POSITIVE run, which was slightly less accurate than the track from the Forecast 3 POSITIVE run (not shown).

The track from the Forecast 2 NEGATIVE run (Figure 13c) clearly had no correspondence to Robyn's track. For all the NEGATIVE runs, the calculated tracks were not really tracks at all but unorganized shifts in the minimum of the broad monsoon trough.

2. TYPHOON INTENSITY

Robyn's intensity in the model was estimated from the strength of the SLP minima shown in Figures 10-12. The intensity of the actual SLP minima for Robyn was estimated from the JTWC maximum sustained winds using a correlation between winds and SLP developed by Atkinson and Holliday (1977). These JTWC derived intensities, along with the Forecast 2 intensities, are shown in Table 2.

The JTWC derived SLP minima were significantly lower than the model's SLP minima. This is probably the result of deficiencies in the NOGAPS representation of tropical cyclone physics, and the limited resolution of NOGAPS. Allowing for these model limitations, the POSITIVE and NO runs showed a development of the SLP minima that was very similar to that estimated from the JTWC winds. The POSITIVE run reached its deepest low, 978 mb, on 07 August at 12Z, when the deepest JTWC low, 927 mb, also occurred. The intensities from the POSITIVE run were noticeably more realistic than those from the NO run; and both were much better than those from the NEGATIVE run. Similar results were found for the Forecast 1 and 3 intensities (not shown).

3. CONCLUSION FOR PREREQUISITE 2

The POSITIVE runs gave relatively accurate simulations of Robyn's track and intensities, while the NEGATIVE runs showed no signs of Robyn. Therefore, we concluded that prerequisite 2 was satisfied.

D. PREREQUISITE 3 – COMPARISONS WITH CLIMATOLOGY

In order to ensure that the model used in this study gave a realistic depiction of the climatological features of the atmosphere, we compared the 20-day time average of the model's 200 mb height and atmospheric heating fields to the observed monthly mean fields for August 1993.

1. 200 MB GEOPOTENTIAL HEIGHTS

The 20-day average 200 mb heights for the Forecast 2 POSITIVE, NEGATIVE, and NO bogus runs are shown in Figure 14. Some of the major features seen in all three averages are the areas of: (1) strong meridional

gradients, indicating the westerly jets; and (2) diffuence over the North and South Pacific, and North and South Atlantic. These time averages are similar to the observed monthly mean heights for August 1993 (Kousky 1993).

The major differences between the model averages are found in a comparison of the NEGATIVE average with the POSITIVE and NO averages. Note in particular that the NEGATIVE average had much weaker jets over the east Asian - North Pacific area and over North America.

The 20-day averages of the Forecast 1 and Forecast 3 runs (not shown) were quite similar to those shown for the Forecast 2 runs.

2. ATMOSPHERIC HEATING

The 20-day average atmospheric heating for the Forecast 2 POSITIVE, NEGATIVE, and NO bogus runs are shown in Figure 15. Note that only the very strongest heating areas are shown in this figure, due to the choice of contouring. This contouring was used in order to highlight the differences in strong heating between the POSITIVE, NO, and NEGATIVE runs. Some of the major features seen in all three averages are the areas of strong heating in the tropical western Pacific and Indian Ocean areas, and in the midlatitude storm track areas. These time averages are roughly similar to the strong heating inferred from the observed monthly mean outgoing long wave radiation (OLR) and precipitation patterns for August 1993 (Kousky 1993). However, the heating in the tropical eastern Pacific appears to be too weak in all three model runs.

The major differences between the model averages are in the western Pacific near the Philippines and Japan, where the NEGATIVE average had much less heating. This is presumably the result of Robyn being absent from the

NEGATIVE run. This heating difference may also explain the 200 mb height differences seen in the western North Pacific.

The 20-day averages of the Forecast 1 and Forecast 3 runs (not shown) were quite similar to those shown for the Forecast 2 runs.

3. CONCLUSION FOR PREREQUISITE 3

The similarities of the average forecast heights and heating to the observed values indicates that prerequisite 3 was met.

E. PREREQUISITE 4 – EFFECTS OF ENSEMBLE AVERAGING

Ensemble averaging is done in order to clarify the common features in the various forecasts. However, it is possible for averaging to produce a result that is unrepresentative of any of the individual forecasts used to calculate the average. Thus, we wanted to check that the ensemble averaging process preserved the major features of its constituent forecasts. We made this check by comparing the 200 mb heights from the Forecast 1, 2, and 3 POSITIVE and NEGATIVE runs with each other and with their ensemble average. Similar comparisons were made for the individual and ensemble average atmospheric heating fields. Figures 16-31 shows these height and heating fields at 2-day intervals.

These figures are discussed in the following two subsections. The emphasis in these discussions is on the ensemble average results (Figures 19, 23, 27, and 31), since, as will be shown, the average fields were very similar to the individual fields.

1. 200 MB GEOPOTENTIAL HEIGHTS

This section presents the evolution of the major features in the 200 mb

geopotential height field over the North Pacific - North American (NP-NA) region for the Forecast 1, 2, and 3 POSITIVE and NEGATIVE runs and the ensemble average of these forecasts. This discussion focuses on the NP-NA region because: (1) Robyn occurred in the western portion of this region (cf. Figures 10-13); and (2) large responses to Robyn were found in this region (cf. Figures 14, 15).

a. RESULTS OF THE POSITIVE FORECASTS

The 200 mb heights from the POSITIVE forecasts are shown in the following figures.

- Forecast 1 – Figure 16
- Forecast 2 – Figure 17
- Forecast 3 – Figure 18
- Ensemble Average – Figure 19

On 09 August 1993 at 00Z, a series of upper-level ridges and troughs extended across the North Pacific from Asia to North America (Figures 16-19). Specifically, 200 mb ridges existed over Japan and the western Gulf of Alaska, while 200 mb troughs were found over Kamchatka and over the most eastern portion of the Gulf of Alaska. The strongest upper level winds were located over east Asia (the Asian - North Pacific jet) and Alaska.

By 11 August at 00Z, the series of ridges and troughs had moved slightly eastward. The ridge that was over Japan had strengthened, moved east of Japan, and was tilted southwest to northeast. The trough that was over Kamchatka had extended to the east-southeast, and the ridge in the Gulf of Alaska had sharpened. The Asian - North Pacific jet had strengthened and extended farther eastward, and the North American jet was evident across the

northwestern US.

Forty-eight hours later on 13 August, the ridge east of Japan had shown no movement, but was sharper and extended farther north into Siberia. The trough east of Kamchatka had moved slightly eastward and strengthened. The ridge in the Gulf of Alaska had flattened. The Asian - North Pacific jet had extended farther to the east and become noticeably stronger over the Aleutians.

By 15 August, the ridge east of Japan was still in place. The trough east of Kamchatka had strengthened. The Asian - North Pacific jet had extended farther into Alaska and the North American jet had become more zonal.

By 17 August, the ridge east of Japan had strengthened slightly but remained in place. The trough east of Kamchatka and the ridge in the Gulf of Alaska had strengthened. The North American jet had strengthened and become very zonal across all of southern Canada.

Two days later on 19 August, the features seen during the preceding week were still present, with the features west of the dateline having strengthened further.

By 21 August, the ridge - trough sequence stretching eastward from east Asia across North America was still in place but had weakened.

This ridge - trough pattern remained in place from 23 through 25 August but was weaker overall than in the preceding week.

In summary, the POSITIVE 200 mb heights showed a very clear and persistent ridge - trough pattern for most of the forecast period. This pattern intensified for much of the forecast period, with the intensification occurring first in the western, and later in the eastern, part of the NP-NA region. Minor differences existed between the individual forecast runs. For example, at the

last few output times of Forecast 1 some of the ridge and trough features were less distinct than in Forecasts 2 and 3. This may have been due to the longer forecast period for Forecast 1.

b. RESULTS OF THE NEGATIVE FORECASTS

The 200 mb heights from the NEGATIVE forecasts are shown in the following figures:

- Forecast 1 – Figure 20
- Forecast 2 – Figure 21
- Forecast 3 – Figure 22
- Ensemble Average – Figure 23

On 09 August 1993 at 00Z, the NEGATIVE 200 mb height pattern (panel c of Figures 20-23) was virtually identical to that in the POSITIVE run (panel c of Figures 16-19). In particular, the NEGATIVE pattern exhibited the same series of troughs and ridges from Asia to North America.

Forty-eight hours later on 11 August, the pattern was still similar except for a weaker ridge over Japan in the NEGATIVE case.

On 13 August, the heights were still similar to those in the POSITIVE case, except for a weaker ridge over Japan and a weaker trough east of Kamchatka in the NEGATIVE case.

By 15 August, the similarities between the NEGATIVE and POSITIVE heights were confined to central and eastern North America. Elsewhere, the ridge - trough pattern seen on 9 and 11 August had weakened further, and the indicated flow had become rather zonal.

From 17 to 21 August, the ridge - trough pattern became even weaker and the flow quite zonal all the way from east Asia to the North Atlantic.

From 23 to 25 August, there was some increased ridging over the northeastern Pacific and western North America. By 25 August, there was relatively strong zonal flow over the northwestern Pacific.

In summary, the NEGATIVE 200 mb heights showed an initial ridge - trough pattern across the NP-NA region that was similar to that from the POSITIVE runs and which generally weakened throughout the forecast period. This weakening progressed from west to east. The differences between the individual NEGATIVE runs were small. Comparison of the POSITIVE and NEGATIVE 200 mb heights shows that they evolved quite differently, with the ridge - trough pattern strengthening in the POSITIVE case and weakening in the NEGATIVE case (compare Figures 16-19 with 20-23). However, in both cases the changes in the ridge - trough pattern progressed from west to east.

2. ATMOSPHERIC HEATING

This section presents the evolution of the major features in the atmospheric heating, Q , field over the North Pacific - North American region for the Forecast 1, 2, and 3 POSITIVE and NEGATIVE runs and the ensemble average of these forecasts.

a. RESULTS OF THE POSITIVE FORECASTS

The heating fields from the POSITIVE forecasts are shown in the following figures:

- Forecast 1 – Figure 24
- Forecast 2 – Figure 25
- Forecast 3 – Figure 26
- Ensemble Average – Figure 27

On 09 August, the most prominent heating was in a circular area between the

Philippines and Japan, where the model representation of Robyn was located (cf. Figure 10). There were also areas of weaker heating just north and south of this strong heating, and in the tropical eastern Pacific.

Two days later on 11 August, the intense heating from Robyn had moved over the Sea of Japan and weakened. The heating just south of Robyn had strengthened and extended to the east, while the heating in the tropical eastern Pacific had strengthened and moved to the northwest.

By 13 August, the heating signal from Robyn had moved farther north and weakened further. The heating east of the Philippines had strengthened while the tropical eastern Pacific heating had weakened.

By 15 August, a small remnant of Robyn's heating was located along the Siberian coast of the Sea of Okhotsk. The heating east of the Philippines and in the tropical eastern Pacific had weakened.

From 17 through 25 August, there was relatively weak heating throughout the NP-NA region.

In summary, typhoon Robyn's heating was clear as Robyn recurved north of the Philippines and moved over the Sea of Japan and eastern Asia. Robyn's heating was the dominant heating seen throughout the NP-NA region during the forecast period.

b. RESULTS OF THE NEGATIVE FORECASTS

The heating fields from the NEGATIVE forecasts are shown in the following figures:

- Forecast 1 – Figure 28
- Forecast 2 – Figure 29
- Forecast 3 – Figure 30

- **Ensemble Average – Figure 31**

On 09 August, moderate heating was found over the Sea of Japan and in the tropical eastern Pacific. The main difference between this heating and that in the POSITIVE cases was the absence of Robyn's heating northeast of the Philippines in the NEGATIVE case.

From 11 through 25 August, the heating events were generally weak and short lived throughout the NP-NA region. This heating was roughly similar to the heating seen in the POSITIVE case, except for the absence of Robyn's heating during 9-15 August.

3. CONCLUSION FOR PREREQUISITE 4

In their major features, the ensemble averages of the height and heating fields from the POSITIVE and NEGATIVE runs were very similar to the height and heating fields from the individual runs. Thus, we concluded that the ensemble average fields were a good representation of the individual forecast fields. Therefore, most of the remaining results will be presented in their ensemble average form.

F. HYPOTHESIS 1 – TELECONNECTIONS ASSOCIATED WITH TYPHOON ROBYN

The 200 mb heights and heating fields presented in the preceding sections indicate that there were large differences in the NP-NA region between the POSITIVE and NEGATIVE runs. These differences represent the model response to typhoon Robyn, and suggest that Robyn may have induced teleconnections in the NP-NA region. To explore these teleconnections further, we examined the ensemble averages of the POSITIVE - NEGATIVE differences

in atmospheric heating, 200 mb heights, and several other fields. These differences represent the model atmosphere's responses to the presence of Robyn. The ensemble averaging of the differences provides a clearer view of the major features in the differences.

1. ENSEMBLE AVERAGE DIFFERENCES IN ATMOSPHERIC HEATING AND 200 MB GEOPOTENTIAL HEIGHTS

Figure 32 shows the POSITIVE – NEGATIVE ensemble average differences in the heating and 200 mb heights. The heating differences are weak except at the beginning of the forecast period. The prominent heating differences occurred from 9-13 August in the western Pacific where the POSITIVE runs located Robyn and where the NEGATIVE runs had no representation of Robyn (Figure 32c,d,e).

The evolution of the height differences in Figure 32 was easier to follow after identifying the major differences and labeling them with the symbols H and L (for highs and lows) and with numbers corresponding to the order in which they first appeared. The seven major height differences in Figure 32 are labeled as shown below and listed in the order of their appearance.

- H1, the first positive difference, which appeared over Japan on 11 August (Figure 32d)
- L1, the first negative difference, which appeared southeast of Kamchatka on 13 August (Figure 32e)
- H2, the second positive difference, which appeared over southern Alaska on 13 August (Figure 32e)
- L2, the second negative difference, which appeared in the northeast Pacific at about 40N, 145W on 15 August (Figure 32f)

- L3, the third negative difference, which appeared over northwestern Canada on 15 August (Figure 32f)
- H3, the third positive difference, which appeared over central Alaska on 21 August (Figure 32j)
- H4, the fourth positive difference, which appeared over southwestern Canada on 21 August (Figure 32j)

As an example of how these differences can be traced through time and space, consider H1 which formed over Japan as Robyn was approaching the Sea of Japan (cf. Figure 10). On 12 August, the magnitude of H1 was over 200 gpm (not shown). Over the next twelve days, H1 slowly weakened and propagated to the east-northeast. On 21 August, H1 was just southeast of Kamchatka. By 25 August, H1 was just south of Alaska, had reversed its weakening trend, and had strengthened to over 300 gpm.

Soon after H1 formed, L1 formed to the east-northeast of H1 (Figure 32e). L1 also propagated slowly to the east, and was at about 35°N, 175°E on 19 August and just west of the northwestern US on 25 August.

H2 formed to the northeast of L1 (Figure 32e) and slightly later than L1 formed. H2 remained near southern Alaska until about 23 August when it dissipated.

L2 and L3 formed soon after H2, with L2 forming to the southeast and L3 forming to the northeast of H2 (Figure 32f). L2 was relatively stationary, remaining over the northeast Pacific for most of the forecast period. But by 25 August, L2 had intensified to -350 gpm and moved over western Canada. L3 formed at a relatively high latitude, 60°N, and propagated slowly to the southeast. L3 strengthened steadily, throughout its existence, reaching -350

gpm by 25 August.

H3 and H4 formed to the north and southeast, respectively, of H2 (Figure 32i). They both grew slowly as they gradually moved eastward. By 25 August, H3 had reached Hudson Bay and H4 had reached south central Canada.

2. CONCLUSION FOR HYPOTHESIS 1

These strong and persistent height differences represent the response of the model to Robyn. Thus, Robyn clearly produced, in the model atmosphere, a significant teleconnection signal over the NP-NA region. Therefore, these results support Hypothesis 2.

A comparison of Figure 32 with Figures 6 and 7 shows that the modeled teleconnection response to Robyn is very similar to: (1) the Northern Hemisphere summer teleconnection response to tropical western Pacific heating anomalies identified by Nitta (1987); and (2) the wind anomaly pattern associated by Harr and Elsberry (1991) with recurving tropical cyclones. Note that the atmospheric levels represented in Figures 6, 7, and 32 are all different. However, all three figures represent time averages for which the vertical structure of the atmosphere is equivalent barotropic. Thus, the three figures do, indeed, show quite similar patterns. These similarities indicate that the modeled teleconnection response to Robyn (Figure 32) may represent the way in which the actual atmosphere responds to tropical cyclones.

Figure 32 also offers some insights into how the teleconnection response to Robyn may have occurred. An inspection of all the panels of Figure 32 shows that the height differences developed first in the western part of the NP-NA region (e.g., H1 and L1 near east Asia), and then farther and farther to the east throughout the forecast period. Also, the area in which the largest height

differences occurred was located progressively farther to the east. The eastward propagation speeds of the site at which new height differences formed, and of the area in which the largest height differences occurred, were much faster than the eastward propagation speeds of the height differences themselves. This suggests that the eastward motion of the teleconnection response was dominated by Rossby wave group propagation, occurring at the faster eastward speeds. The slower eastward propagation of the individual height differences represents Rossby wave phase propagation.

Note also that most of the growth in the individual height differences occurred well after and far from Robyn (cf. Figures 10 and 13), although H1 formed over Japan as Robyn was approaching southern Japan. Also, several of the height responses grew rapidly for several days after they formed and then gradually weakened (e.g., L1 and H2). And some of the differences grew only slowly until late in the forecast period when they started to grow rapidly (e.g., L2 and L3). And some had more than one period of strong growth (e.g., H1). These results suggest that the growth of the individual height differences: (1) was not a simple and direct response to the heating differences associated with Robyn; and (2) was affected by more than simple Rossby wave energy propagation. The next two sections explore potential sources of energy for the growth of the response as Hypotheses 2 and 3 are investigated.

G. HYPOTHESIS 2 – THE JET'S ROLE IN TELECONNECTIONS

This section investigates Hypothesis 2 which concerns the jet's role in the teleconnection process. As discussed by Woll (1993), Hypothesis 2 can be expressed in terms of the following components:

- the teleconnection pattern, defined by the 200 mb height differences, has a characteristic relationship to the jet;
- the jet acts as a wave guide for QG wave energy propagation; and
- areas of potential barotropic instability (BTI) may be important wave energy sources.

These three components of Hypothesis 2 are addressed in the three subsections that follow. The jets used in these subsections was calculated from the ensemble average of the 200 mb zonal and meridional winds from the POSITIVE runs. Jet axes within these winds were defined by winds that were greater than or equal to 30 m/s. The jets calculated from the POSITIVE runs were chosen for these analyses because they best represented the jets that were present during and after Robyn's occurrence.

1. 200 MB HEIGHT DIFFERENCES AND THE JETS

Figure 33 displays the ensemble average POSITIVE – NEGATIVE 200 mb geopotential height differences shown in Figure 32 but with the jets indicated by heavy black lines.

The first positive height difference, H1, appeared on 10 August over the Sea of Japan, and just south of the east Asian jet (not shown). By 11 August, H1 was still centered just south of the jet and both H1 and the jet had strengthened (Figure 33d). This spatial relationship between H1 and the jet also occurred on 13 August, when L1 was centered just north of the jet (Figure 33e).

On 15 and 17 August, H1 was southwest of the jet, L1 was still centered just north of the jet, and H2 was centered just south of the jet that extended across southern Alaska (Figure 33f,g). On 17 August, the Alaska jet and H2 had strengthened, and L3 was in an early development stage and located north of the southern Canada jet. On 19 August, H1 and H2 were both found just south

of their local jets, while L3 was just north of the Canada jet (Figure 33h). These relationships were maintained on 21 August, when H4 was in its early stages and on the south flank of the jet across southern Canada (Figure 33i). On 23 and 25 August, H4 was still at or just south of the Canada jet, while L3 was still just north of this jet (Figure 33j,k). The strong growth of L3 that occurred from 23 to 25 August was accompanied by a strengthening of the jet located just south of L3.

In summary, there was a fairly consistent relationship between most of the major height differences and their local jets. The positive height differences tended to form just south of their jets, while the negative differences formed just north. The height differences and their local jets tended to strengthen and weaken together, with the strongest height differences (over 400 gpm) occurring when a strong jet axis was nearby.

Note that the *relationship between the height differences and the jet* seen in Figure 33 suggests that variations in the heights associated with the wave response may have produced propagating jet variations. That is, as the wave response propagated through the atmosphere, it may have produced height variations which led to wind variations. For example, eastward propagation of wave energy led to the strongest height differences being located progressively farther to the east (Figure 32). This, in turn, led to the strongest jets being located progressively farther to the east. These jets were situated just north of the positive height differences and just south of the negative differences, as would be expected from geostrophic reasoning (Figure 33).

Similar relationships between height differences and jets were found by Woll (1993) in his study of the response to Yuri. However, in that case the individual

height differences and jet tended to propagate eastward together. In the Robyn case, the individual height differences tended to propagate more slowly than the jet.

2. THE JETS AND THE WAVE RESPONSE

This section uses the quasi-geostrophic (QG) wave activity flux (Plumb 1985) to examine the propagation and sources and sinks of the energy associated with the wave response to Robyn (Figure 32). Chapter II, Section F1, and Woll (1993) give overviews of this flux and explanations of how and why this flux is used in this type of study.

The following characteristics are useful in interpreting the flux patterns.

- The flux vectors are oriented parallel to the direction of wave energy propagation.
- The flux vector length is proportional to the amount of energy being propagated.
- An area of flux divergence is an area of wave energy gain, or an energy source.
- An area of flux convergence is an area of wave energy loss, or an energy sink.

We calculated the QG wave activity flux vectors from the ensemble average of the POSITIVE – NEGATIVE 200 mb geopotential height differences (Figure 32). Thus, the fluxes represent the wave energy propagation associated with the teleconnection response to Robyn. Figure 34 shows these fluxes along with the ensemble average POSITIVE 200 mb jet axis (wind speeds > 30 m/s), the same jet that was shown in Figure 33.

Figure 34c shows that on 09 August 1993, the wave energy propagation was

weak throughout the NP-NA region. Note that this was also a time when the height differences were weak (Figure 32c).

On 11 August, flux vectors of moderate magnitude were located over and near Japan (Figure 34d). Note that the stronger fluxes were approximately parallel to the jet along the jet's south flank. Note also that these fluxes diverged from an area over the Sea of Japan, indicating that there was a wave energy source along the jet's south flank, in the vicinity of Robyn (Figure 10d).

On 13 August, there were strong fluxes in the northwest Pacific directed to the northeast (Figure 34e). Near Kamchatka, the fluxes were oriented perpendicular to the jet, but further to the west and east they were roughly parallel to the jet. The fluxes were strongly divergent in an area east of Japan and southeast of Kamchatka.

On 15 August, the largest fluxes had propagated eastward and were parallel to the jet south and east of Kamchatka and over southern Alaska (Figure 34f). The flux divergence indicated an energy source near the western end of the Aleutians, along the north flank of the Alaska jet.

By 17 August, the strongest fluxes were located still farther to the east, over the central North Pacific (Figure 32g). Over most of this area, the fluxes were roughly perpendicular to the jet. The flux divergence indicated energy sources near the jet entrance over the northwest Pacific, and near the jet exit over the northern Gulf of Alaska. Note that the strong fluxes south of Alaska formed an arcing pattern, with the fluxes directed: (1) eastward and poleward over the Aleutians; and (2) eastward and equatorward over the northeast Pacific. Note also that the fluxes were perpendicular to the local 200 mb height difference contours (see L1 and H2 in Figure 32g).

By 19 August, the strong fluxes were still farther to the east (Figure 34h). Over western Canada the fluxes paralleled the jet. Over the Gulf of Alaska, they were directed eastward and equatorward from a divergent area along the jet.

On 21 August, the strongest fluxes were located over Canada, but these were weaker fluxes than the those seen during the preceding week (Figure 34i). 21 August was also a time of relatively weak height differences (Figure 32i). Over much of the NP-NA region, the fluxes were approximately parallel to the jets. One notable exception was over eastern Canada, where the fluxes crossed the jet. The strongest energy source region was over northern Canada, near where L3 was intensifying (Figure 32i).

The flux pattern on 23 August was similar to that on 21 August, but the source region over northern Canada had shifted to the southeast (as had L3, Figure 32j). Also, the fluxes in the central North Pacific were more spatially coherent and stronger.

By 25 August, these North Pacific fluxes had strengthened and propagated to the east-northeast to a position over the Gulf of Alaska (as had H1 and L2, Figure 32k). The strong flux divergence over the Gulf of Alaska indicated a major wave energy source in that area. Over much of southern Canada, the fluxes were roughly parallel to the jet.

In summary, The QG wave activity fluxes had a relatively consistent relationship with the jets. In particular, the fluxes often paralleled the jets, indicating that the jets were acting as wave guides in these situations. Also, strong flux divergence regions were often associated with the jet flanks, suggesting that the jets may have been an energy source for the wave response to Robyn. Similar results were found by Woll (1993) in his study of the

response to Yuri. However, arcing energy propagation paths were more common, and the energy paths were more confined to lower latitudes, in his results. These differences were probably related to the seasonal differences in the background flow for this study and Woll's study.

3. BAROTROPIC INSTABILITY

The association of wave energy source regions with the jet flanks seen in Figure 34 suggests that barotropic instability (BTI) may have been a factor in providing energy to the wave response (Figures 33 and 34). Figure 35 shows areas of potential BTI, as determined from a local application of the Rayleigh-Kuo criterion: $\beta - \frac{\partial^2 u}{\partial y^2} = 0$. The zonal flow used in this calculation was the ensemble average 200 mb zonal wind from the POSITIVE runs. As Figure 35 shows, some of the largest areas where this condition was met tended to occur along the flanks of the jets displayed in Figures 33 and 34. Note that the contours shown in Figure 35 give a general indication of areas where BTI was possible. These potentially unstable areas may have been inside and/or outside the closed contours. Woll (1993) and Chapter II, Section F2, provide more detailed discussions of potential barotropic instability and its application to this type of study.

Figure 35 also shows the wave activity fluxes and jets seen in Figure 34. In our interpretation of Figure 35, we have assumed that areas where flux divergence and potential BTI were collocated were areas where barotropic energy conversions may have been important in amplifying the wave response to Robyn.

An overview of figure 35 shows that areas of potential BTI were generally zonally elongated and scattered throughout the NP-NA region. The larger

areas tended to lie along the jet flanks. (e.g., on 15, 19-25 August, Figure 35f,h-k). At several times, the flux divergence areas were located close to and had shapes similar to the BTI areas (e.g., on 11, 15, 17, 21, and 25 August, Figures 35d,f,g,i,k). This was also true on a number of days not shown in Figure 35.

In summary, it appears that BTI may have been part of the mechanism by which energy was supplied to the wave response to Robyn. Thus, BTI may help explain how the response evolved: (1) after Robyn had dissipated; and (2) in ways that were apparently not related to simple Rossby wave energy propagation (see Section F). The association of the BTI areas with the jets indicates that energy from the jet played a role in amplifying the wave response, as well as in guiding the response (see Section G2). These results are similar to those found by Woll (1993).

4. CONCLUSION FOR HYPOTHESIS 2

The results shown in Figures 33, 34, and 35 indicate that the jets played a major role in the development of the teleconnection response to Robyn. The jet acted both as a wave guide and energy source for the wave response. Thus, these results support Hypothesis 2.

H. HYPOTHESIS 3 – THE ROLE OF ROSSBY WAVE SOURCES IN TELECONNECTIONS

This section investigates the possibility that a Rossby wave sources contributed to the teleconnections caused by a tropical cyclone. Woll (1993) concluded that the model results from his study of super typhoon Yuri met the four prerequisites and two hypotheses discussed earlier in this chapter. However, Woll (1993) did not explore Hypothesis 3. Thus, this hypothesis was

examined using both the Yuri and the Robyn results. In this examination, we used several ensemble average POSITIVE – NEGATIVE difference fields to calculate the Rossby wave source, its components, and other terms of interest in the vorticity equation, (6). The calculations for Yuri are presented first. Then these results are compared to those from Robyn.

1. THE ROSSBY WAVE SOURCE

Figure 36 shows the ensemble average POSITIVE – NEGATIVE 200 mb Rossby wave source differences for the Yuri forecasts (Woll 1993) in the western and central North Pacific from 29 November - 3 December 1991. Figure 37 shows the corresponding 200 mb geopotential height differences.

On 29 November at 12Z, the major Rossby wave source difference was a negative feature over and to the east of Honshu (Figure 36a). This was also the location of the dominant height difference, a positive difference, at this time (figure 37a). This height difference was the initial signal in the teleconnection wave response to Yuri described by Woll (1993). The ensemble average POSITIVE SLP and atmospheric heating showed that Yuri was located at about 25°N, 140°E at this time (Woll 1993, not shown). Thus, the major Rossby wave source difference and the major 200 mb height difference were collocated, and Yuri was well to the south of both of them.

From 29 November at 12Z through 01 December at 00Z, both the source difference and the height difference seen on 29 November intensified and moved about ten degrees to the east (Figures 36b-d, 37b-d). During this period, Yuri moved to the northeast until 01 December at 00Z, it was at about 33°N, 155°E (Woll 1993, not shown). Thus, Yuri at this time was just south of the source and height differences seen in Figures 36d and 37d.

From 01 December at 12Z through 03 December at 00Z, the source difference east of Japan moved to the east-northeast and dissipated (Figure 36e-h). The height difference during this period moved approximately with the source difference but did not dissipate (Figure 37e-h). Yuri also moved with, but just to the south of, the source difference (Woll 1993, not shown). During this period, Yuri evolved into a midlatitude system and dissipated (Woll 1993).

In summary, there was a negative Rossby wave source east of Japan early in the POSITIVE Yuri forecasts that was not present during the NEGATIVE Yuri forecasts. This source formed to the north of the model's Yuri and was collocated with the first wave response to Yuri. Furthermore, the wave response grew as the source grew, but did not dissipate as the source did. These results suggest that the early development of the wave response to Yuri may have been initiated by the Rossby wave source.

2. THE ROSSBY WAVE SOURCE COMPONENTS

The divergent wind advection and the stretching terms form the Rossby wave source. Figures 38 and 39 show the ensemble average POSITIVE -NEGATIVE differences in these two terms at 200 mb. These differences correspond to the difference fields shown in Figures 36-37. A comparison of Figure 38 with Figure 39 shows the relative importance of divergent wind advection and vortex stretching in producing the Rossby wave source differences seen in Figure 36.

Figures 38 and 39 show that the major negative source difference east of Japan (Figure 36) was dominated by the divergent wind advection from 29 November at 12Z through 01 December at 00Z. However, vortex stretching was a significant contributor too. From 01 December at 12Z through 03 December at 00Z, vortex stretching was dominant.

Examination of the terms that compose ADVDIV in (5) showed that the features seen in Figure 38 were mainly the result of the divergent wind advection of relative vorticity rather than planetary vorticity (not shown).

3. THE RELATIVE VORTICITY AND DIVERGENT WINDS ASSOCIATED WITH THE ROSSBY WAVE SOURCE

Figure 40 shows the 200 mb relative vorticity difference corresponding to the difference fields shown in Figures 36-39. Figure 41 shows the 200 mb divergent wind difference corresponding to the difference fields shown in Figure 36-39. These fields were examined in order to understand the evolution of the portion of the Rossby wave source difference caused by the advection of absolute vorticity by the divergent wind, the ADVDIV term in (5).

Figure 40a shows two major relative vorticity differences on 29 November at 12Z: a negative zonal feature east of Japan and a positive circular feature near Yuri's position south of Japan and east of the Philippines. Strong relative vorticity gradients (cf. (5)) can be inferred from both of these features. The negative feature represents the south flank of the corresponding jet difference (not shown). The negative feature is also collocated with the negative Rossby wave source area seen in Figure 36a and the positive height response seen in Figure 37a.

From 29 November at 12Z through 01 December at 00Z, the negative feature strengthened and moved to the east, while the positive feature weakened and moved to the north-northeast (Figure 40a-d). The negative feature moved with the Rossby wave source difference and the height difference seen in Figures 36 and 37, while the positive feature moved approximately with Yuri (Woll 1993, not shown). Note that the local intensification of the negative feature

represented the local rate of change in the relative vorticity described by (6). This intensification was very consistent with the intensification of the negative source difference shown in Figure 36a-d.

The divergent wind differences were strongly divergent over and to the northeast of Yuri from 29 November at 12Z through 01 December at 00Z (Figure 41a-d). The divergent wind differences to the northeast of Yuri were associated with a midlatitude synoptic system located northeast of Yuri and southeast of Japan (Woll 1993). This system was more intense in the POSITIVE Yuri runs than in the NEGATIVE Yuri runs. This relative intensification led to the divergent wind differences northeast of Yuri (Figure 41).

Comparison of the relative vorticity and divergent wind differences (Figures 40 and 41) indicated that the portion of the Rossby wave source caused by the divergent wind advection of relative vorticity was relatively large and negative just south of the jet axis east of Japan. This suggests that the divergent wind advection of relative vorticity was important in the development of the Rossby wave source difference (Figure 36). However, the divergent wind difference that contributed to this source difference was caused by both the difference in Yuri's divergent winds and the difference in the midlatitude system's divergent winds.

4. THE RELATIVE IMPORTANCE OF THE ROSSBY WAVE SOURCE IN THE VORTICITY EQUATION

The Rossby wave source, S , is one term in the vorticity equation (6). To understand the importance of S to the vorticity balance given by (6), we compared S with the relative vorticity tendency and advection by the rotational wind (ADVROT) at 200 mb. This comparison was made in the western Pacific

area during the 29 November - 3 December period when *S* seemed to be important in initiating the wave response to Yuri (Figures 36 and 37). All three terms had the same magnitude, with ADVROT being the largest and the tendency being the smallest. In general, these three terms did not balance each other. Thus, the twisting and/or vertical advection terms were also important in the vorticity balance for this location and time.

In summary, our analyses of the Rossby wave source, *S*, for Yuri indicated that *S* was an important part of the mechanism that initiated the teleconnection wave response to Yuri. *S* was shown to be associated with Yuri and its enhancement of a nearby midlatitude synoptic system. The impact of *S* on the wave response started well before Yuri reached the location at which the wave response started. This was because Yuri's divergent wind signal, and the divergent wind signal from the enhanced midlatitude system, extended well beyond Yuri to an area of strong relative vorticity gradient along the jet near Japan.

5. COMPARISON OF THE ROSSBY WAVE SOURCES FOR YURI AND ROBYN

The analyses of the Rossby wave source for the Yuri results led us to make the same analyses for the Robyn results. These analyses showed that the Rossby wave source had a very similar role in the development of the wave response to Robyn.

Figure 42 shows the ensemble average POSITIVE – NEGATIVE 200 mb Rossby wave source differences for the Robyn forecasts in the western and central North Pacific from 09 August - 12 August 1993 (cf. Figure 36 for Yuri

results). Figure 43 shows the corresponding 200 mb geopotential height differences (cf. Figure 37 for Yuri results). The major source difference during this period was the negative feature approximately over the Sea of Japan from 09 August at 12Z through 12 August at 00Z. The major height difference during this period was the positive feature over the Sea of Japan from 09 August at 12Z through 10 August at 12Z; and over and just east of Japan from 11 August at 00Z through 12 August at 12Z. This is the same height difference, H1, discussed in Section F1 and shown in Figures 32 and 33.

On 09 August at 00Z, there were only scattered weak source differences and no detectable height differences (Figures 42a and 43a). Twelve hours later, there was a pair of weak positive and negative source differences over the Yellow Sea (Figure 42b), and, just to the east, the first sign of H1 (Figure 43b). The ensemble average POSITIVE SLP and heating fields show that Robyn at this time was to the southeast of this source difference pair, approximately over Kyushu (cf. Figures 10c and 27c).

By 10 August at 00Z, the source difference pair and H1 had strengthened (Figures 42c and 43c), and Robyn had moved to just southeast of the negative source difference (not shown).

By 10 August at 12Z, the source difference pair had weakened substantially (Figure 42d), H1 had strengthened (Figure 43d), and Robyn had moved only slightly to the north (not shown). A weak positive source difference had also formed to the northeast of the Yellow Sea in association with a weak negative height difference.

On 11 August at 00Z, the two positive source differences were merged and placed close to the negative height difference just northeast of the Yellow Sea

(Figure 42e). The negative source difference was over the Sea of Japan, and a strengthened H1 was just to the northeast (Figure 43e). Robyn was in approximately the same location as the negative source difference (Figures 10d and 27d).

These source difference and height difference features were similar on 11 August at 12Z, except that they had all strengthened (Figures 42f and 43f). Robyn had moved slightly farther north (not shown).

During the next 24 hours, the source difference pair weakened (Figure 42g,h), and H1 and the much smaller negative height difference maintained their intensities while moving to the east-northeast (Figure 43g,h). Robyn weakened and moved slightly farther north to about 40°N (not shown).

Examination of the ADVDIV and vortex stretching terms (not shown) showed that ADVDIV was the primary contributor to the strong negative Rossby wave source difference located near the Sea of Japan. This source difference developed on the east flank of the meridionally oriented jet that was located along the eastern edge of the Sea of Japan on 09-10 August (Figure 33). Thus, this negative source difference is similar to the negative source difference that formed in the Yuri case on the south flank of the jet over Japan (Figure 36).

The positive source difference just east of the negative source difference (Figure 42) was caused by both ADVDIV and vortex stretching, but vortex stretching effects were larger. The other source differences seen in Figure 42 were caused primarily by vortex stretching.

In summary, the development of the Rossby wave source in the Robyn case was quite similar to that in the Yuri case. The relative importance of ADVDIV and vortex stretching was also similar. The development of positive 200 mb

height responses in association with negative Rossby wave source differences was also the same. This indicates that in both cases the wave response was initiated by the Rossby wave source; in particular, the ADVDIV term in S . The sign of the initial wave response was consistent with the sign of the source difference. That is, both corresponded to anticyclonic flow. This suggests that the phasing of the wave response may be governed, at least initially, by the sign of S . For the Yuri and Robyn cases, the sign of S was determined by the sign of the divergent wind and the sign of the relative vorticity gradient along the jet.

6. CONCLUSION FOR HYPOTHESIS 3

These Rossby wave source results provide strong support for Hypothesis 3. In particular, these results suggest that the interaction of the divergent upper level outflow from a tropical cyclone with an extratropical jet may initiate an extratropical wave response to the tropical cyclone. Note, too, that the results presented in this section also support Hypothesis 2 concerning the importance of the jet in the teleconnection process.

I. COMPARISON OF MODEL AND ANALYZED HEIGHT FIELDS

We performed a preliminary verification of the NOGAPS 20-day forecasts used in this study. This was done by visually comparing the ensemble average POSITIVE and NEGATIVE 200 mb geopotential heights with 200 mb geopotential height analyses from the National Meteorological Center (NMC). The focus in this verification was on the strong, large-scale structures in the 200 mb heights. Figure 44 shows the NMC upper-level heights from 09 August through 23 August 1993, at two day intervals.

Comparison of Figure 19c with Figure 44c shows that on 09 August at 00Z the POSITIVE heights and the analyzed heights were in very good agreement. The POSITIVE heights remained very similar to the analyses until 13 August at 00Z when the model slightly over built the ridge over the Gulf of Alaska (Figures 19e and 44e). In other areas, this 13 August forecast was good.

Forty-eight hours later, on 15 August, the POSITIVE heights had a ridge-trough-ridge pattern over East Asia and the North Pacific that was too strong and located too far to the west (Figures 19f and 44f).

On 17 and 19 August, the POSITIVE heights were too wavy in the western Pacific and too zonal over the US (Figures 19g,h and 44g,h).

On 21 and 23 August, the POSITIVE heights had become more zonal and more similar to the zonal structures seen in the NMC analyses (Figure 19i,j and 44i,j).

The ensemble average NEGATIVE 200 mb heights (Figure 23) were also compared to the NMC heights (Figure 44). On 09 August, the NEGATIVE heights were quite good (Figures 23c and 44c).

On 11 August, the midlatitude ridging in the NEGATIVE heights between China and the dateline was too weak (Figures 23d and 44d). The NEGATIVE structures were also out of phase over the northeast Pacific and North America on 19 August (Figures 23h and 44h).

On 21 August, the NEGATIVE heights were too wavy over the east Asia - western North Pacific area, and too zonal over the northeast Pacific and North America (Figures 23i and 44i). By 23 August, the area of excessive waviness had propagated eastward and was located over most of the North Pacific (Figure 23j and 44j).

The ensemble average POSITIVE forecast clearly gave a better simulation than the ensemble average NEGATIVE forecast of the observed 200 mb heights. However, both forecasts had problems in simulating some of the major ridges and troughs. There were some situations in which the POSITIVE ridges and troughs were too strong, suggesting that the processes that produced long waves in the POSITIVE runs may have been too active. The reverse may have been true for the NEGATIVE runs (cf. Figure 23d-f). These possible explanations for problems in the simulations are, of course, relevant to modeling the wave response to Robyn and should be pursued in future studies.

IV. CONCLUSIONS

A. SUMMARY

In this study, we used an operational global data assimilation system and forecast model to explore how individual tropical cyclones in the western North Pacific affect the global atmosphere over periods of weeks. Thus, we examined the short term teleconnections caused by a single tropical cyclone. Our primary focus was on typhoon Robyn during August 1993. But we also extended the work of Woll (1993) by conducting some additional studies of super typhoon Yuri during November - December 1991.

The data assimilation and modeling procedures used in this study were successful in allowing us to produce realistic simulations of the global atmosphere with and without the typhoon. Thus, we were able to compare the forecasts with the typhoon to the forecasts without the typhoon to find the impacts of the typhoon. We also used these comparisons to identify the processes by which these impacts occurred.

Our results were very clear in several respects.

- The response to the typhoon across the North Pacific - North American region was strong and persistent. For example, in the Robyn case, the 200 mb height responses were approximately 100-400 gpm and persisted for several days to more than a week.
- The responses showed distinct Rossby wave train characteristics, with eastward group velocities exceeding relatively slow eastward phase velocities.
- Advection of relative vorticity by the upper level divergent wind

from the typhoon was important in initiating the wave response. This initiation process was most pronounced where the divergent wind intersected the east Asian - North Pacific jet. This process may have been important in determining the phase of the wave response, by determining the sign of the first disturbance in the wave train.

→ The subsequent growth and propagation of the wave response was not directly affected by the tropical cyclone but was influenced by the extratropical jets. The jets acted to guide and amplify the response. The amplification may have resulted from barotropic instabilities along the jets.

→ The most realistic forecasts, those which included the typhoon, gave relatively good simulations of the major observed features of the upper troposphere, which were the main features of interest for this study.

These results support the hypotheses tested in this study and are consistent with the results from several other teleconnection studies. In particular, the model's circulation responses are very similar to the height anomalies associated by Nitta (1987) with tropical western Pacific heating anomalies, and the flow anomalies linked by Harr and Elsberry (1991) to recurving tropical cyclones.

B. THE UPPER-LEVEL HEIGHT PATTERNS ASSOCIATED WITH OTHER RECURVING TYPHOONS DURING 1993

The strong and persistent response to Robyn prompted us to wonder how well the Robyn case represents the typical response to a western Pacific typhoon during the northern summer. We performed a preliminary study of this

issue by examining the NMC analyzed upper tropospheric heights and winds during and after four other typhoons that occurred during 1993. These were typhoons Cecil, Ed, Flo, and Yancy. As with Robyn, each of these typhoons existed at or above typhoon strength for at least three days, and each recurved into the midlatitudes over the western North Pacific region.

We compared the heights and winds at common stages in the evolution of each typhoon, using the recurvature stage as a reference point on a relative time scale. We found that the circulation patterns for Robyn and the four other typhoons were similar.

For example, three days prior to recurvature, there were, in all five cases: (1) a ridge south of Japan; (2) a trough near northeastern China; (3) a trough near southwestern Alaska; and (4) a ridge near the northwestern US (not shown).

At recurvature, the common features were: (1) a ridge near southern Japan (the same ridge found three days earlier); (2) a trough near northeastern China; (3) a trough near Kamchatka; and (4) a ridge over the western Gulf of Alaska. For the Robyn case, the features at recurvature can be seen in Figure 44c.

Three days after recurvature, the common features were: (1) a strong ridge over Japan; (2) a cyclone east of Kamchatka; (3) a ridge over the Gulf of Alaska; and (4) a trough over western North America. The post-recurvature features for the Robyn case can be seen in Figure 44e.

These common features indicate that northern summer recurving typhoons may evolve in association with certain characteristic NP-NA circulation features (cf. Harr and Elsberry 1991). In addition, these common features indicate that the Robyn case examined in this study is probably representative of other

recurving typhoons.

C. IMPLICATIONS FOR EXTENDED-RANGE FORECASTING

The results of this study and of Woll (1993) may be useful in improving extended-range forecasts. Of particular interest for such forecasting are the very strong and persistent responses to the typhoons. These responses occurred well after the typhoons dissipated. So certain typhoons may be useful as warnings of circulation changes that may occur in one to two weeks. Since these circulation changes have large amplitudes, these typhoons would also be warnings of significant changes in the strength and location of the jets and storm tracks.

Figure 45 shows schematically the jet changes found in the forecasts with and without Robyn. The jets in this figure represent the ensemble average 200 mb flow in the POSITIVE (with Robyn) and NEGATIVE (without Robyn) forecasts during the second week of the forecast period. The two jets are dramatically different, with the jet in the POSITIVE case being much wavier than the jet in the NEGATIVE case. Similarly dramatic differences were found for the Yuri case (Woll 1993). Obviously, a better understanding of the processes that cause such large, and persistent, jet variations would be very useful in extended-range forecasting.

D. RECOMMENDATIONS FOR FUTURE WORK

The results of this study were very exciting. The teleconnections associated with typhoon Robyn add strong support to Woll's (1993) results for super typhoon Yuri. However, additional work needs to be performed on several

fronts.

1. ADDITIONAL CASE STUDIES

The similarities between the Robyn and Yuri results are encouraging. But more cases should be studied. This would be especially useful for understanding how the variations in the background conditions affect the response to a recurving tropical cyclone.

The strong dependence of the response on the wave guiding and amplification features of the jets suggest that disturbances other than tropical cyclones may produce teleconnections. Thus, additional case studies using a variety of disturbances would be useful. Some examples of these disturbances are:

- Straight moving tropical cyclones;
- Recurving tropical cyclones in the Bay of Bengal;
- *Recurving tropical cyclones in the Atlantic;*
- Tropical cyclones occurring in various seasons of the year;
- Tropical super cloud clusters;
- Active and break events in the Asian monsoon, and
- Strong midlatitude synoptic systems.

Studies with a wide variety of disturbances would be helpful in clarifying the relative importance of the intensity of the disturbance and the strength of the background flow (e.g., the jets).

2. FURTHER STUDY OF TELECONNECTION MECHANISMS

Many questions remain about the mechanisms behind the teleconnections seen in this and other studies (e.g., Harr and Elsberry 1991, Woll 1993). A partial list of unanswered questions includes:

- How much energy does the tropical cyclone contribute to the teleconnection? How is this energy contributed?
- How does the jet guide wave energy? Is a wavy jet as effective a wave guide as a zonal jet?
- How is QG wave energy released in areas of potential barotropic instability?
- How does wave energy feed back into the jet? What processes are operating in the energy sink regions?

Teleconnection energetics are particularly problematic. One example of this was found in the results for 11 August, when the divergence of the wave activity fluxes over the Sea of Japan indicated an energy source (Figure 34d). This energy source was very close to both Robyn (cf. Figure 10d) and to an area of potential BTI (Figure 35d). This overlap indicates that the energetics at this important stage in the development of the teleconnection were probably rather complex.

In this study, the conclusions about the importance of BTI (Chapter III, Section G) are quite tentative. This is because the Rayleigh-Kuo criterion is a crude diagnostic tool for identifying the existence of BTI, especially in zonally wavy flows. For example, this tool does not account for BTI arising from shear in the meridional flow. Thus, other tools need to be applied (e.g., calculations of the barotropic kinetic energy conversions).

Additional research on these and related issues is currently being conducted at the Naval Postgraduate School and the Naval Research Laboratory in Monterey, California.

The results of this study hold positive implications for improvements in extended-range forecasting. If additional studies find that short term

teleconnections can be accurately forecast, it may be possible to more accurately predict large scale steering flows. Persistent weather patterns could then be anticipated, which would allow planners to make informed decisions, thus benefiting all of society.

APPENDIX A - TABLES

Model Run	What it does	What it describes
POSITIVE	displays atmosphere with tropical cyclone; standard NOGAPS bogusing used to develop initial conditions	tropical cyclone, background flow, and interactions
NO	displays the atmosphere with the tropical cyclone, however no bogusing used to develop initial conditions	tropical cyclone, background flow, and interactions
NEGATIVE	tropical cyclone removed in the development of initial conditions	background flow
POSITIVE-NO	displays the difference between the POSITIVE bogus and the NO bogus model runs	the circulation due to the POSITIVE bogus enhancement of the tropical cyclone
NO-NEGATIVE	displays the difference between the NO bogus and the NEGATIVE bogus model runs	the circulation due to the NO bogus representation of the tropical cyclone
POSITIVE-NEGATIVE	displays the difference between the POSITIVE bogus and the NEGATIVE bogus model runs	the circulation due to the POSITIVE bogus representation of the tropical cyclone

Table 1. Overview of the model runs, according to the tropical cyclone bogusing procedure used to develop the model initial conditions (first three rows of table). Overview of the model differences, according to the bogusing procedures (bottom three rows).

Date Time (1993)	POSITIVE	NO	NEGATIVE	JTWC
07 AUG 12Z	978 23N 133E	988 23N 133E	1001 30N 123E	927 21N 132E
08 AUG 00Z	980 23N 132E	987 25N 133E	1004 15N 113E	927 23N 131E
08 AUG 12Z	979 25N 130E	987 25N 133E	1000 30N 103E	933 25N 130E
09 AUG 00Z	980 28N 130E	987 28N 133	999 30N 103E	943 28N 129E
09 AUG 12Z	983 28N 128E	988 30N 133E	998 30N 103E	948 31N 129E
10 AUG 00Z	982 30N 130E	989 30N 133E	998 30N 105E	963 35N 130E
10 AUG 12Z	987 30N 130E	991 30N 133E	997 30N 105E	976 38N 134E
11 AUG 00Z	993 30N 130E	994 30N 135E	998 30N 105E	987 42N 138E

Table 2. Strength and location of the typhoon Robyn minimum sea level pressure (SLP minima), in mb, for the Forecast 2 POSITIVE, NO, and NEGATIVE runs, plus the JTWC best estimates of minimum SLP at the specified times.

APPENDIX B – FIGURES

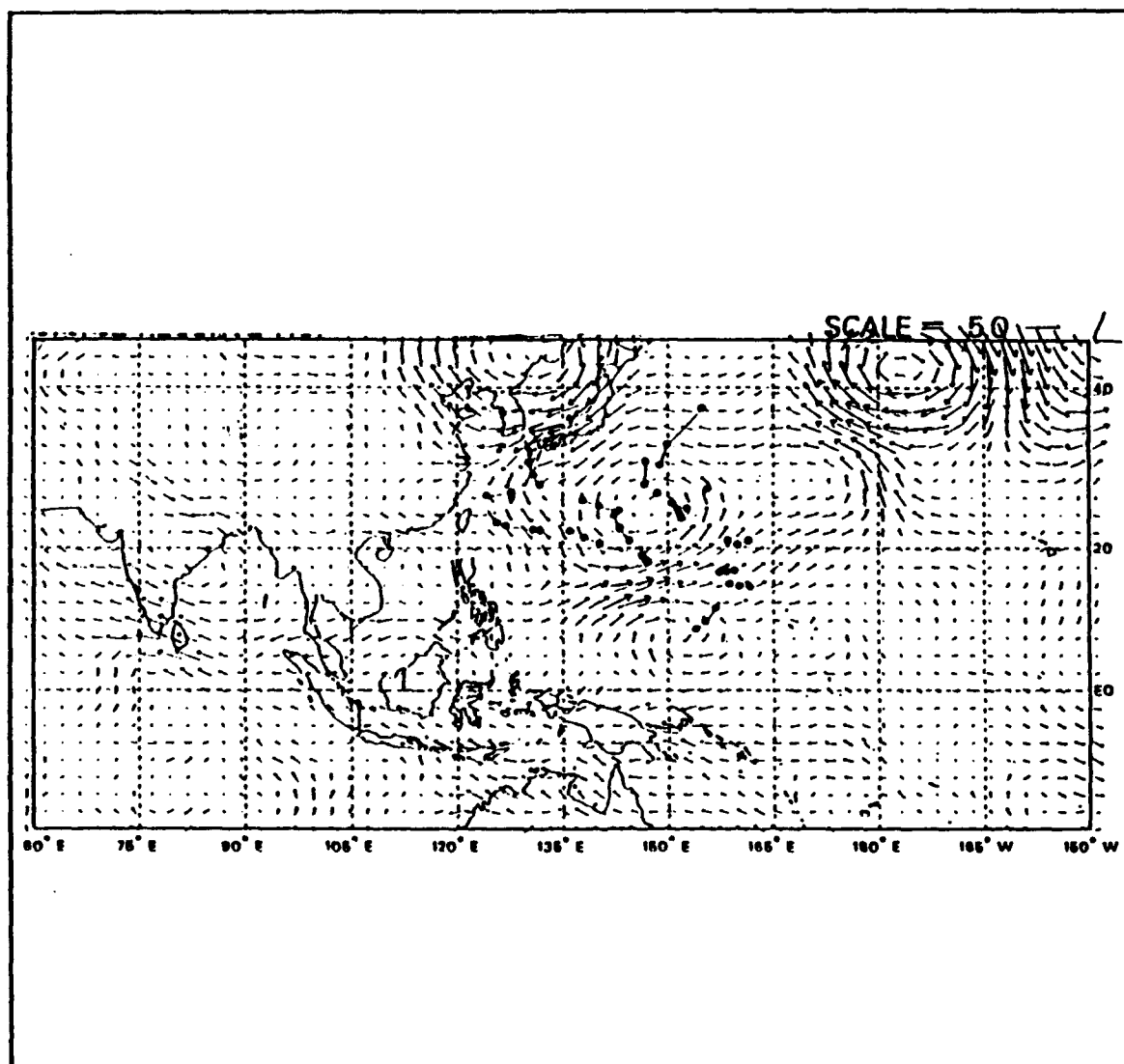


Figure 1. Composite of 700 mb wind anomalies for June-October 1979-1982. Compositing done only for periods during which recurving tropical cyclones existed in western Pacific. Maximum vector corresponds to approximately 5 m/s (from Harr and Elsberry 1991).

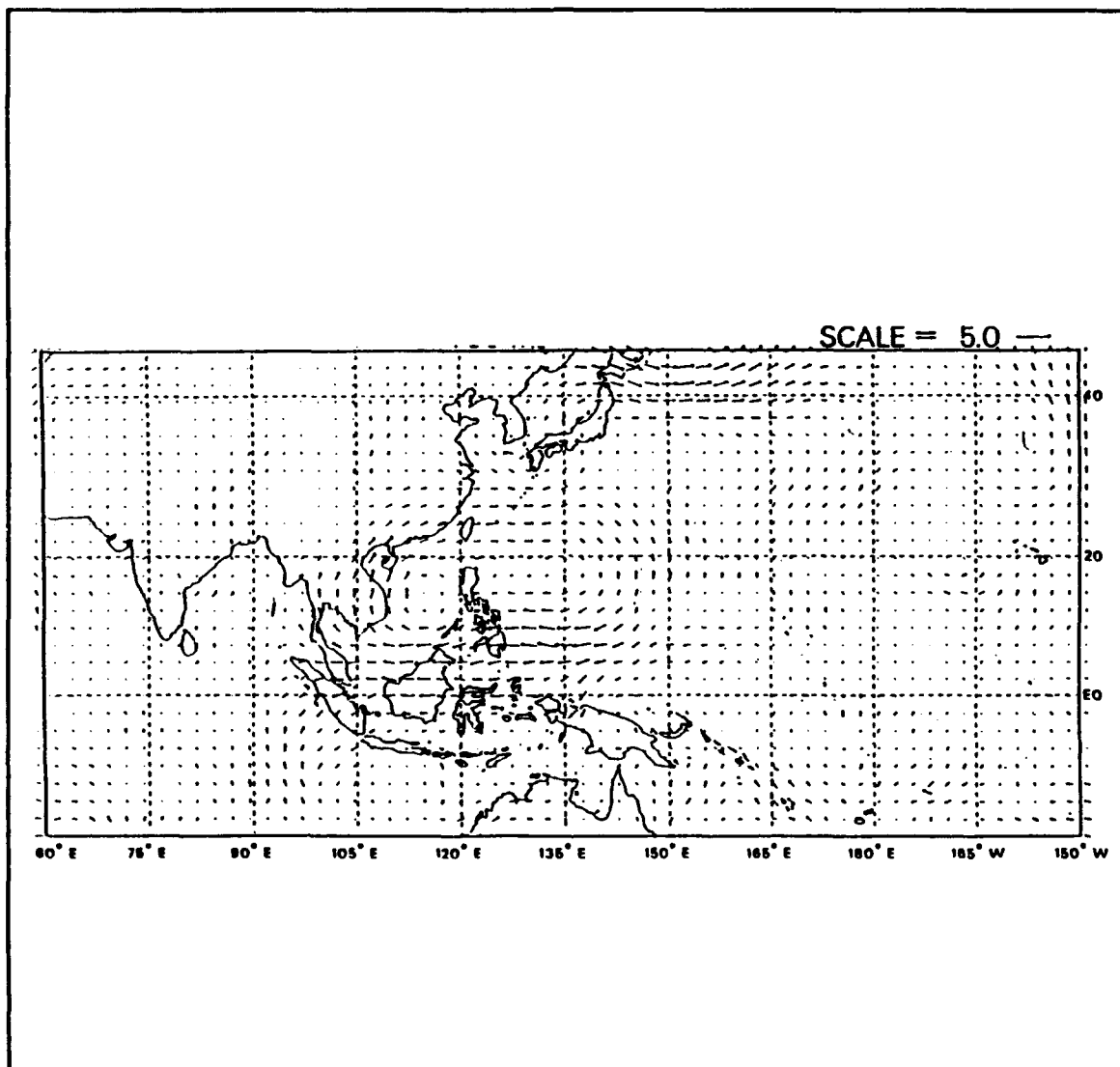


Figure 2. Composite of 700 mb wind anomalies for June-October 1979-1982. Compositing done only for periods during which there was no tropical cyclone activity in the western Pacific. Maximum vector corresponds to approximately 5 m/s (from Harr and Elsberry 1991).

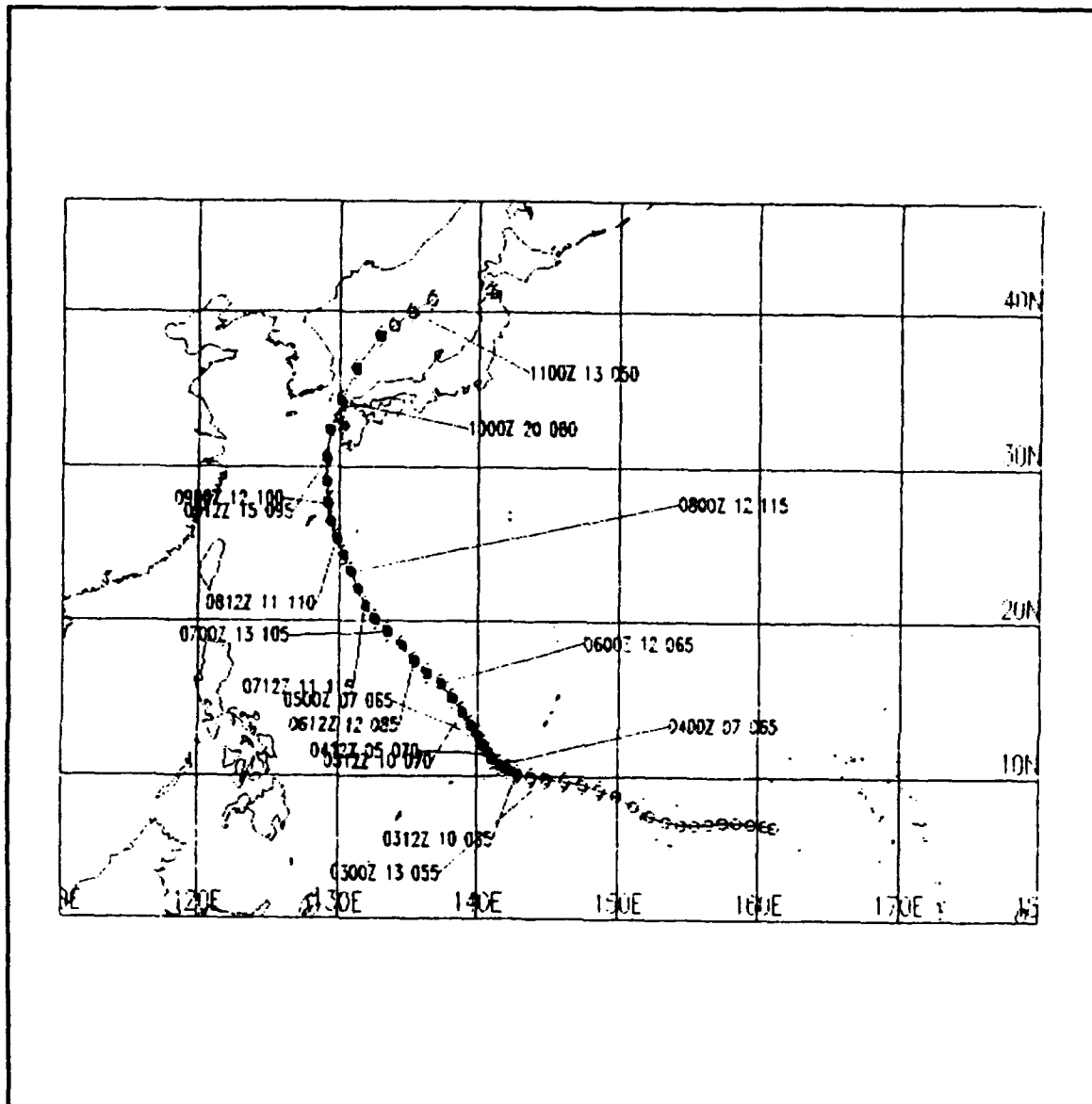


Figure 3. The JTWC best track for typhoon Robyn based on Robyn's positions at six-hour intervals. At selected times and locations, Robyn's propagation speed and maximum sustained wind speeds (in nautical miles/hour) are shown.

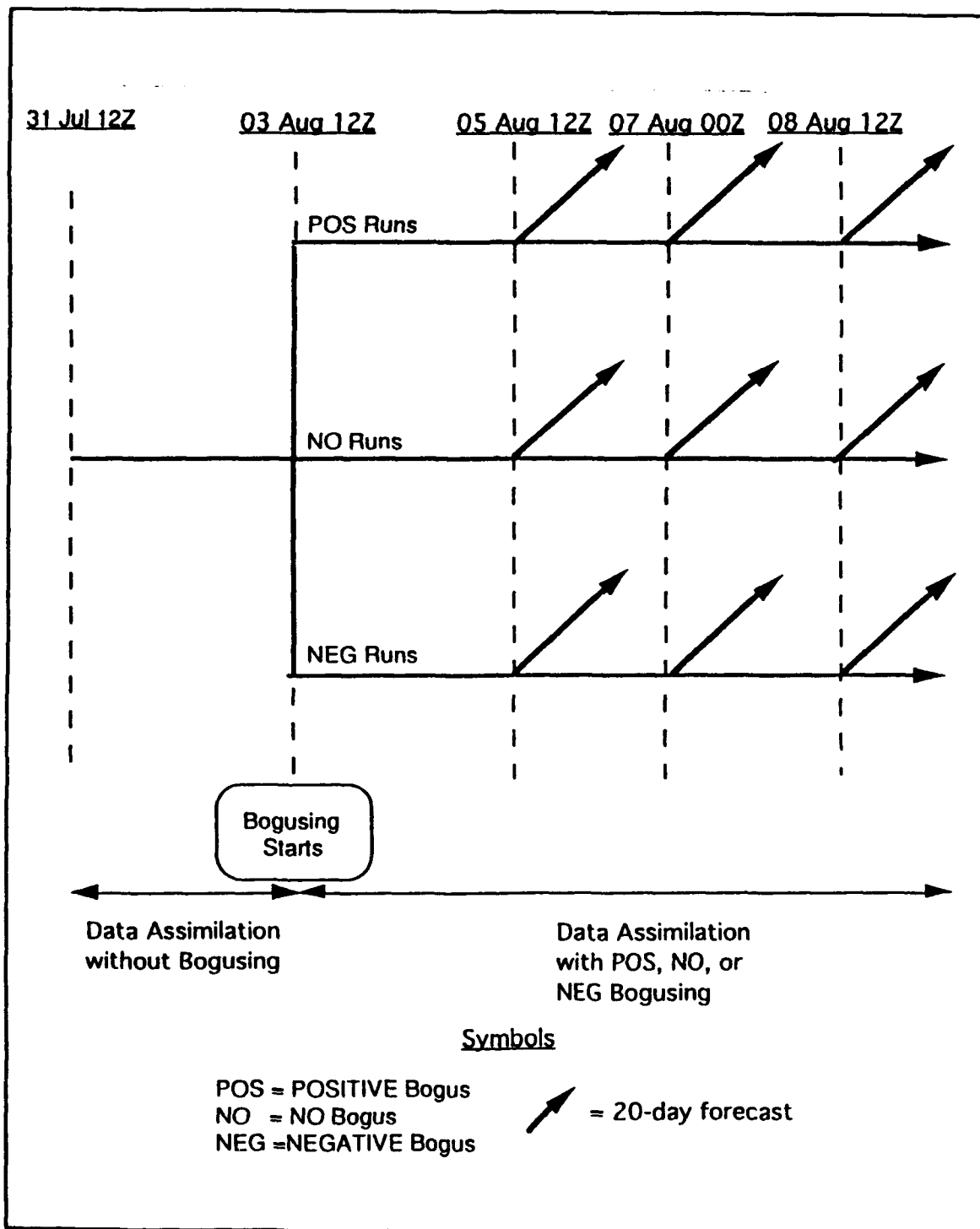


Figure 4. Schematic of the data assimilation and tropical cyclone bogusing procedures for the nine model runs. Bogusing started when Robyn's winds reached 13 m/s. Bogusing continued until the start of each model run.

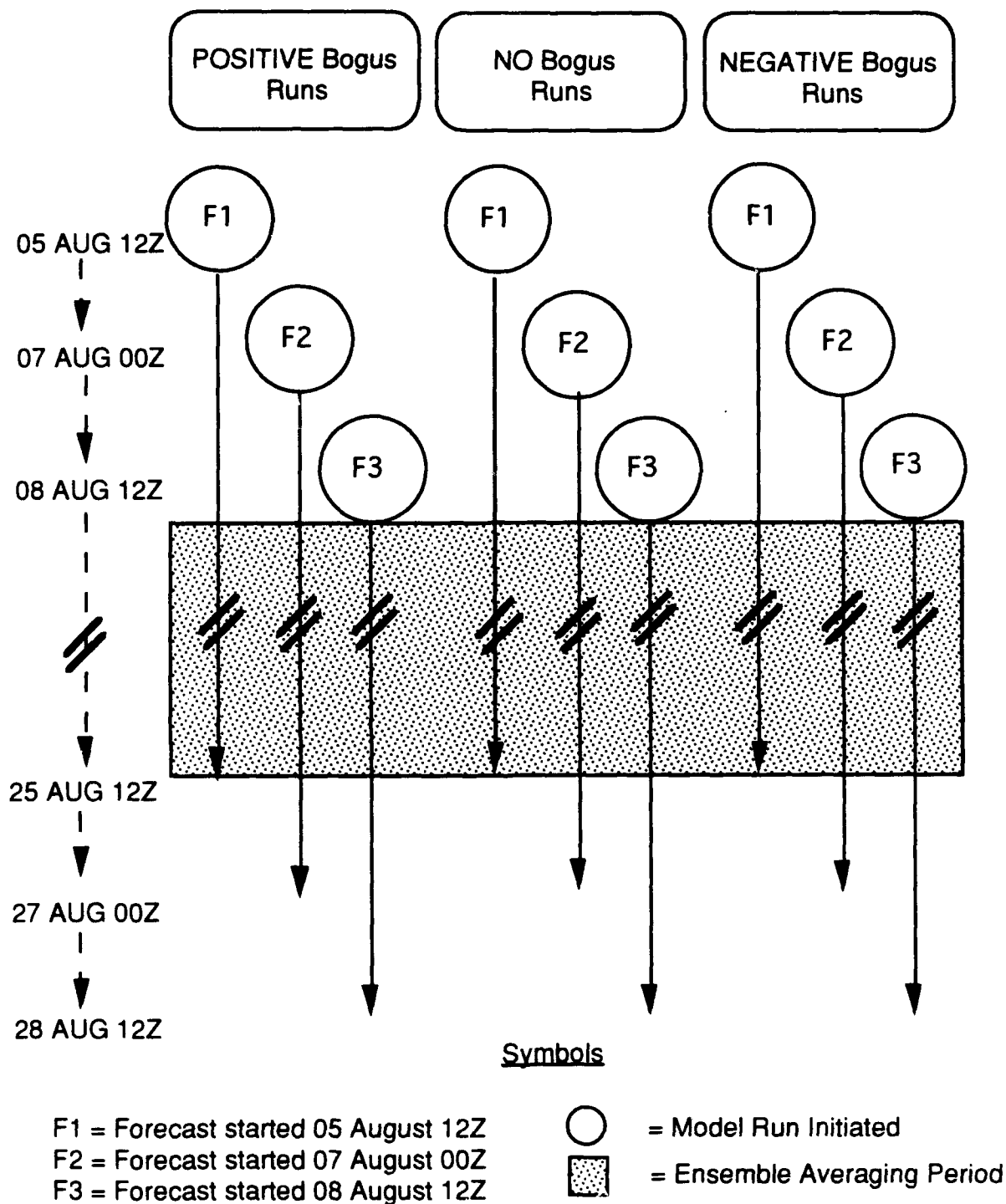


Figure 5. Schematic of nine Robyn model runs conducted, showing standard data assimilation periods, modified data assimilation (i.e., bogusing) periods, 20-day forecast periods, and ensemble averaging periods. Note that lines are not drawn to scale.

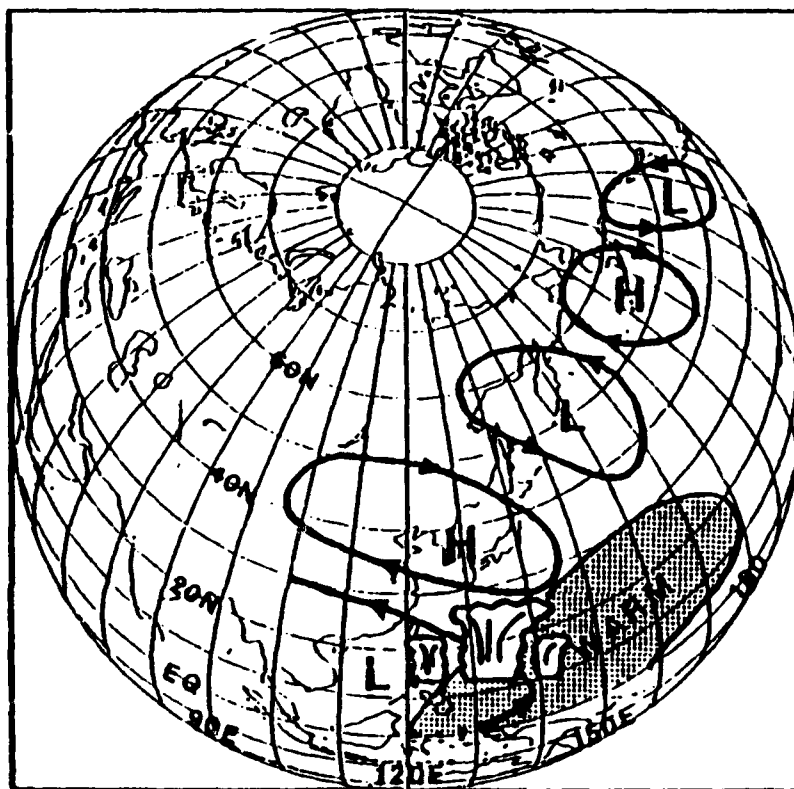


Figure 6. Schematic of 500 mb height anomalies associated with increased convection during northern hemisphere summers with warmer than normal SST in the tropical western Pacific. H denotes positive height anomaly, L denotes negative height anomaly (from Nitta 1987).

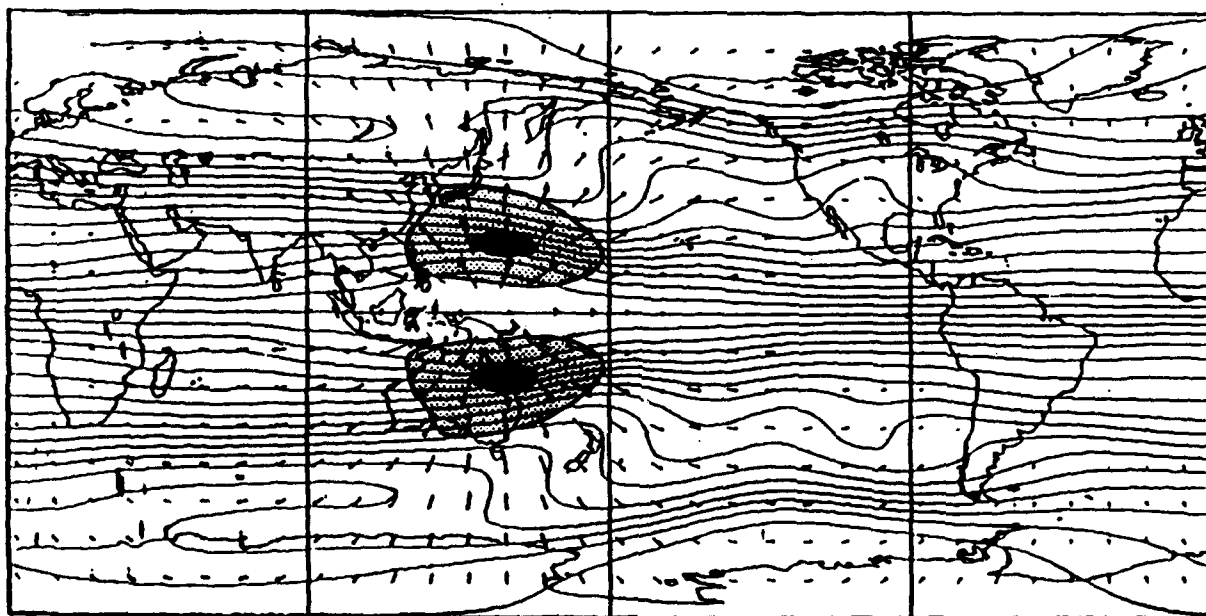


Figure 7. Schematic of modeled upper tropospheric Rossby wave sources due to advection of absolute vorticity by steady divergent winds emanating from the equatorial western Pacific. Wavy contours indicate stream function. Vectors indicate divergent wind (maximum wind is about 5 m/s). Shading along subtropical western Pacific jets indicates negative Rossby wave sources (from Sardeshmukh and Hoskins 1988).

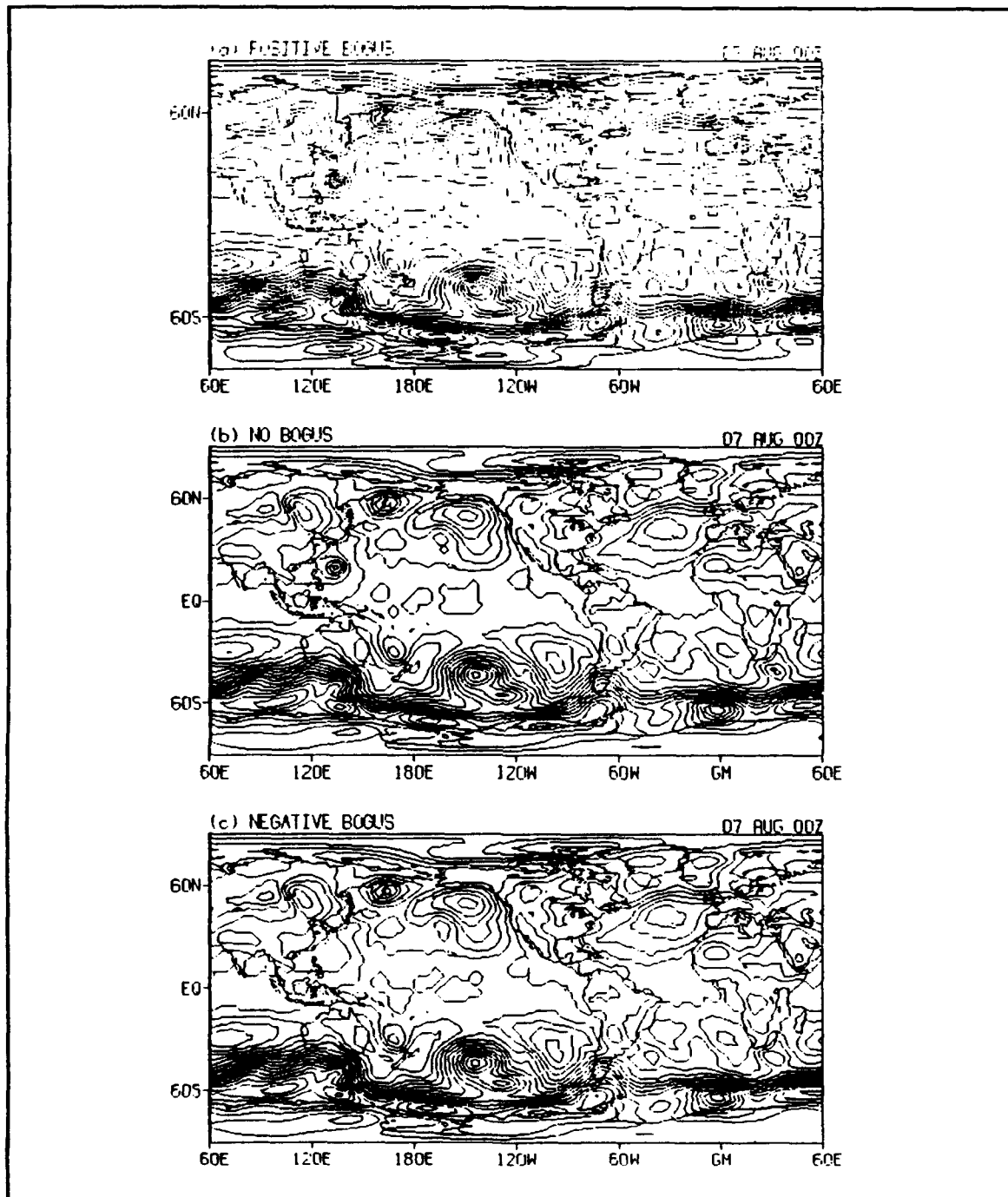


Figure 8. Sea level pressure initial conditions for Forecast 2: (a) POSITIVE, (b) NO, (c) NEGATIVE runs. Contour interval is 4 mb.

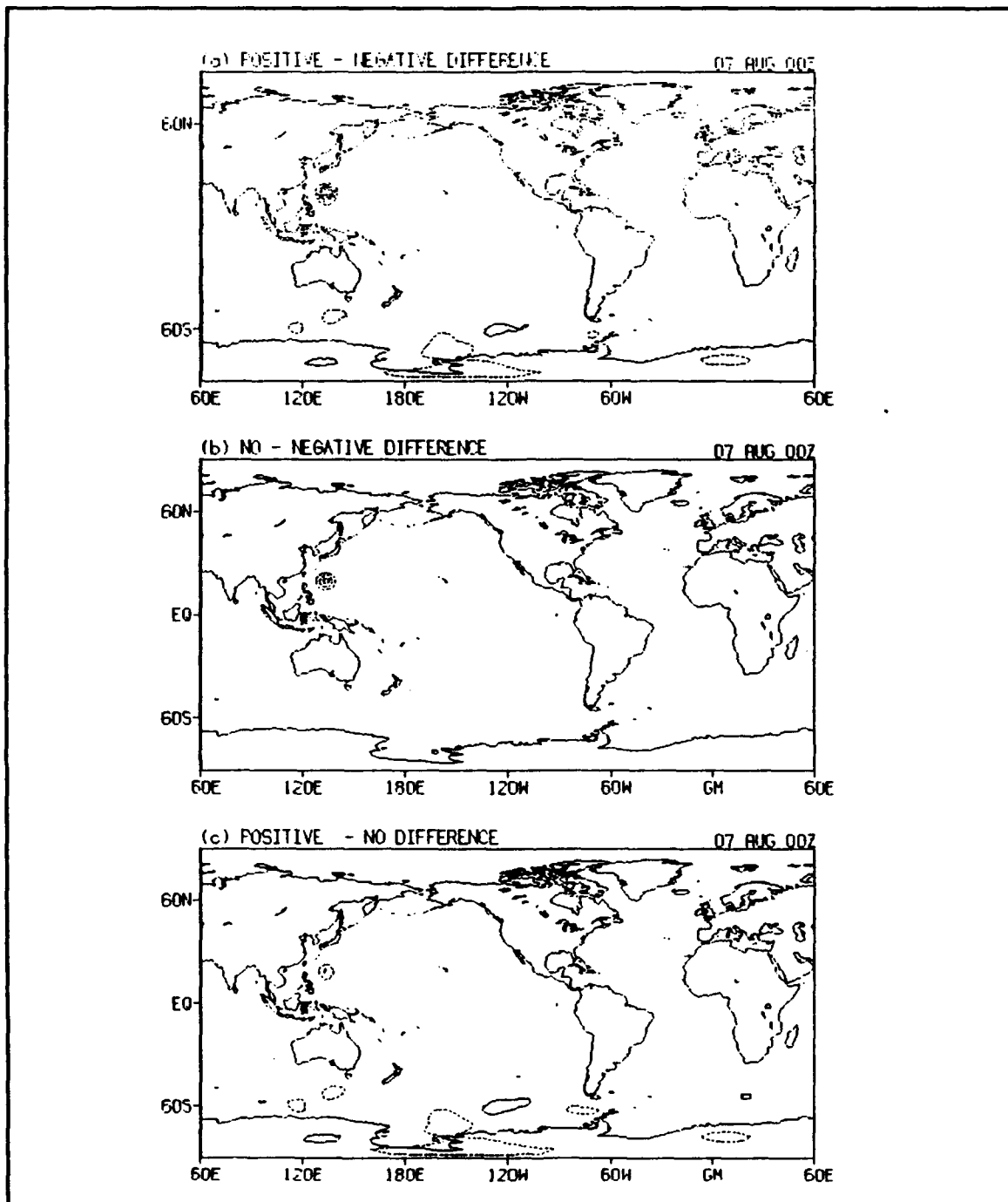


Figure 9. Differences in sea level pressure initial conditions for Forecast 2: (a) POSITIVE - NEGATIVE, (b) NO - NEGATIVE, (c) POSITIVE - NO differences. Contour interval is 4 mb. Zero contour omitted.

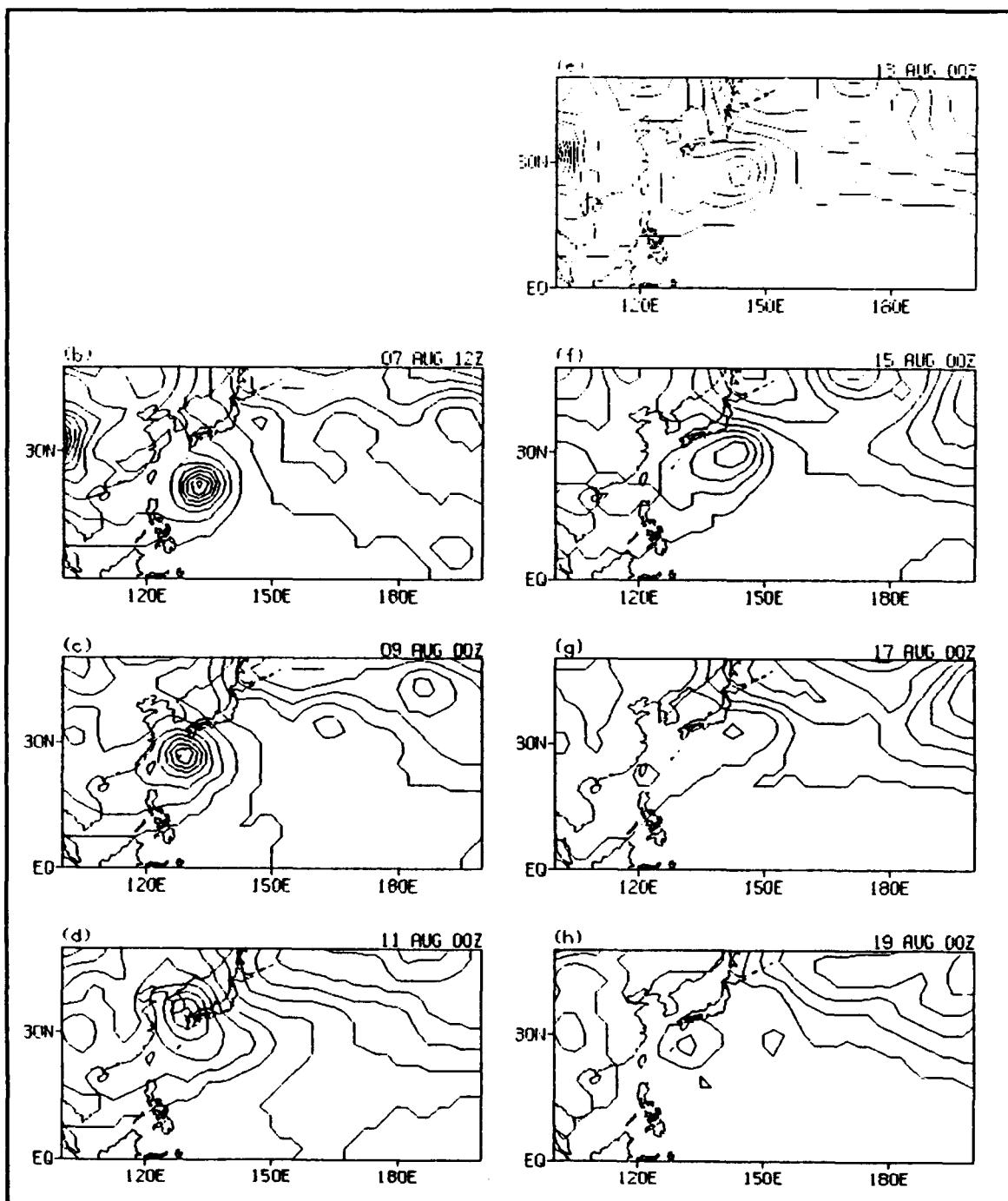


Figure 10. Sea level pressures in the western Pacific at selected times for Forecast 2 POSITIVE run. Contour interval is 4 mb. Panel (a) omitted to retain consistency between this and other figures.

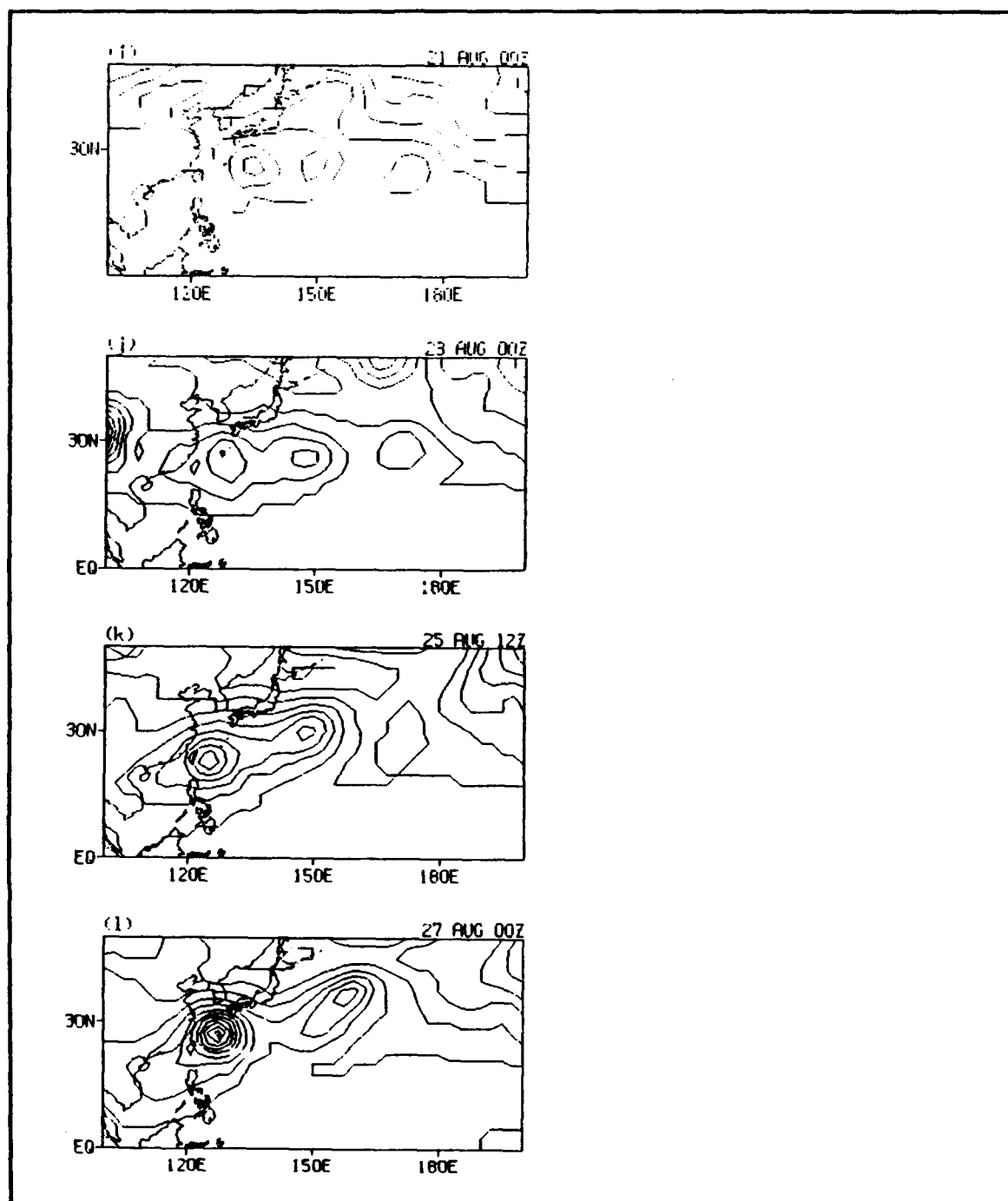


Figure 10. (continued)

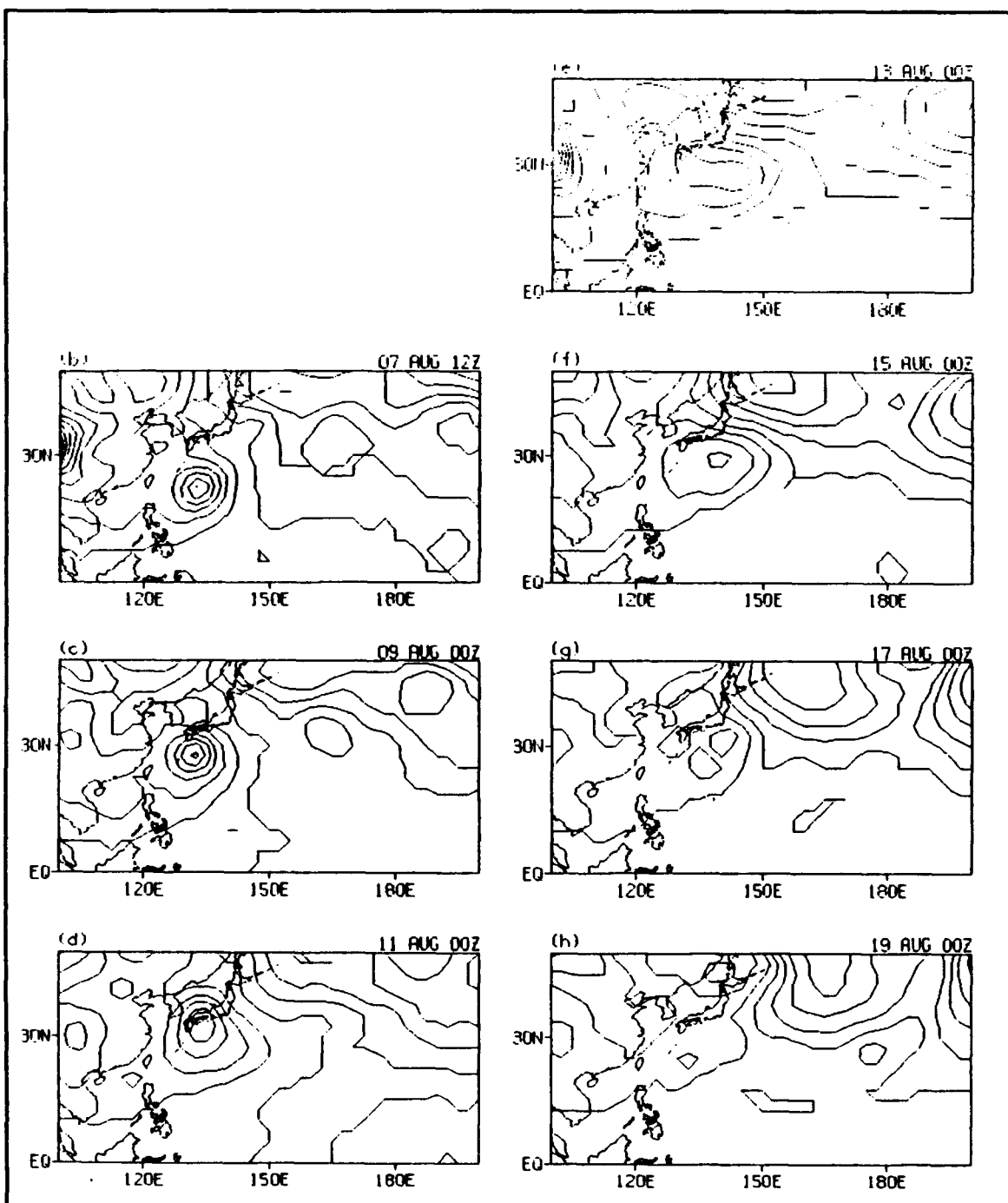


Figure 11. Sea level pressures in the western Pacific at selected times for Forecast 2 NO run. Contour interval is 4 mb. Panel (a) omitted to retain consistency between this and other figures.

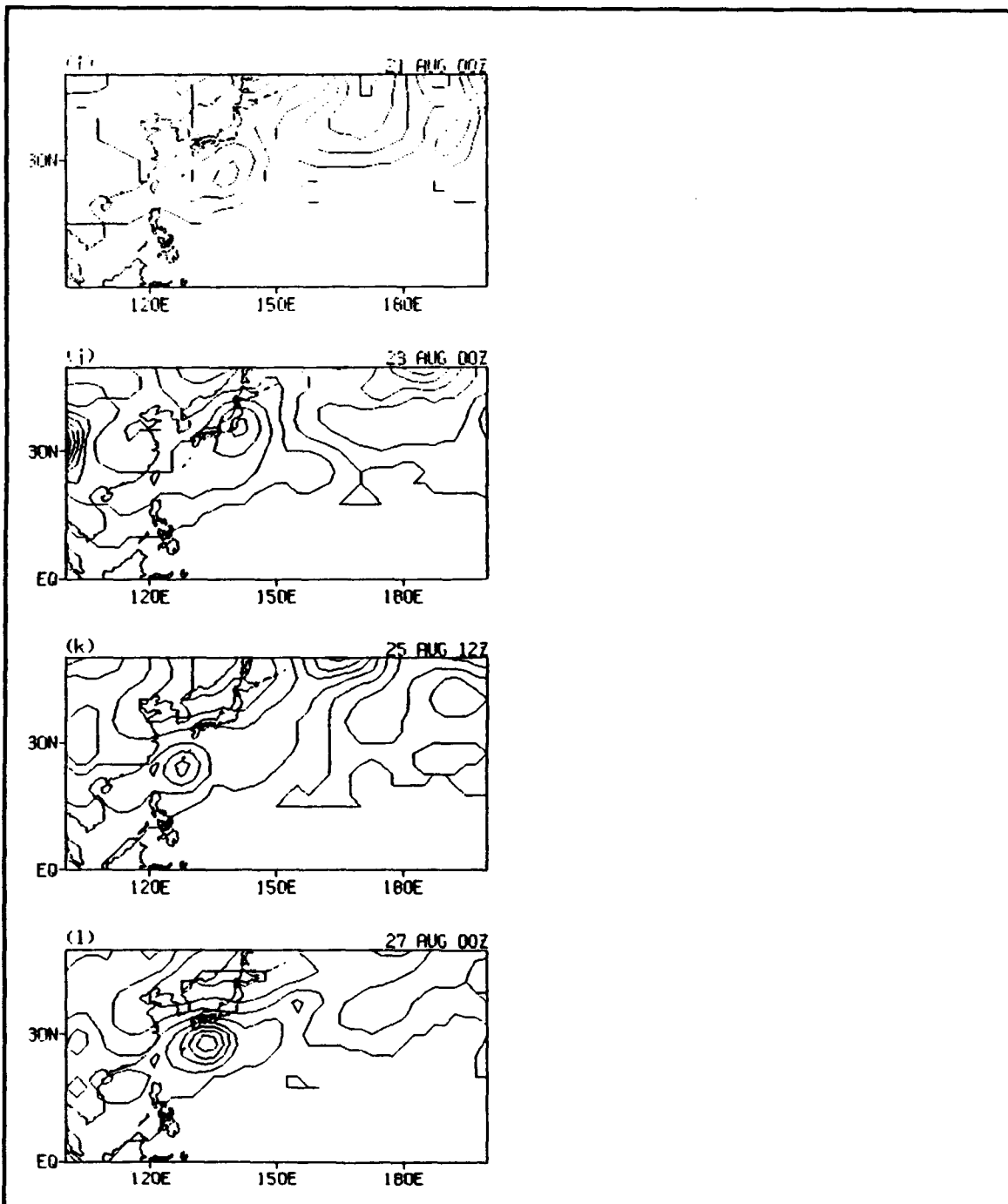


Figure 11. (Continued).

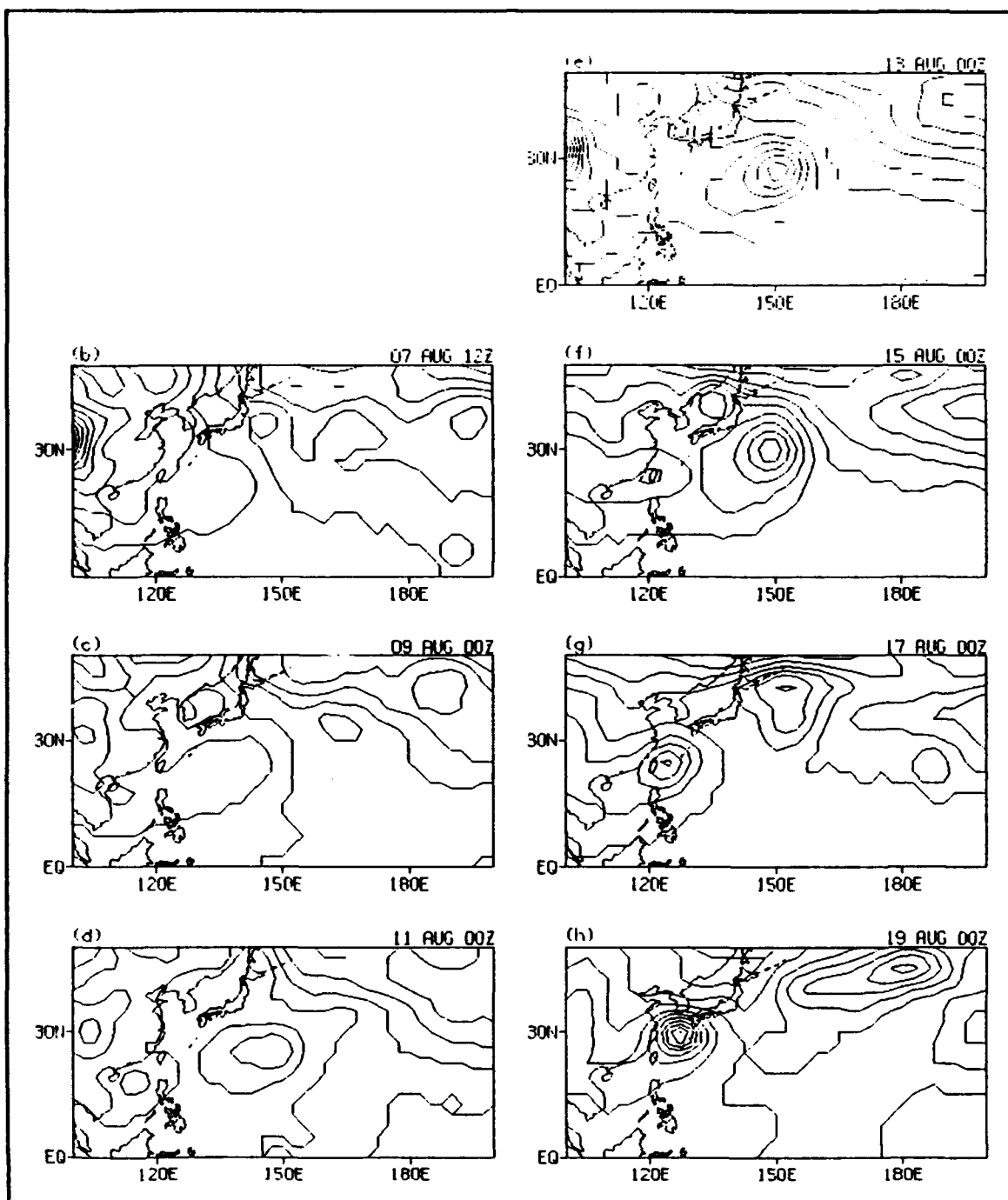


Figure 12. Sea level pressures in the western Pacific at selected times for Forecast 2 NEGATIVE run. Contour interval is 4 mb. Panel (a) omitted to retain consistency between this and other figures.

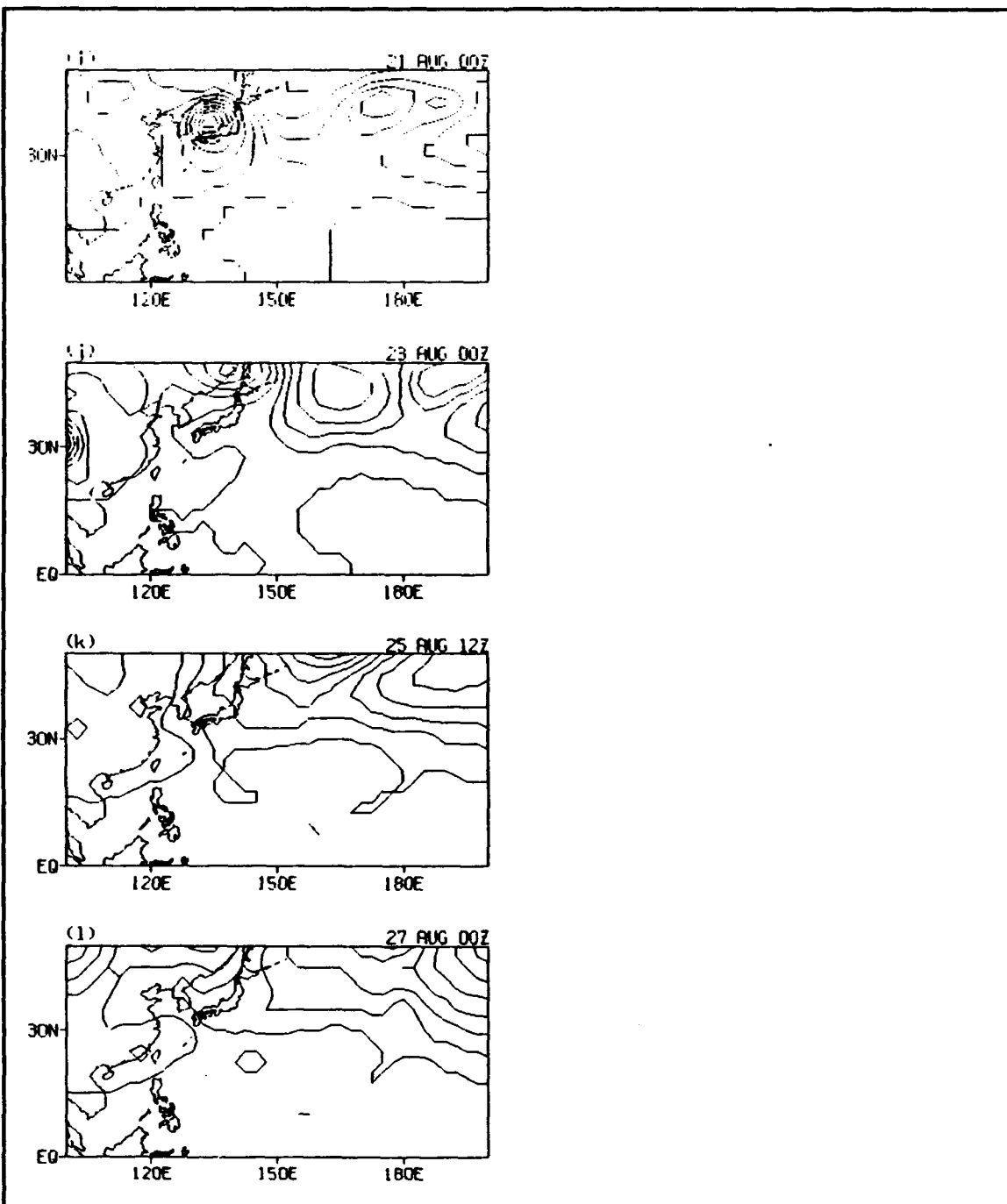


Figure 12. (Continued).

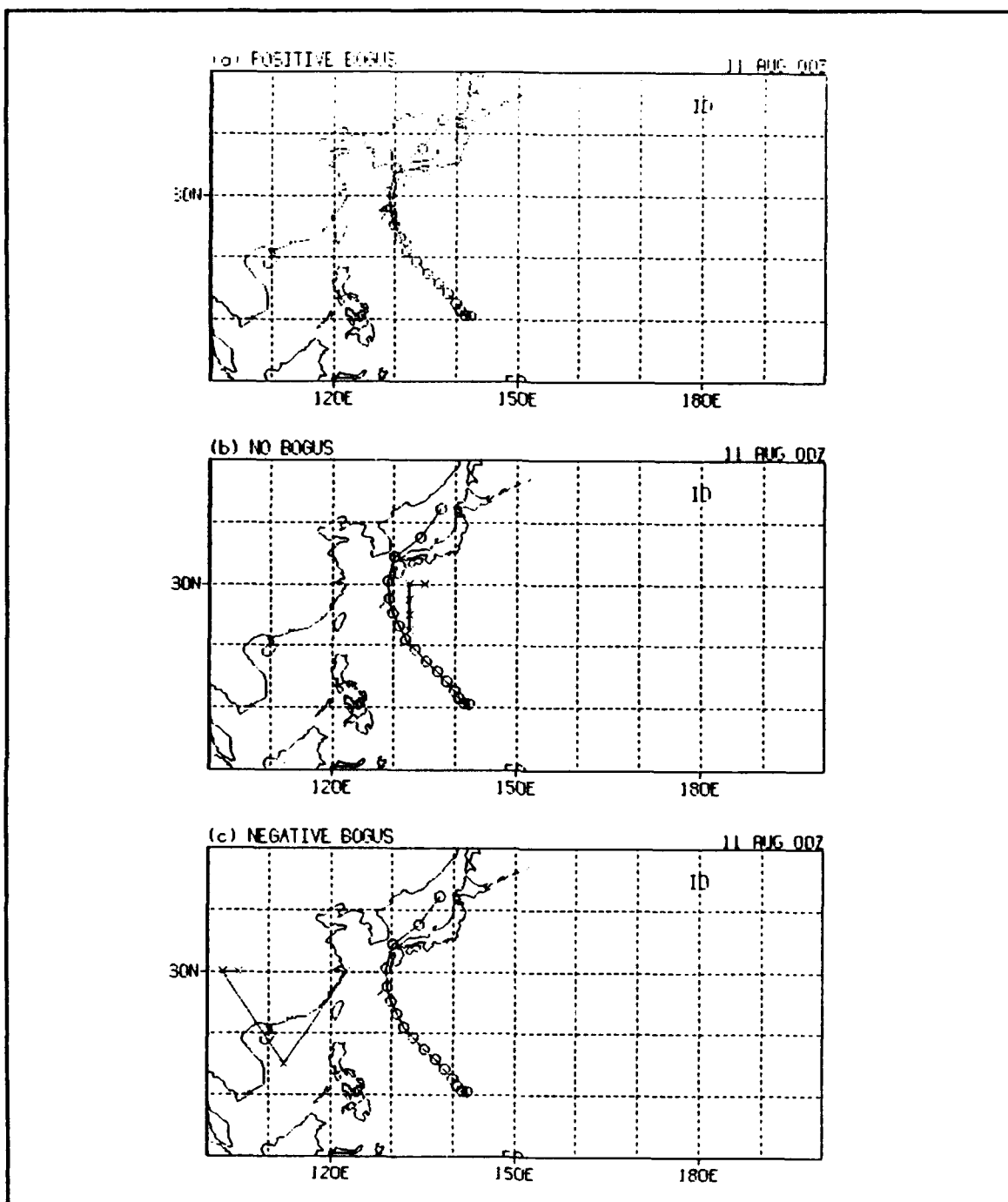


Figure 13. Typhoon Robyn tracks (crosses) from Forecast 2: (a) POSITIVE, (b) NO, (c) NEGATIVE runs. Circles denote JTWC best track for Robyn.

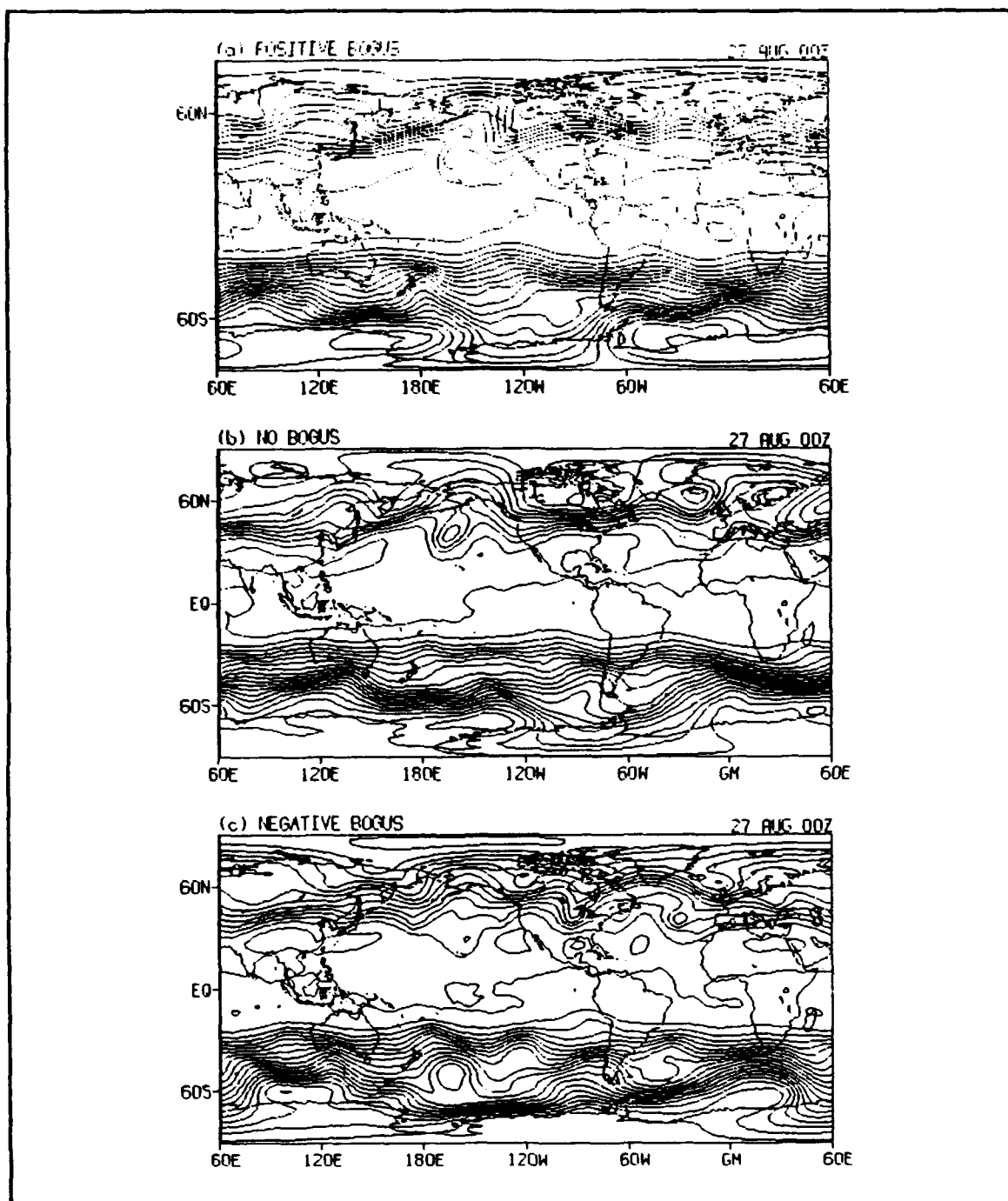


Figure 14. 20-day average 200 mb geopotential heights for Forecast 2: (a) POSITIVE, (b) NO, (c) NEGATIVE runs. Minimum contour is 10500 gpm. Contour interval is 100 gpm.

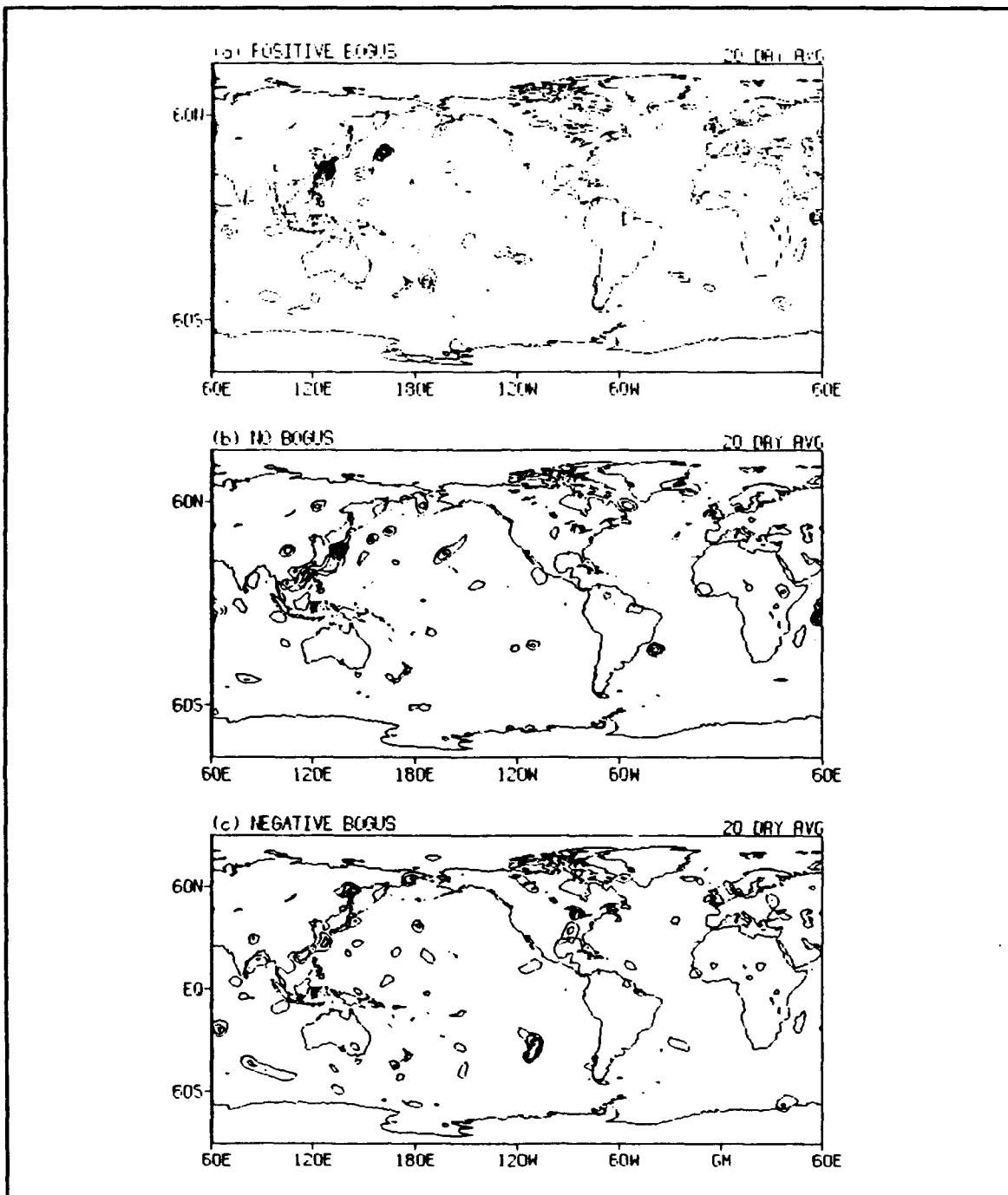


Figure 15. 20-day average atmospheric heating for Forecast 2: (a) POSITIVE, (b) NO, (c) NEGATIVE runs. Minimum contour is 2°C/day. Contour interval is 2°C/day.

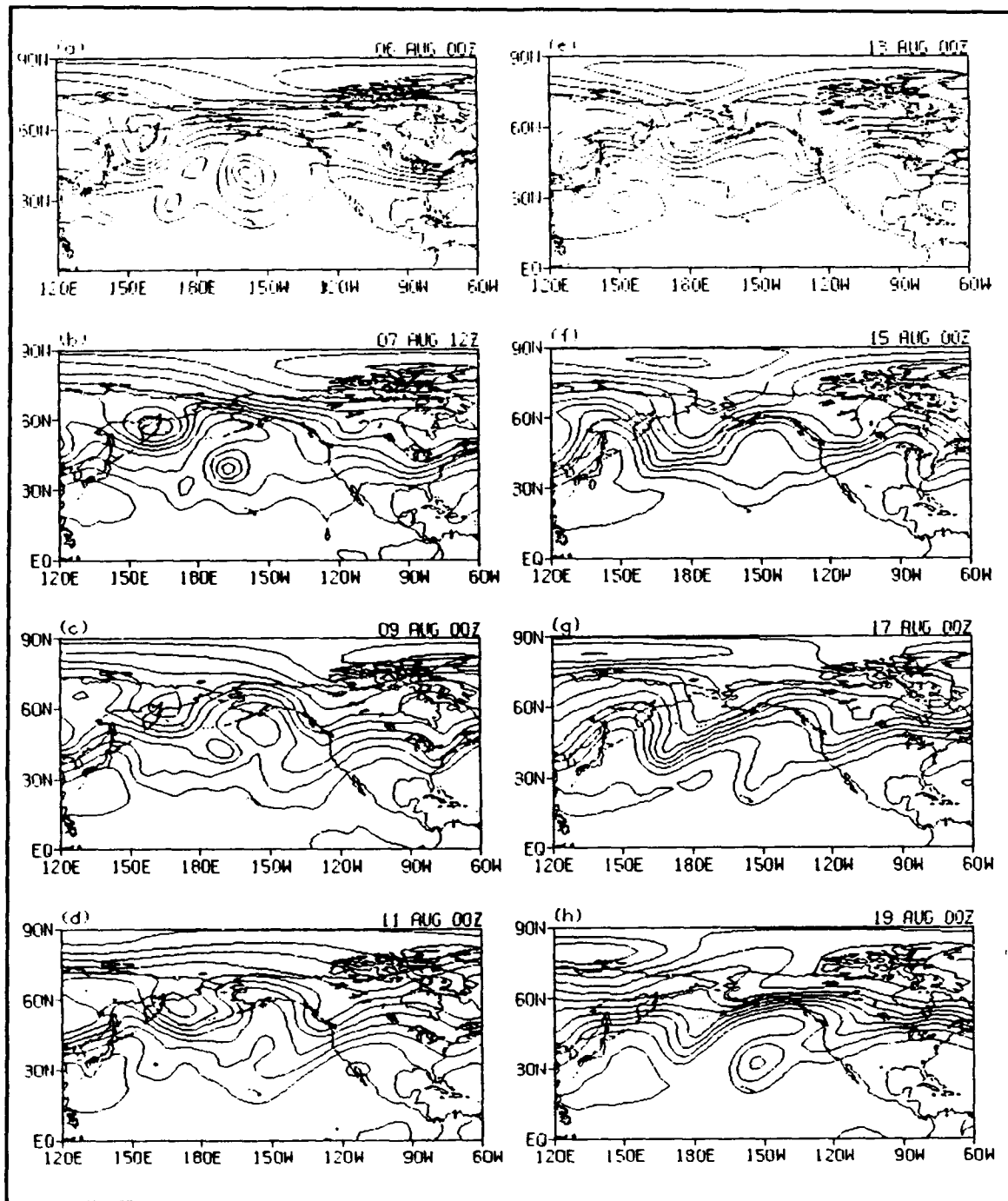


Figure 16. 200 mb geopotential heights at selected times for Forecast 1 POSITIVE run. Minimum contour is 10500 gpm. Contour interval is 100 gpm.

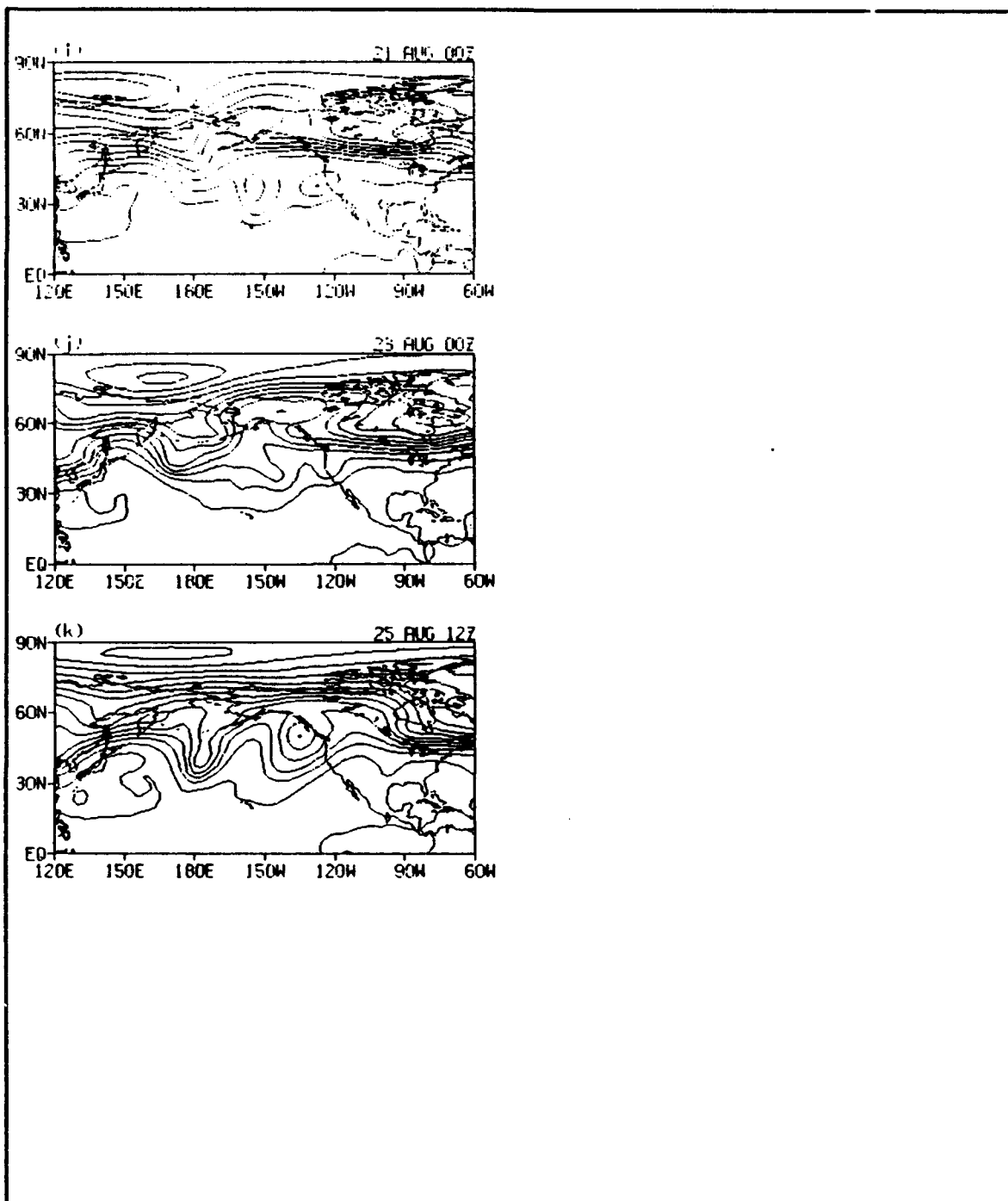


Figure 16. (Continued).

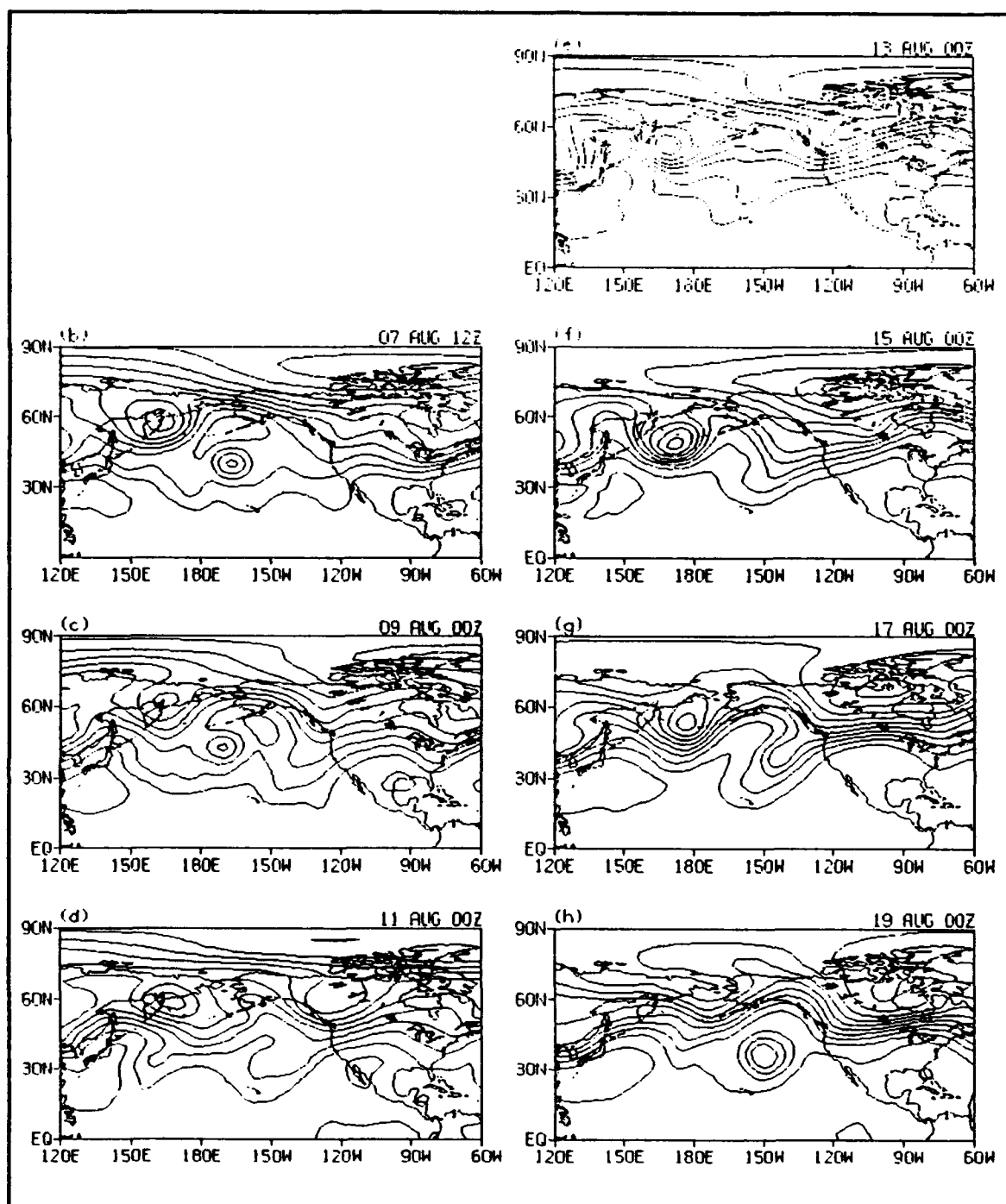


Figure 17. 200 mb geopotential heights at selected times for Forecast 2 POSITIVE run. Minimum contour is 10500 gpm. Contour interval is 100 gpm. Panel (a) omitted to retain consistency between this and other figures.

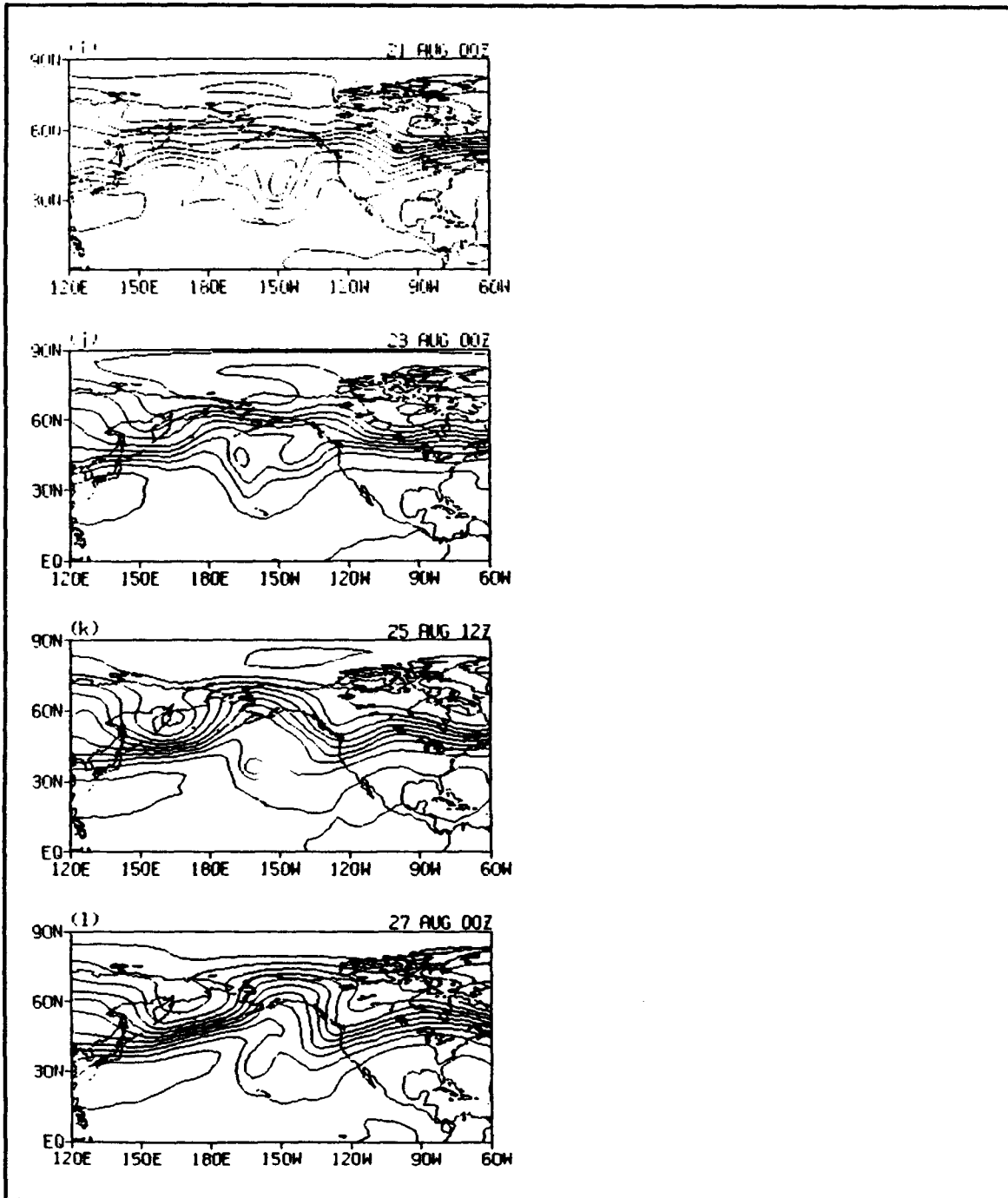


Figure 17. (Continued).

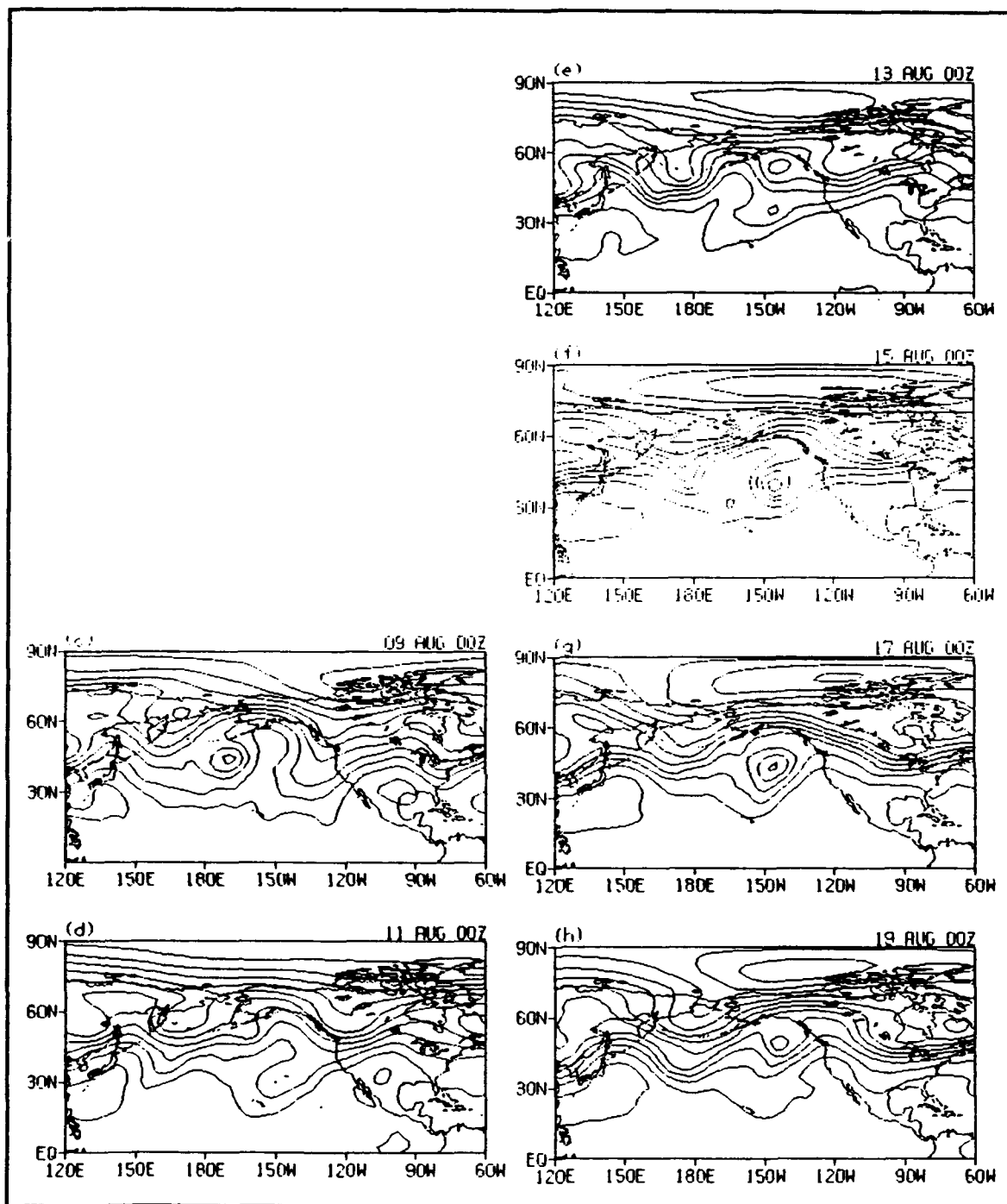


Figure 18. 200 mb geopotential heights at selected times for Forecast 3 POSITIVE run. Minimum contour is 10500 gpm. Contour interval is 100 gpm. Panels (a) and (b) omitted to retain consistency between this and other figures.

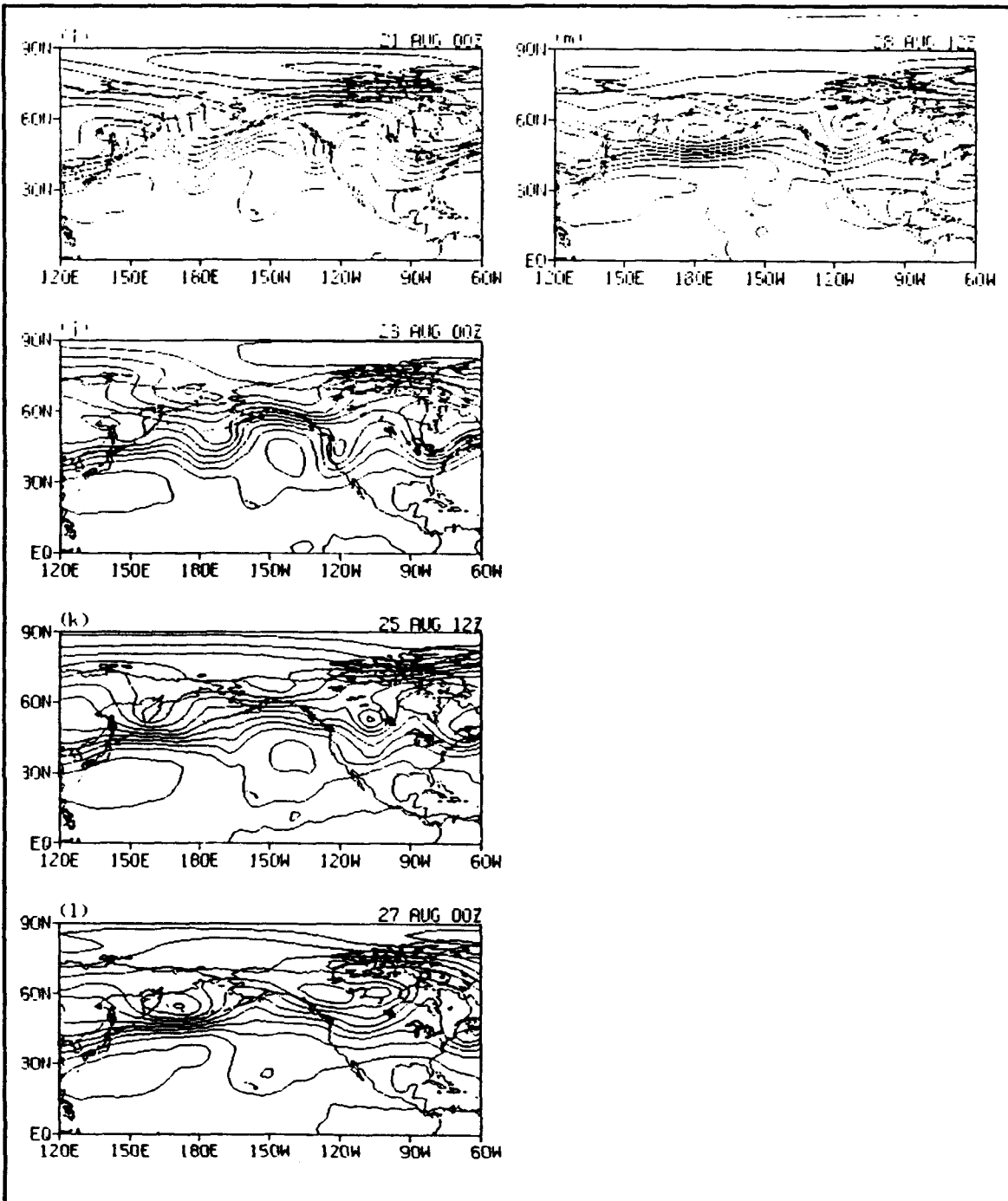


Figure 18. (Continued).

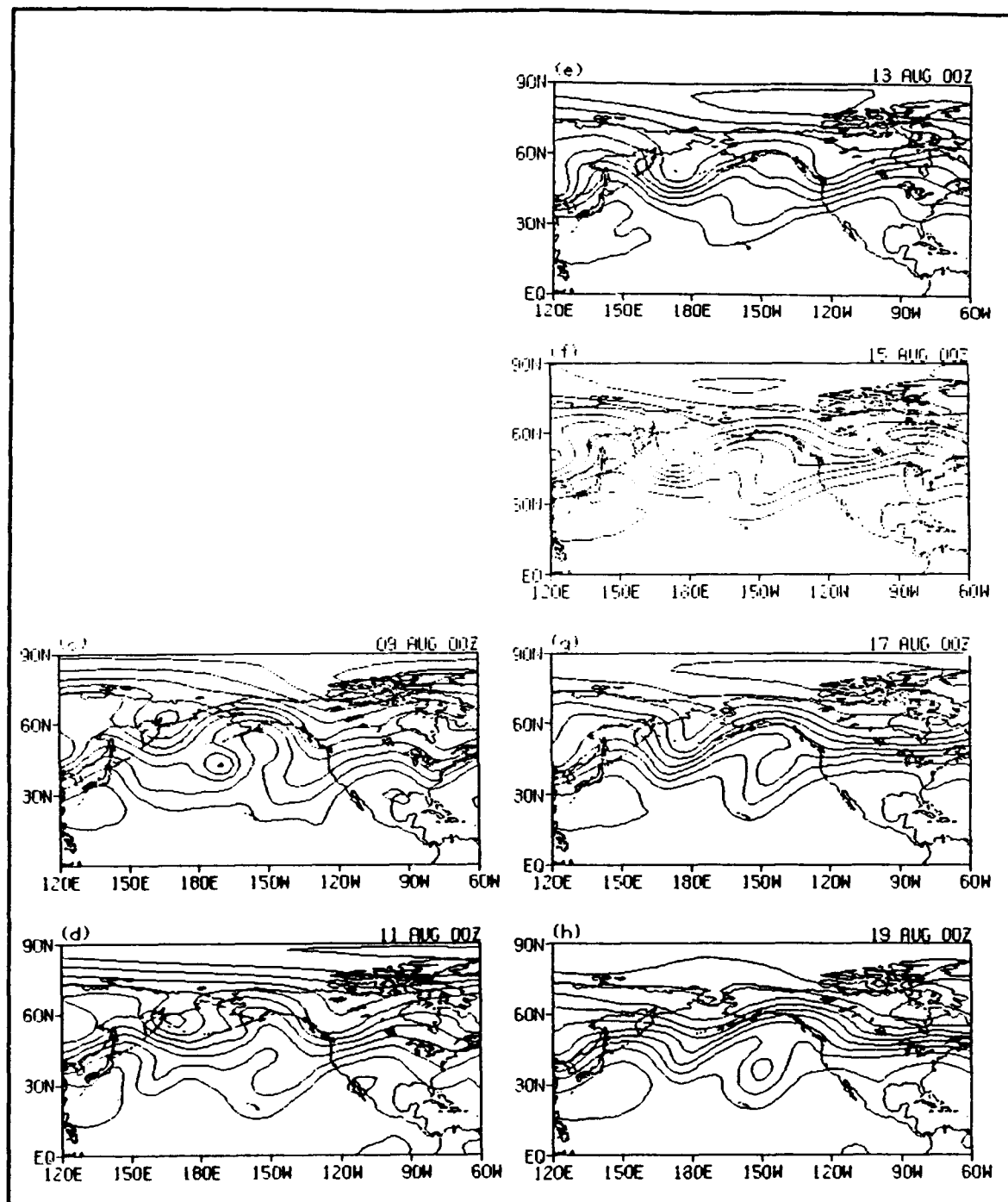


Figure 19. 200 mb geopotential heights at selected times for Ensemble Average POSITIVE run. Minimum contour is 10500 gpm. Contour interval is 100 gpm. Panels (a) and (b) omitted to retain consistency between this and other figures.

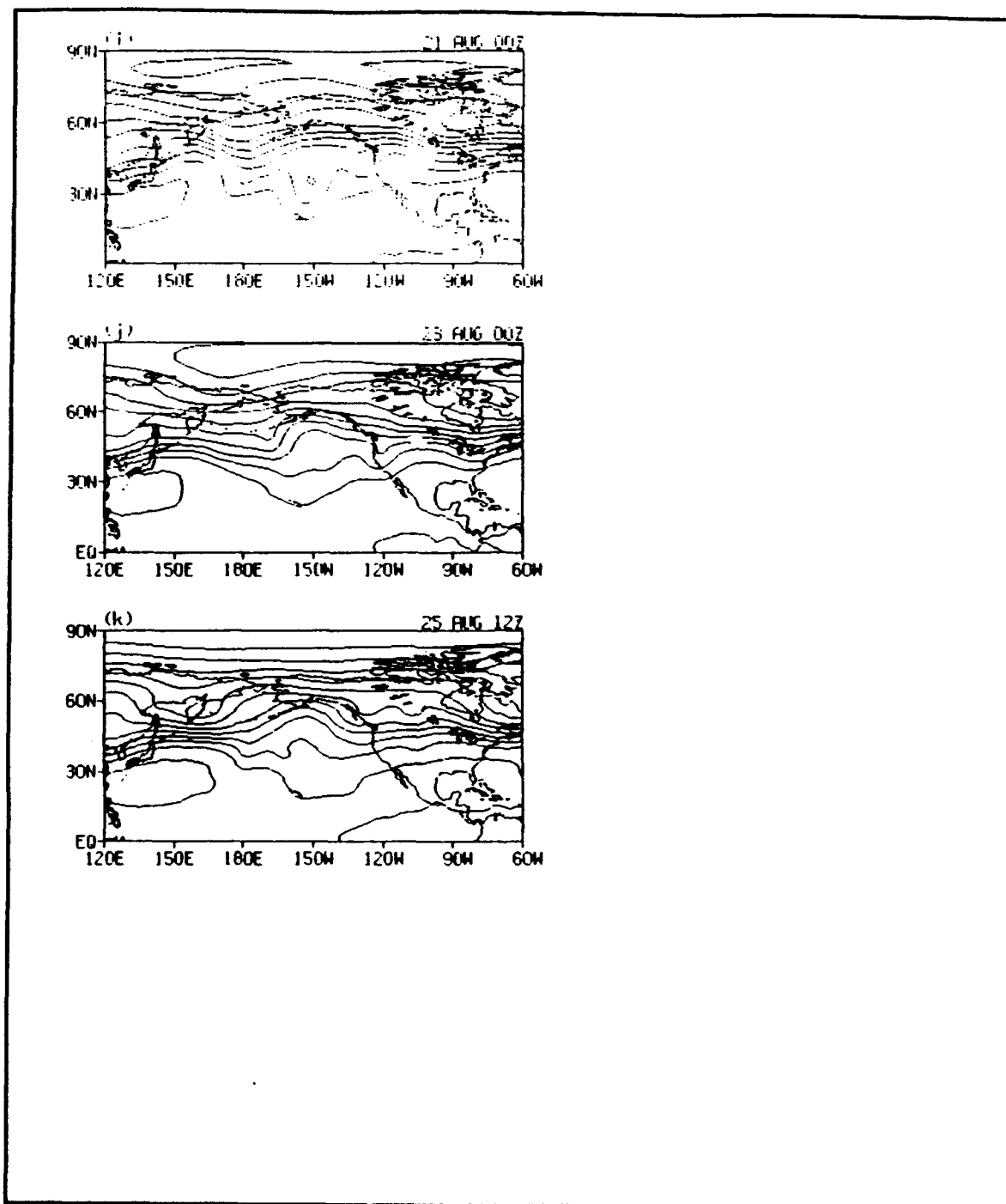


Figure 19. (Continued).

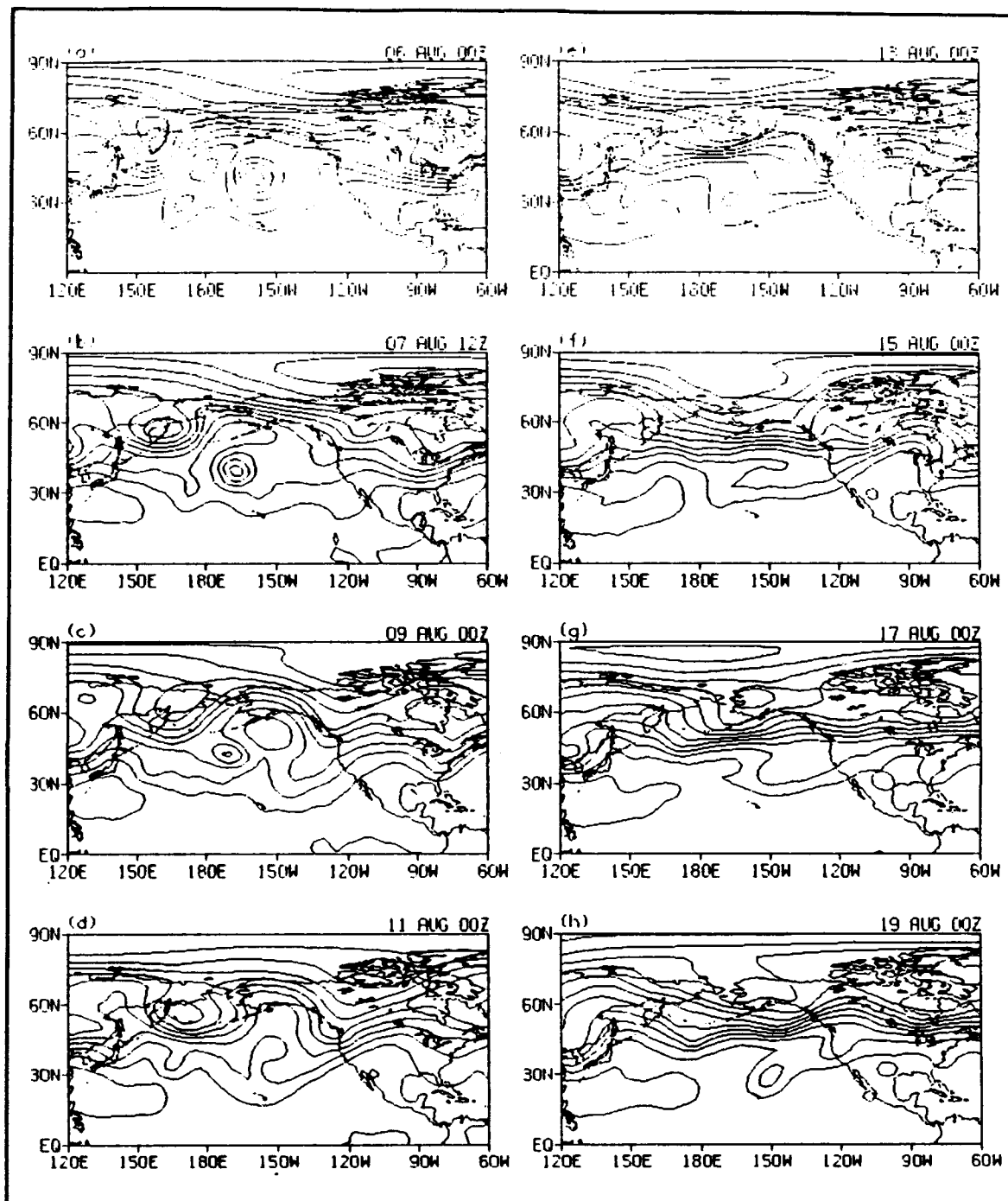


Figure 20. 200 mb geopotential heights at selected times for Forecast 1 NEGATIVE run. Minimum contour is 10500 gpm. Contour interval is 100 gpm.

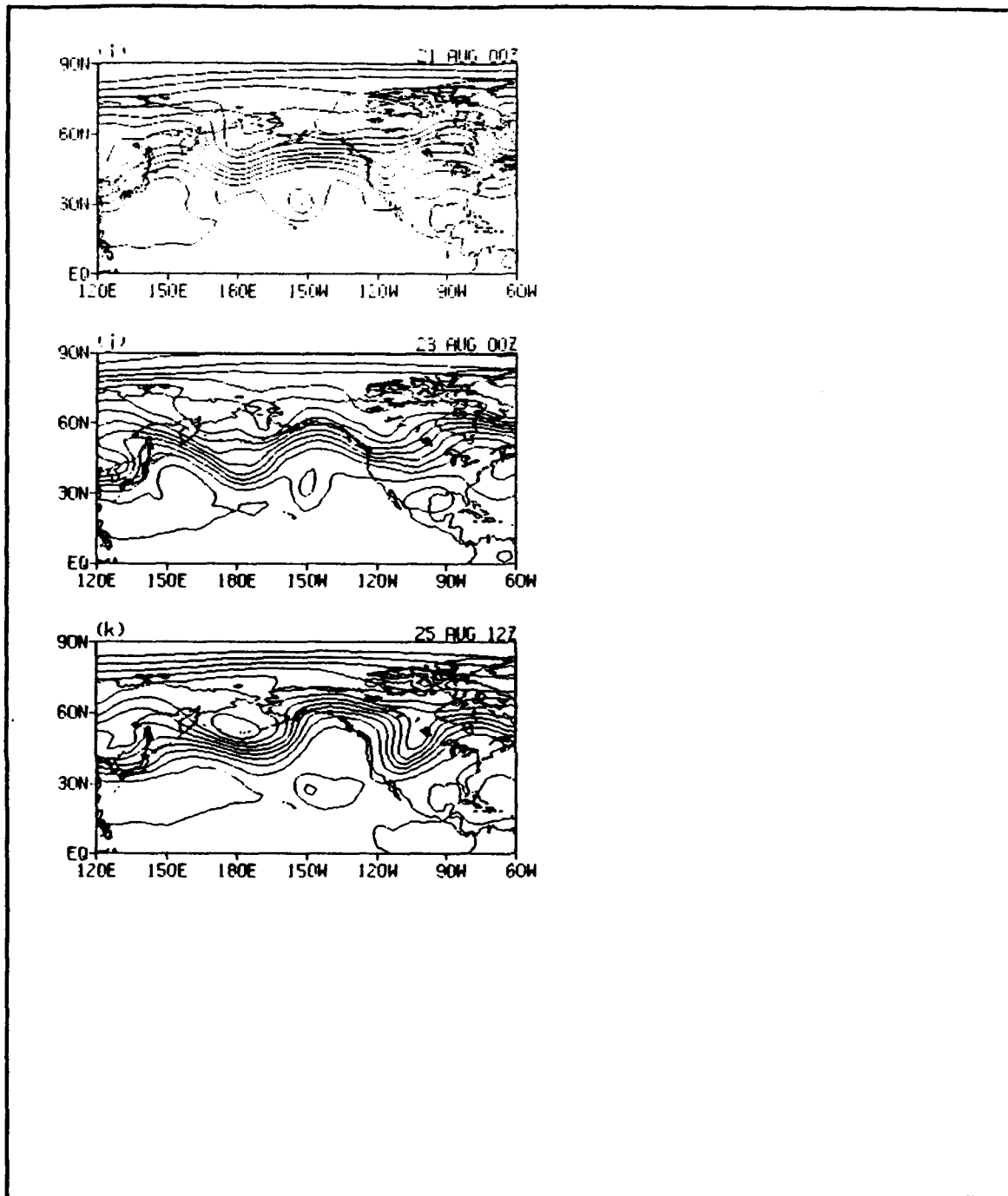


Figure 20. (Continued).

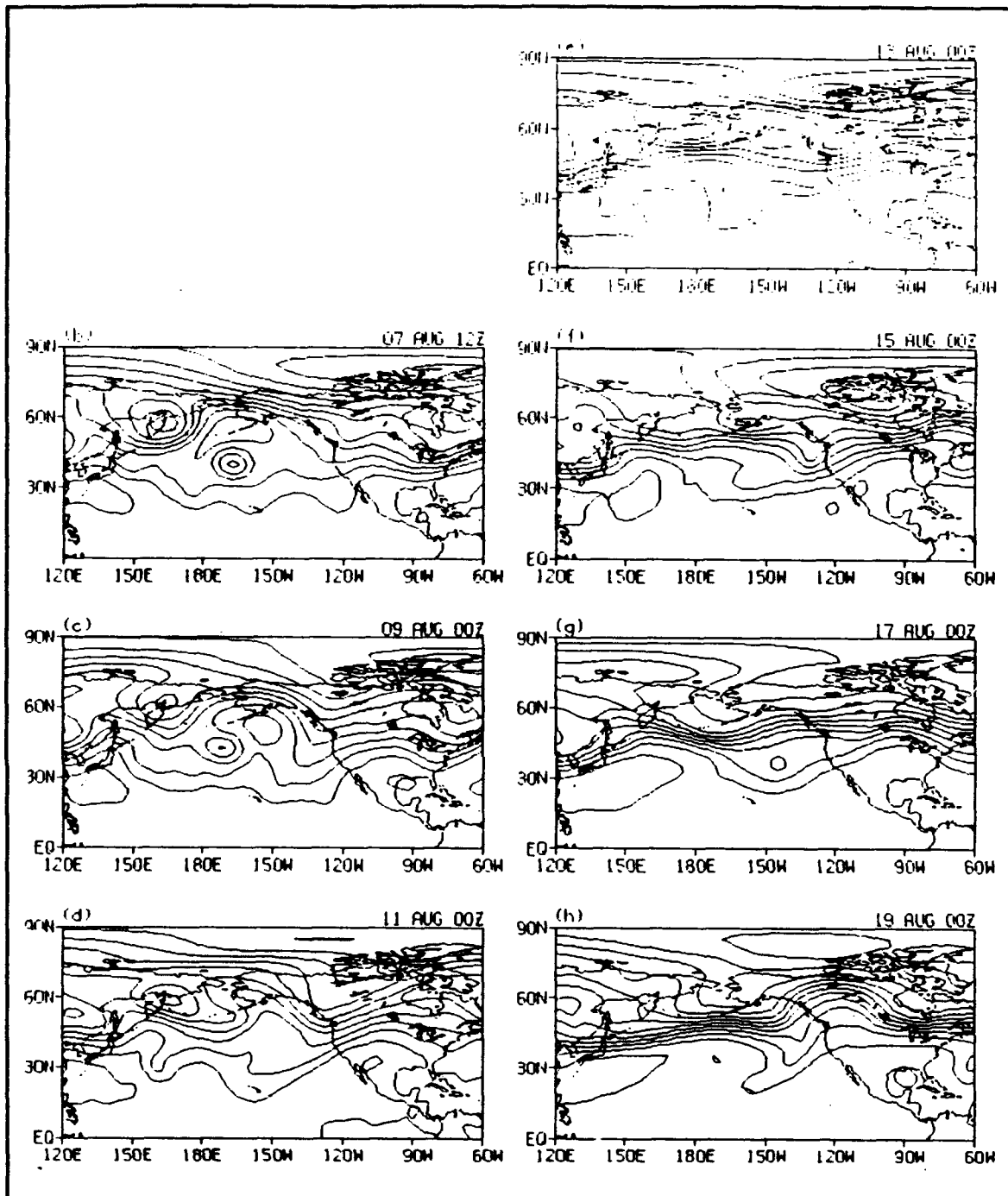


Figure 21. 200 mb geopotential heights at selected times for Forecast 2 NEGATIVE run. Minimum contour is 10500 gpm. Contour interval is 100 gpm. Panel (a) omitted to retain consistency between this and other figures.

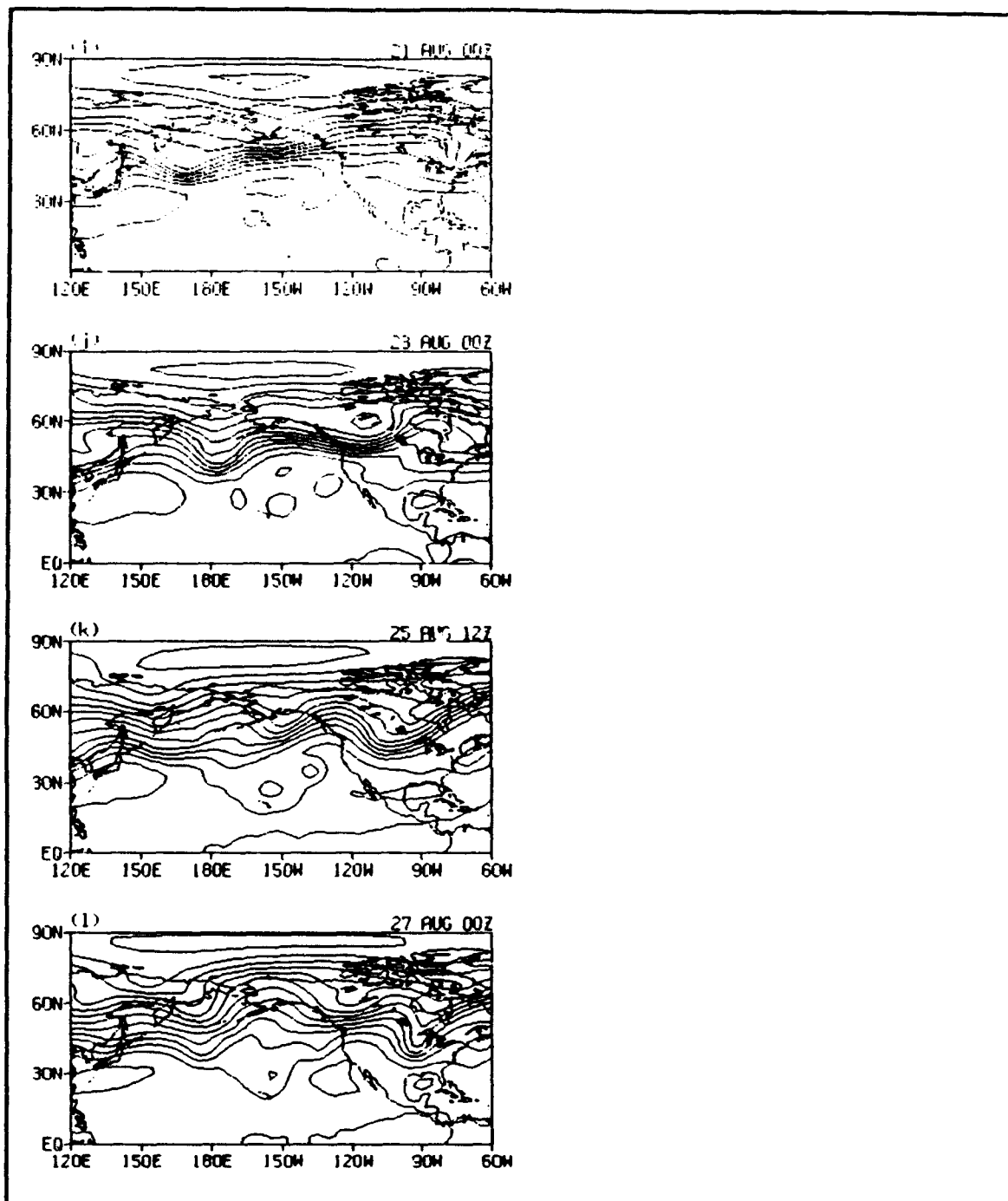


Figure 21. (Continued).

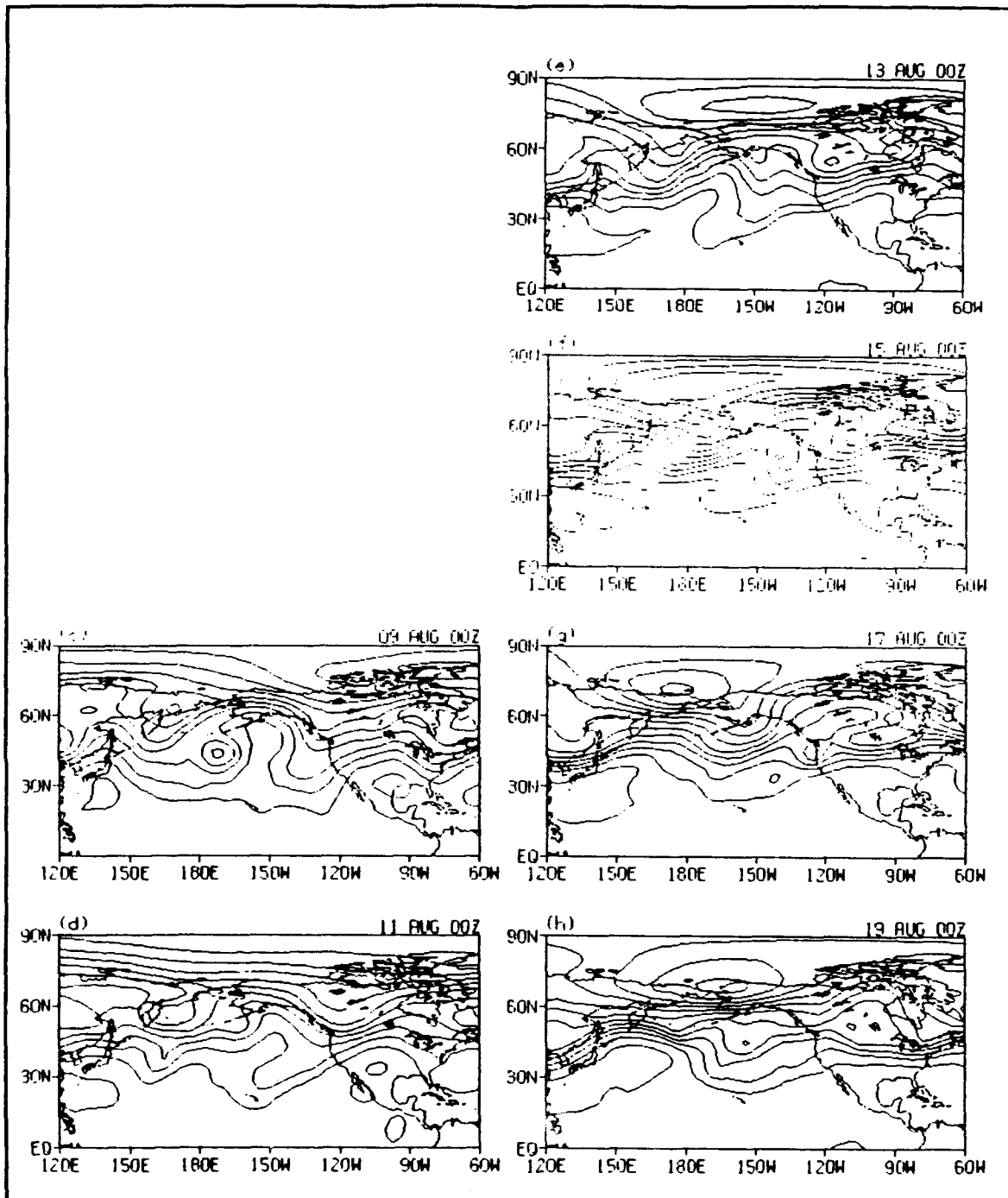


Figure 22. 200 mb geopotential heights at selected times for Forecast 3 NEGATIVE run. Minimum contour is 10500 gpm. Contour interval is 100 gpm. Panels (a) and (b) omitted to retain consistency between this and other figures.

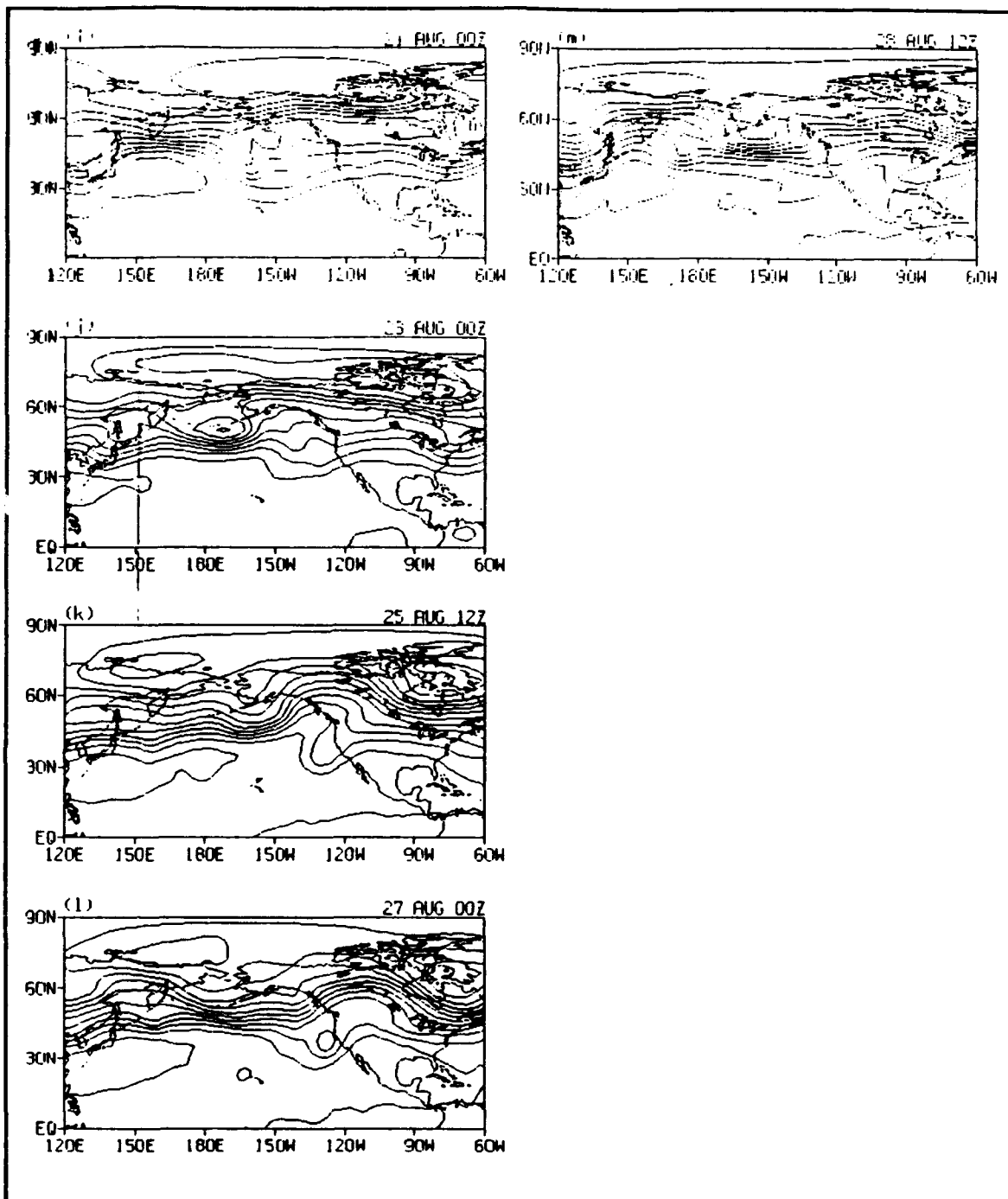


Figure 22. (Continued).

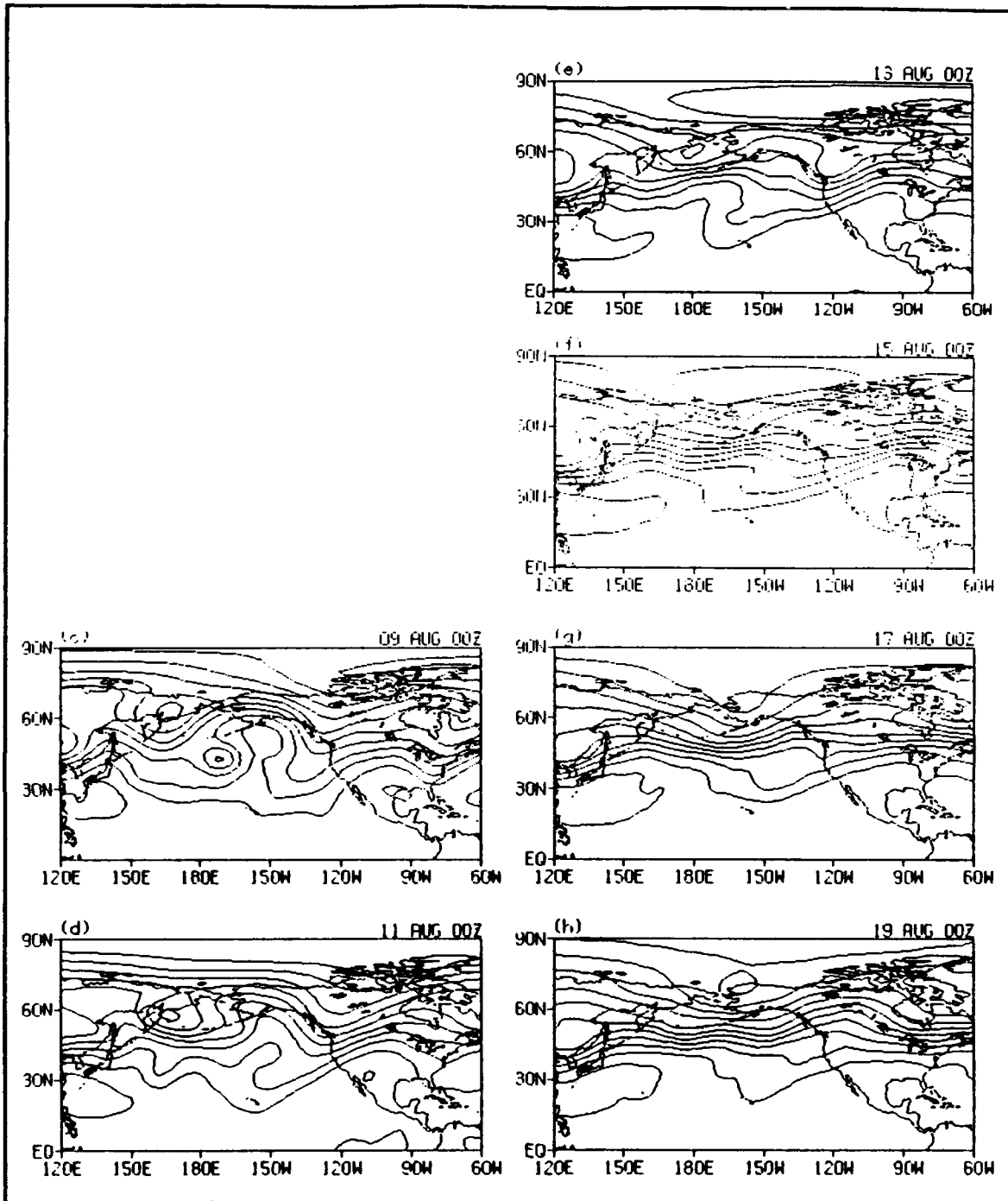


Figure 23. 200 mb geopotential heights at selected times for Ensemble Average NEGATIVE run. Minimum contour is 10500 gpm. Contour interval is 100 gpm. Panels (a) and (b) omitted to retain consistency between this and other figures.

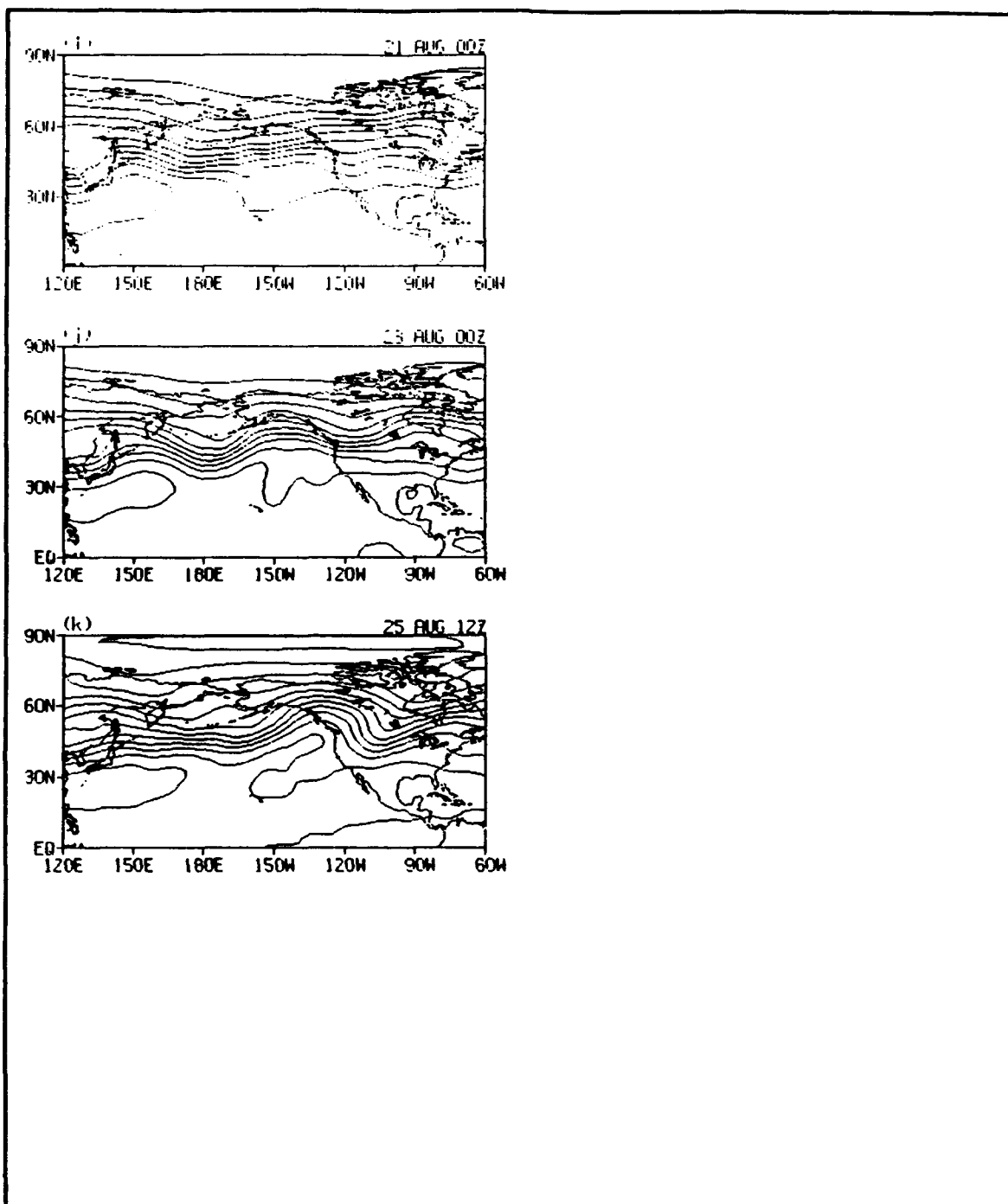


Figure 23. (Continued).

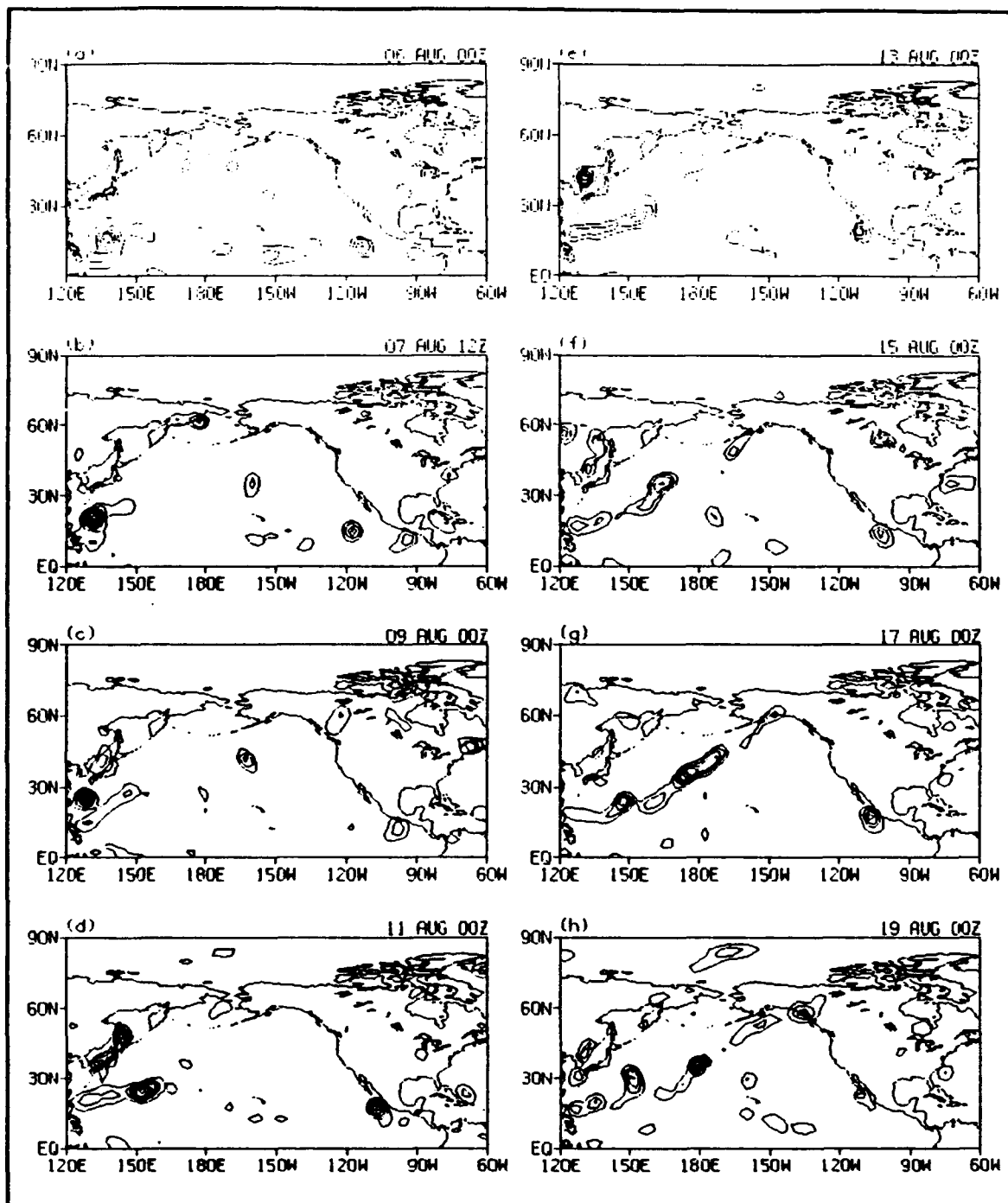


Figure 24. Atmospheric heating at selected times for Forecast 1 POSITIVE run. Minimum contour is 2°C/day. Contour interval is 2°C/day.

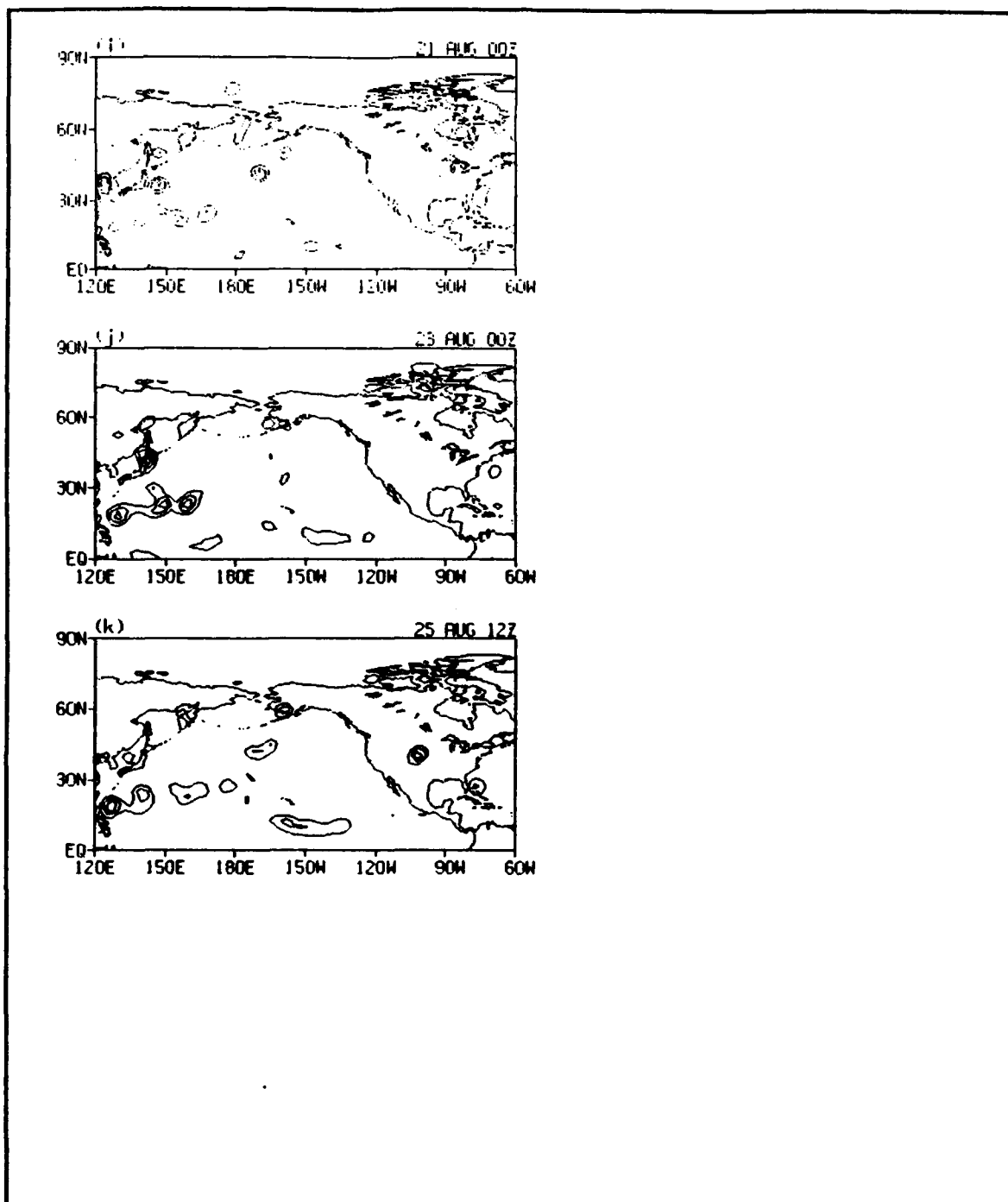


Figure 24. (Continued).

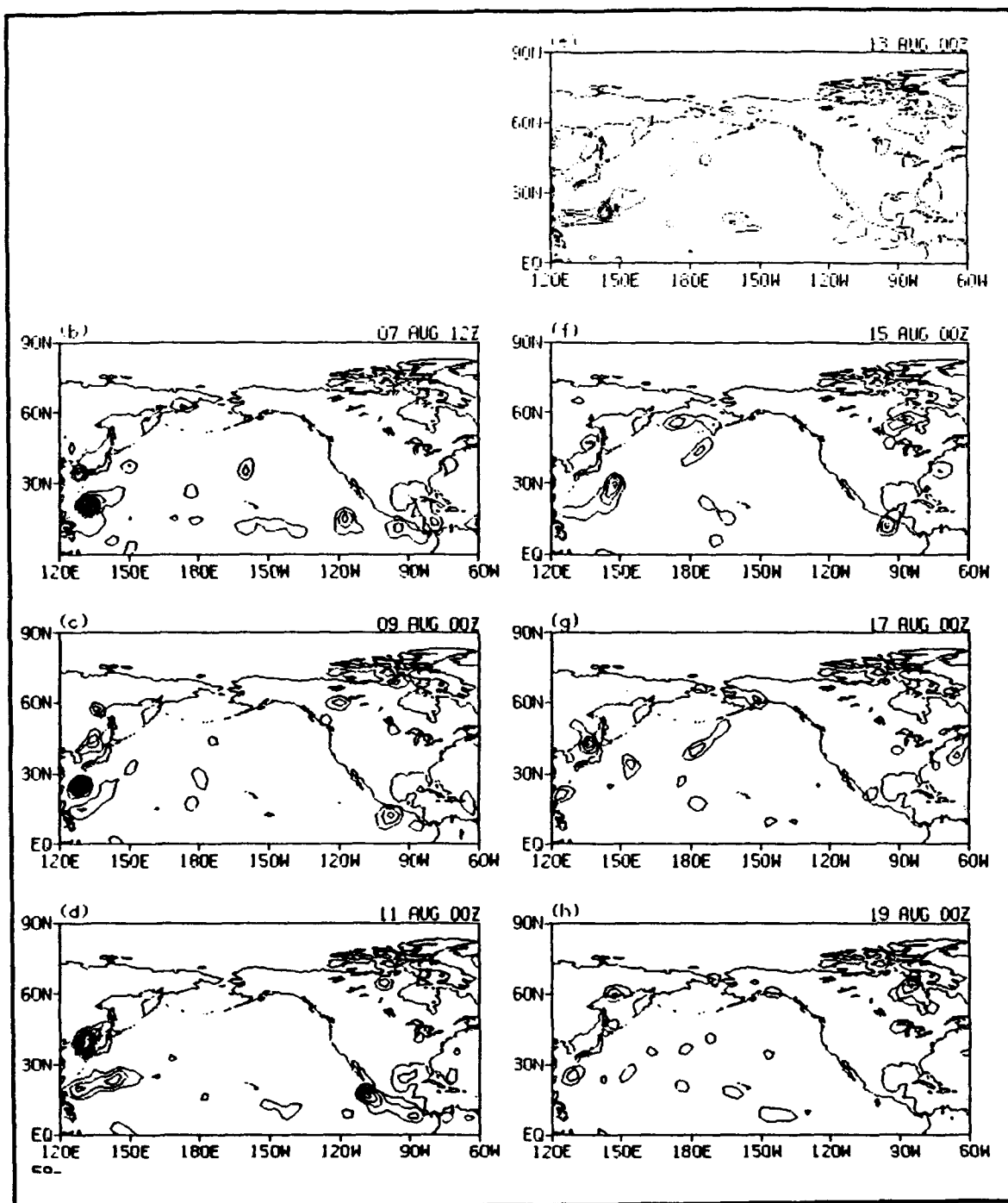


Figure 25. Atmospheric heating at selected times for Forecast 2 POSITIVE run. Minimum contour is 2°C/day. Contour interval is 2°C/day. Panel (a) omitted to retain consistency between this and other figures.

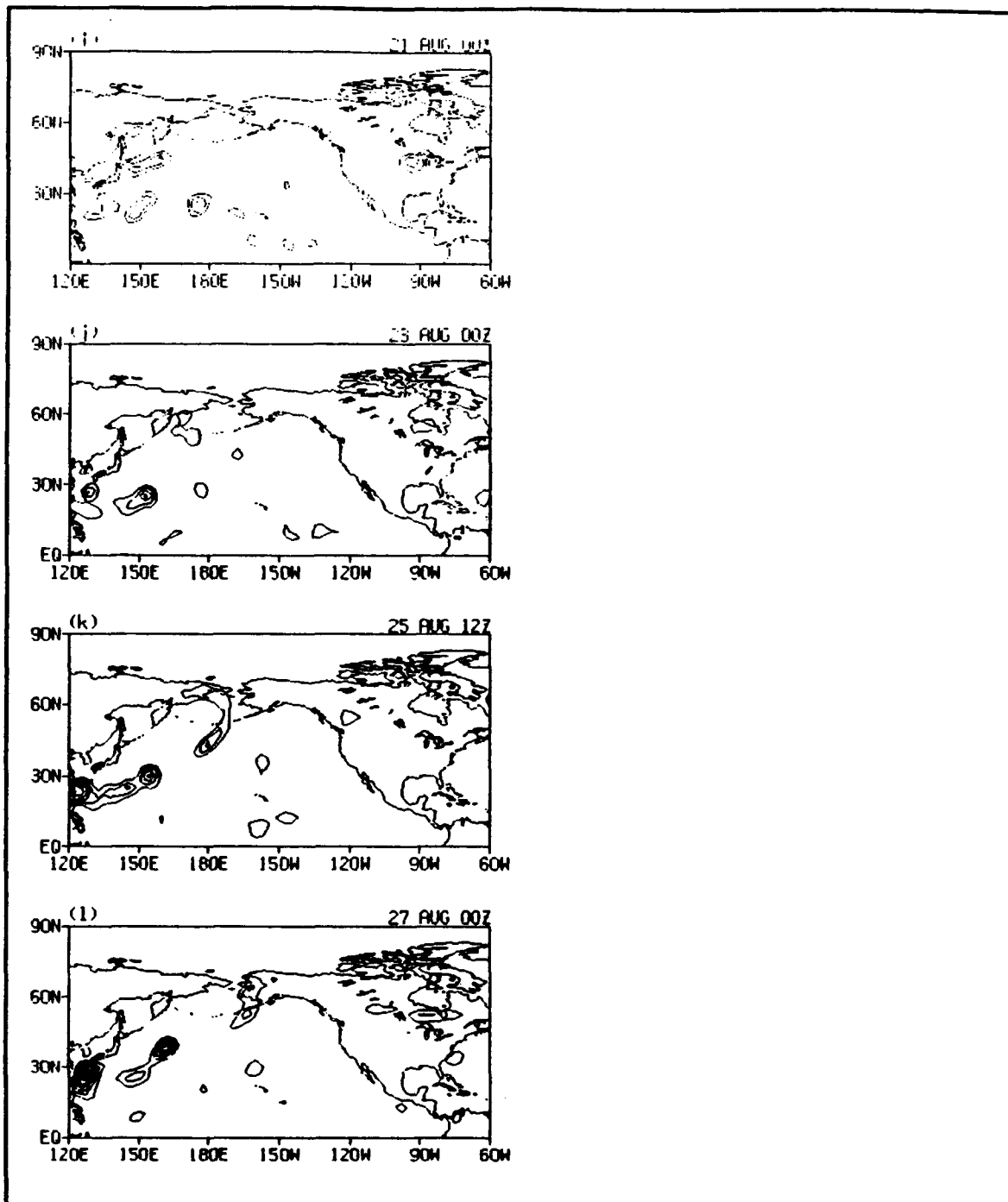


Figure 25. (Continued).

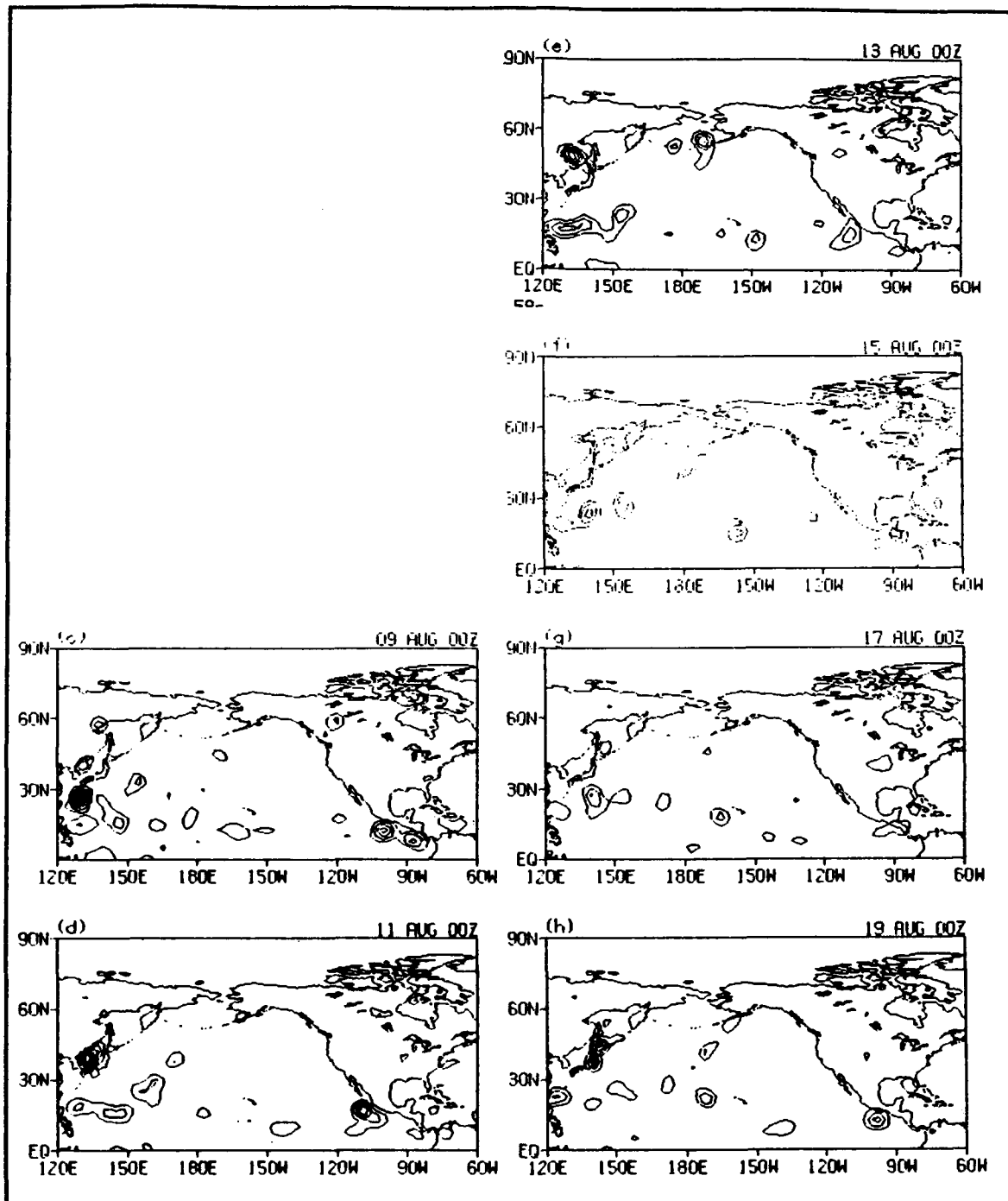


Figure 26. Atmospheric heating at selected times for Forecast 3 POSITIVE run. Minimum contour is 2°C/day. Contour interval is 2°C/day. Panels (a) and (b) omitted to retain consistency between this and other figures.

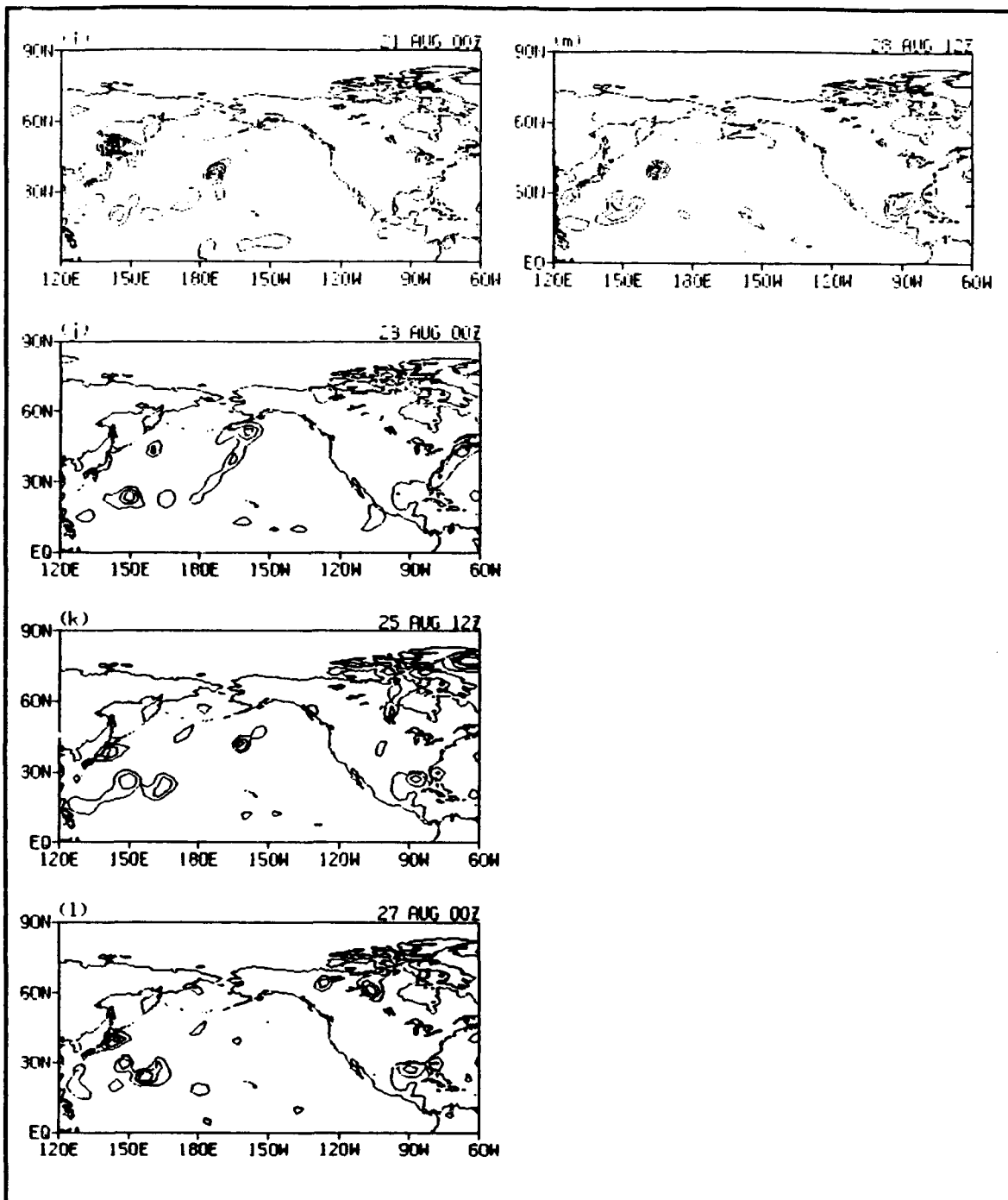


Figure 26. (Continued).

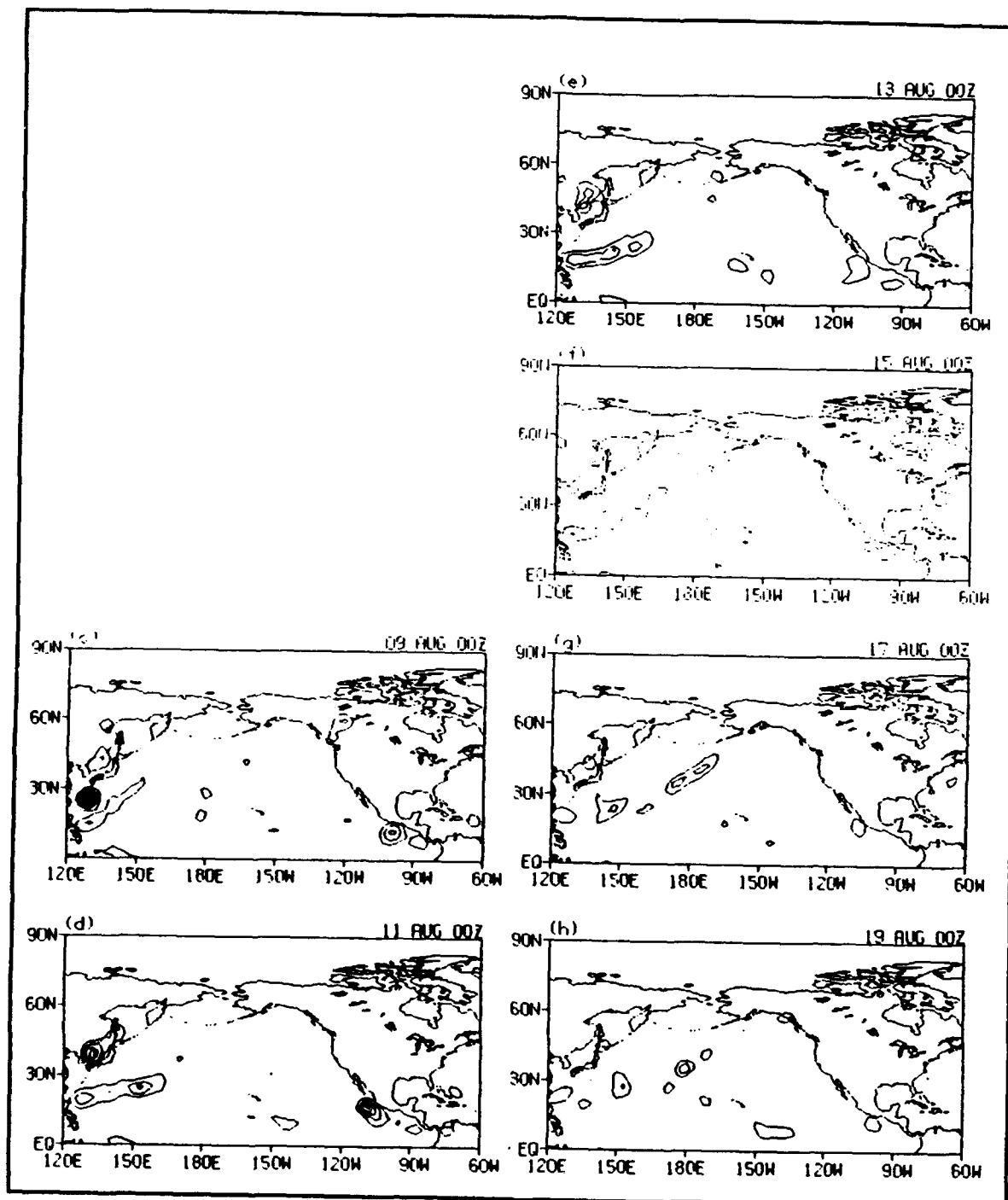


Figure 27. Atmospheric heating at selected times for Ensemble Average POSITIVE run. Minimum contour is 2°C/day. Contour interval is 2°C/day. Panels (a) and (b) omitted to retain consistency between this and other figures.

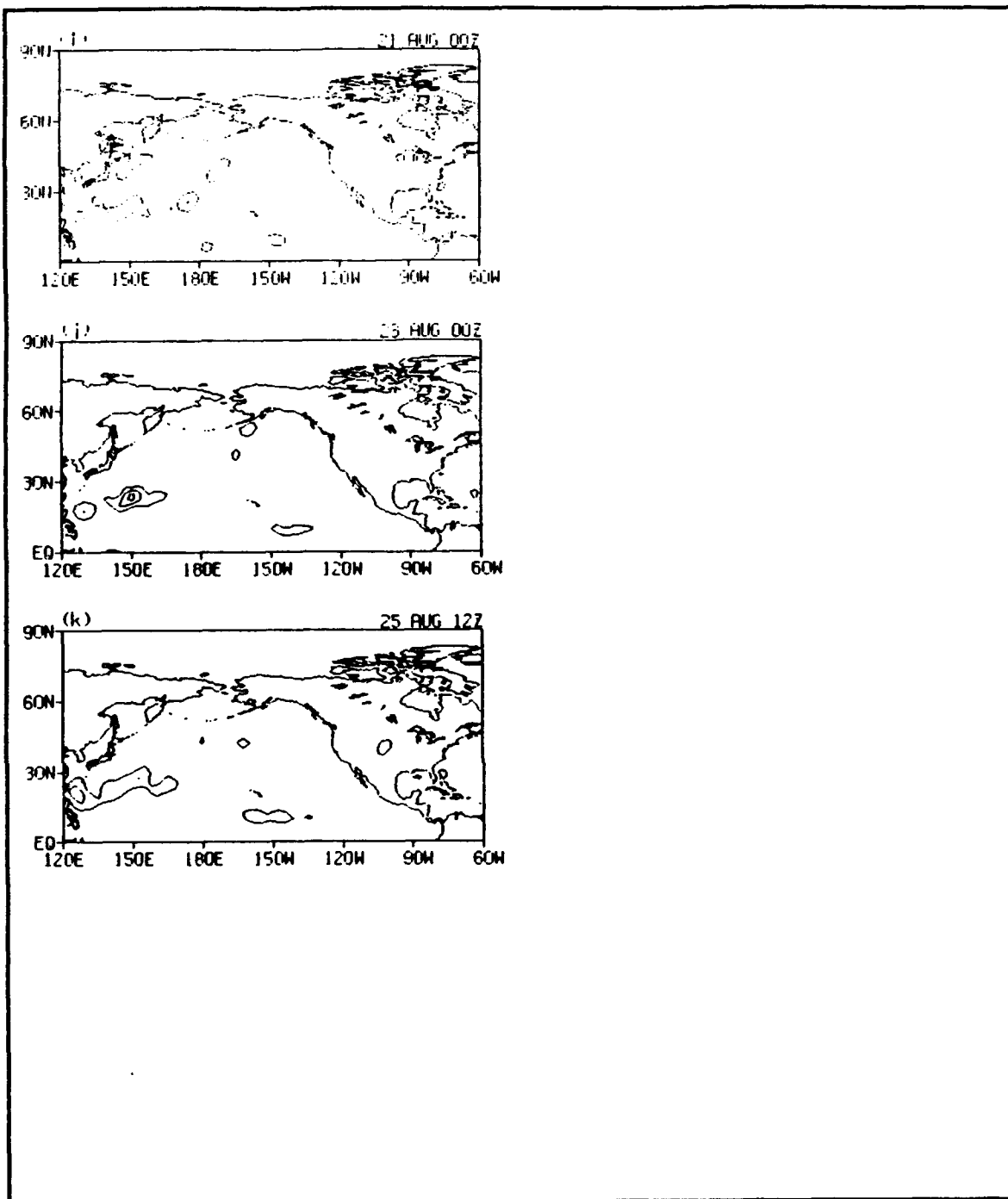


Figure 27. (Continued).

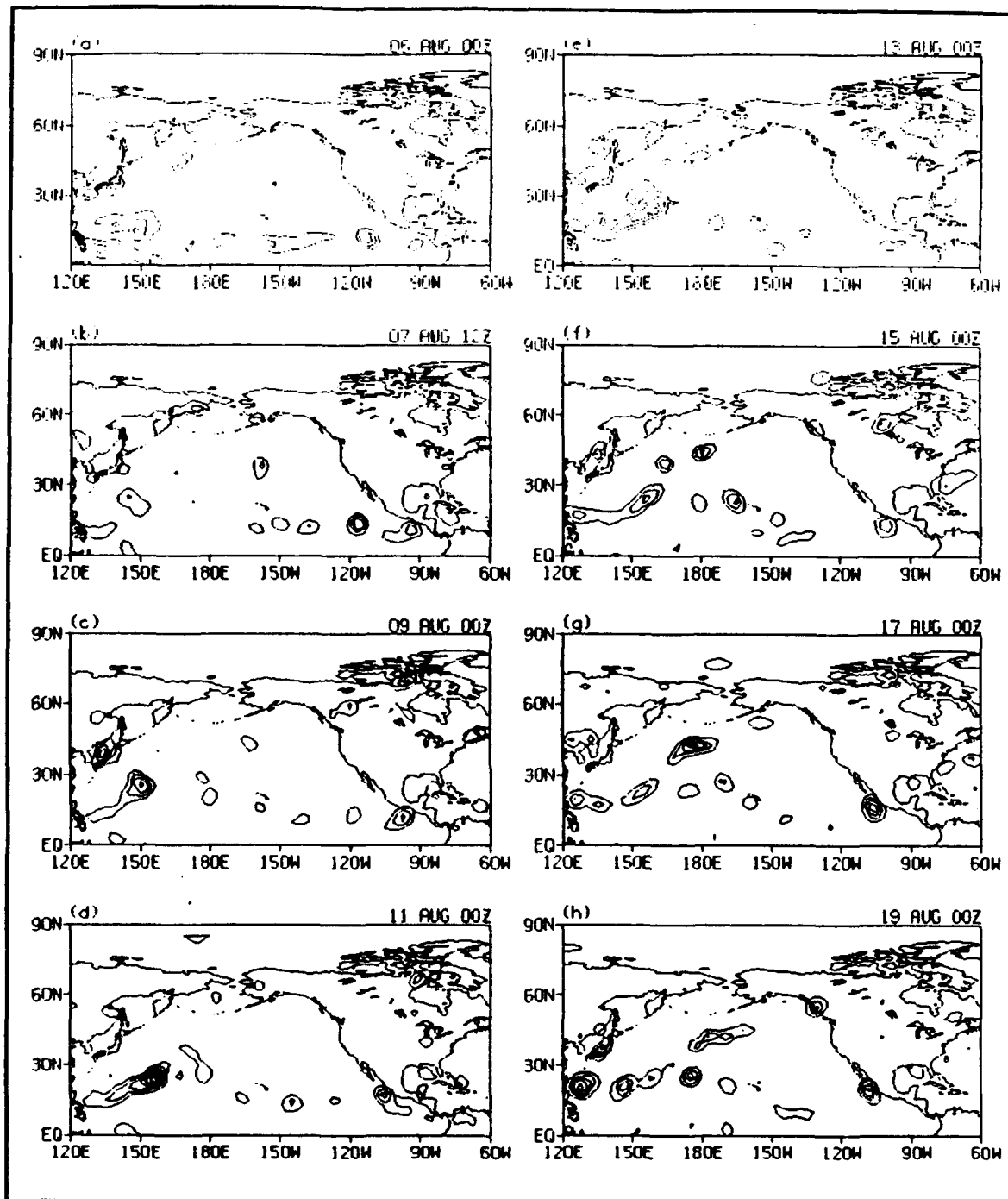


Figure 28. Atmospheric heating at selected times for Forecast 1 NEGATIVE run. Minimum contour is 2°C/day. Contour interval is 2°C/day.

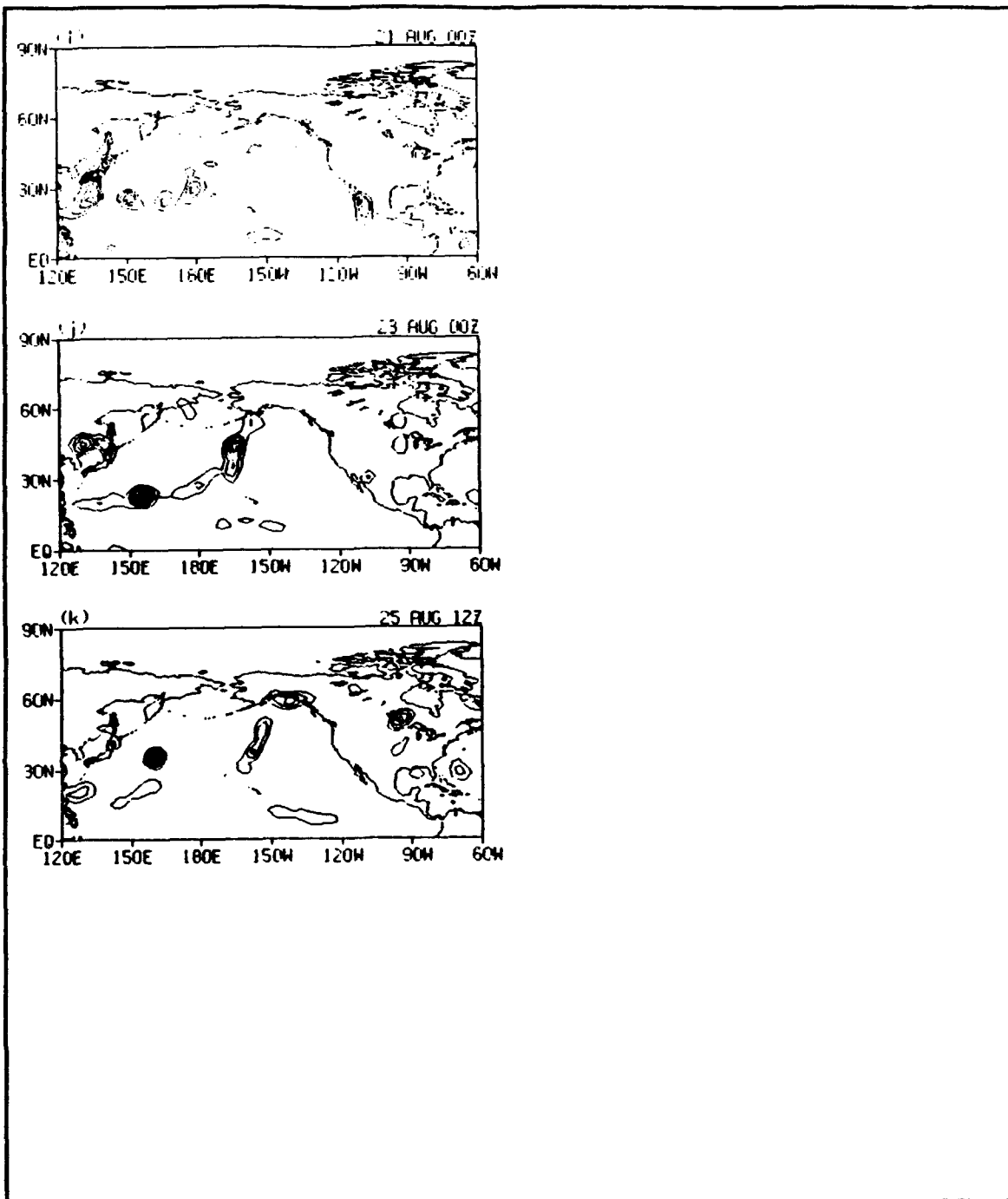


Figure 28. (Continued).

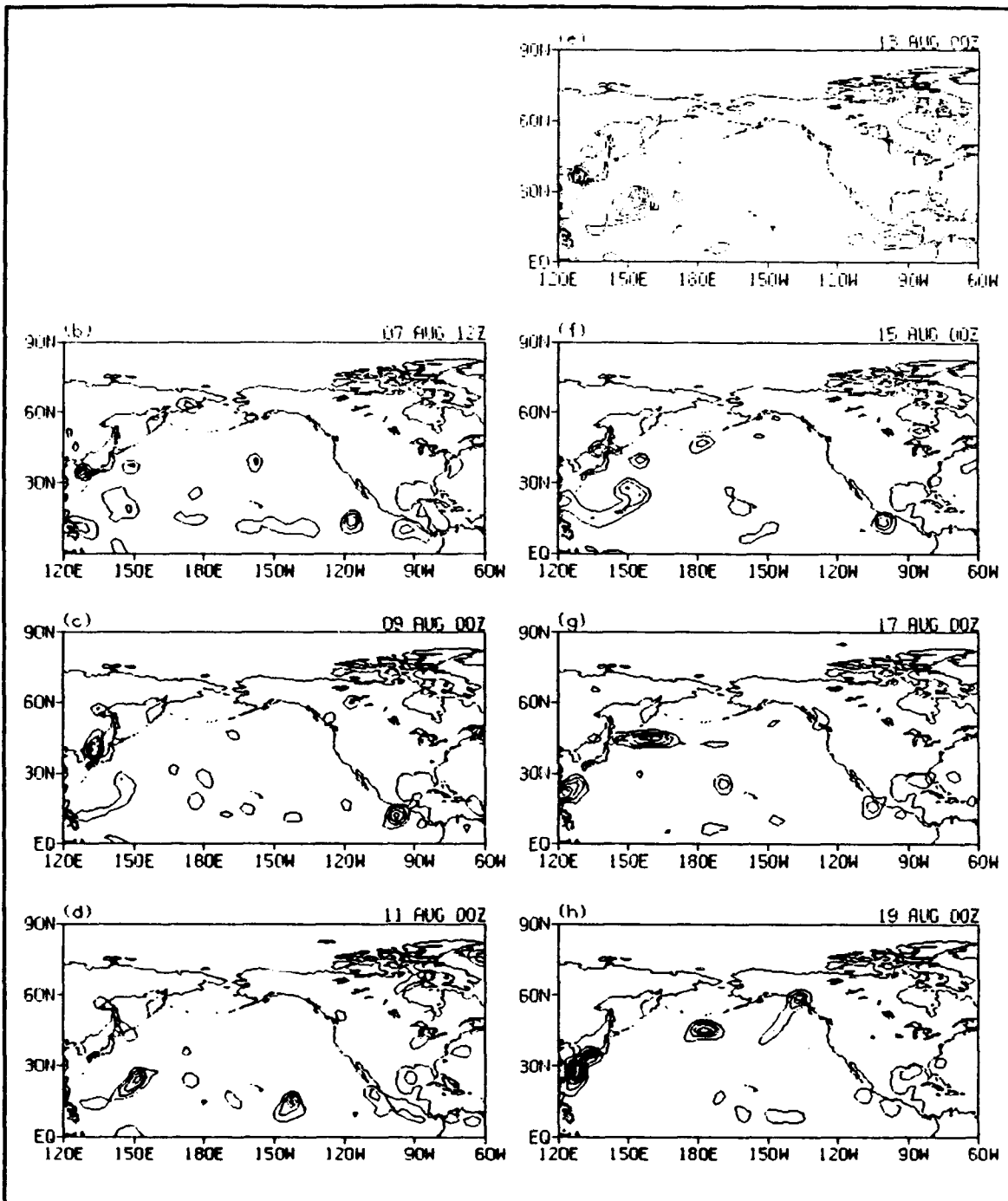


Figure 29. Atmospheric heating at selected times for Forecast 2 NEGATIVE run. Minimum contour is 2°C/day. Contour interval is 2°C/day. Panel (a) omitted to retain consistency between this and other figures.

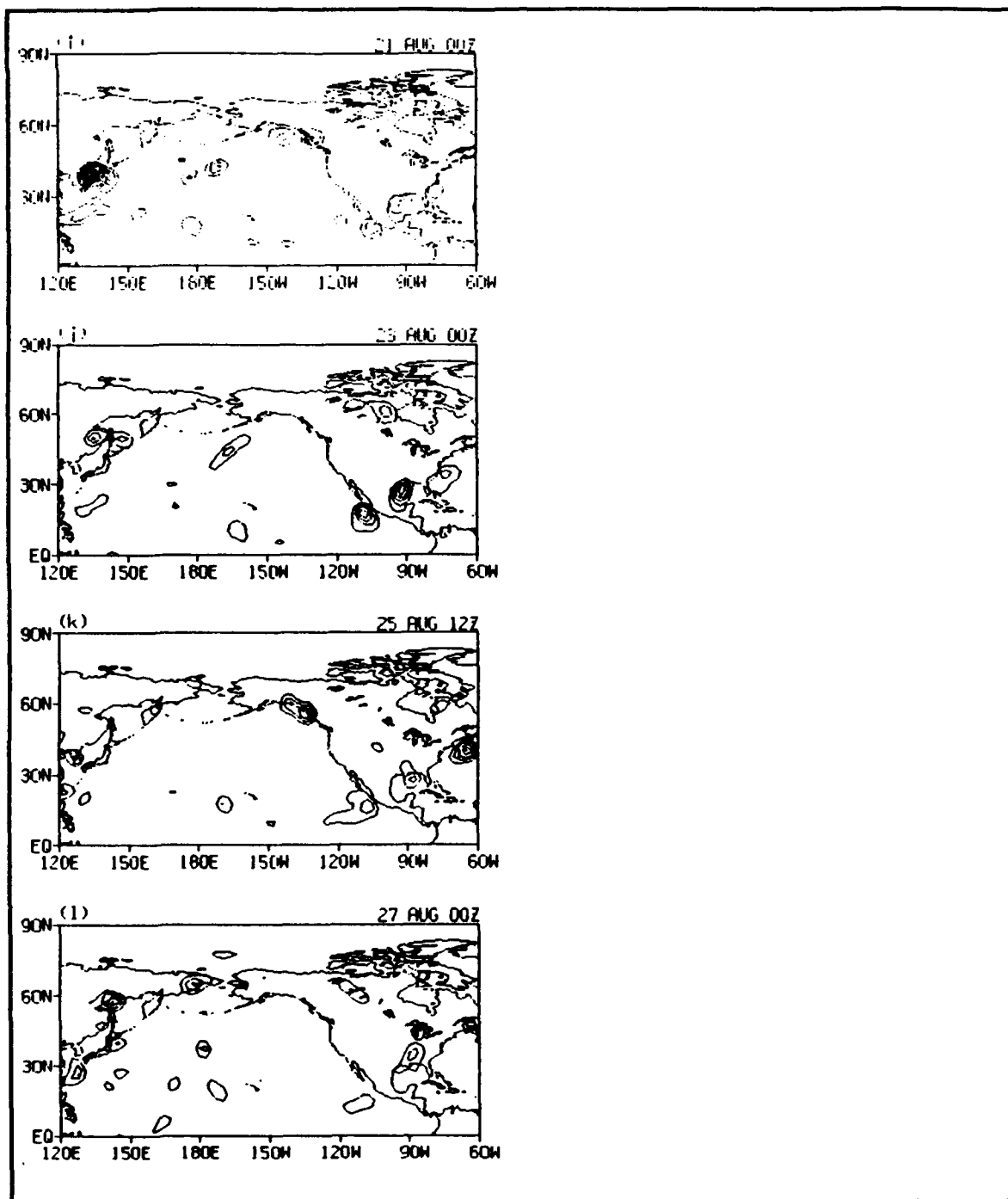


Figure 29. (Continued).

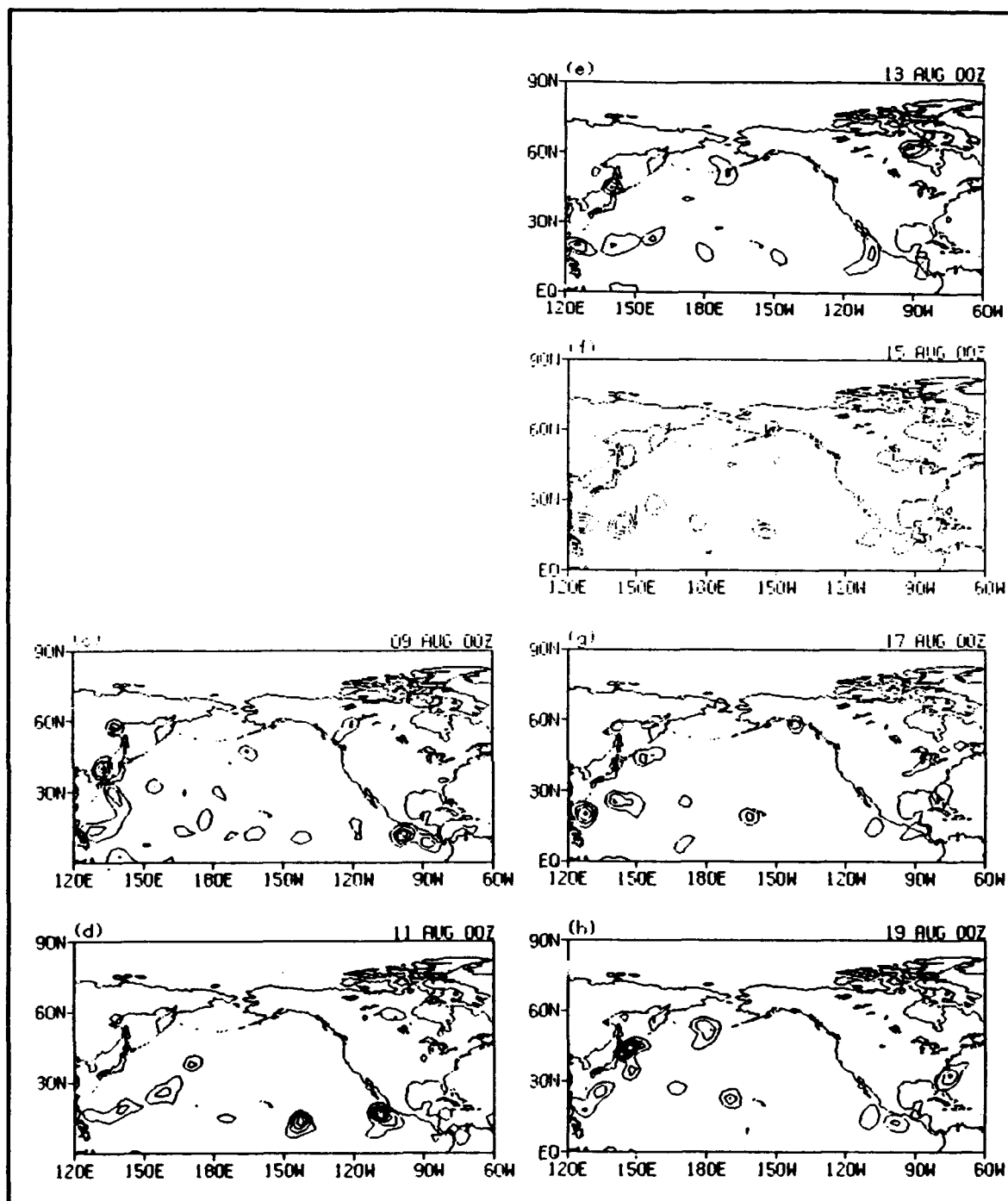


Figure 30. Atmospheric heating at selected times for Forecast 3 NEGATIVE run. Minimum contour is 2°C/day. Contour interval is 2°C/day. Panels (a) and (b) omitted to retain consistency between this and other figures.

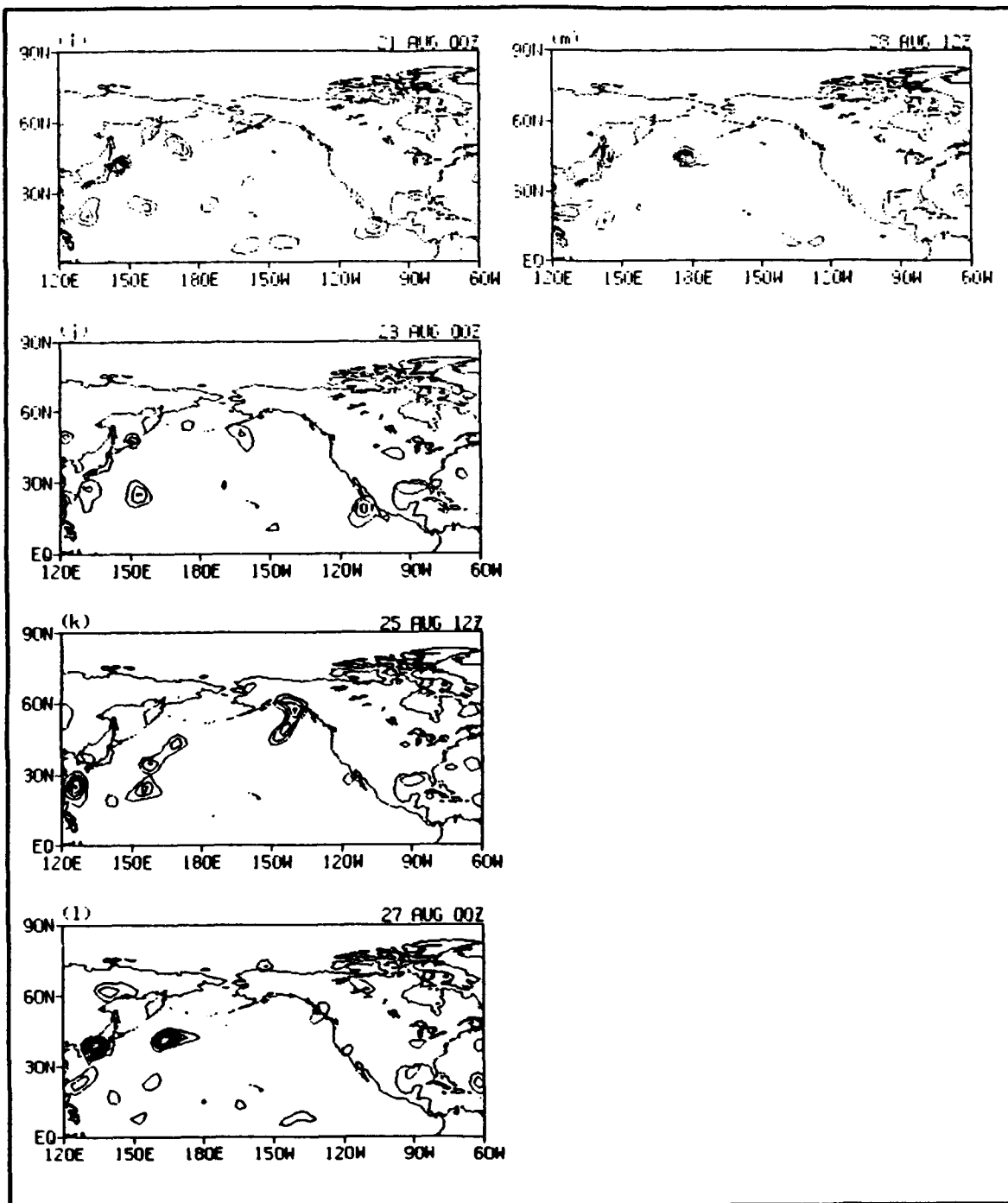


Figure 30. (Continued).

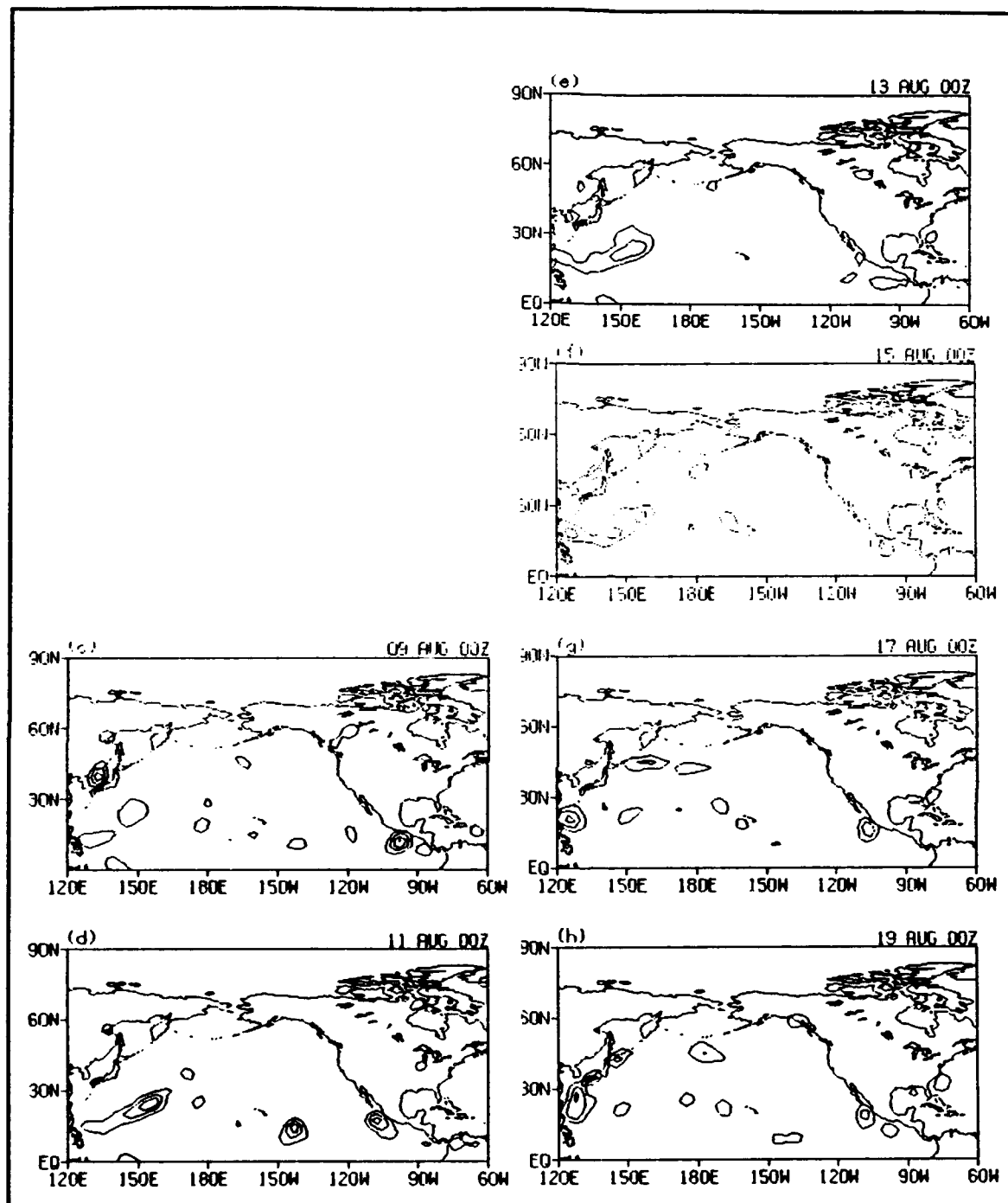


Figure 31. Atmospheric heating at selected times for Ensemble Average NEGATIVE run. Minimum contour is 2°C/day. Contour interval is 2°C/day. Panels (a) and (b) omitted to retain consistency between this and other figures.

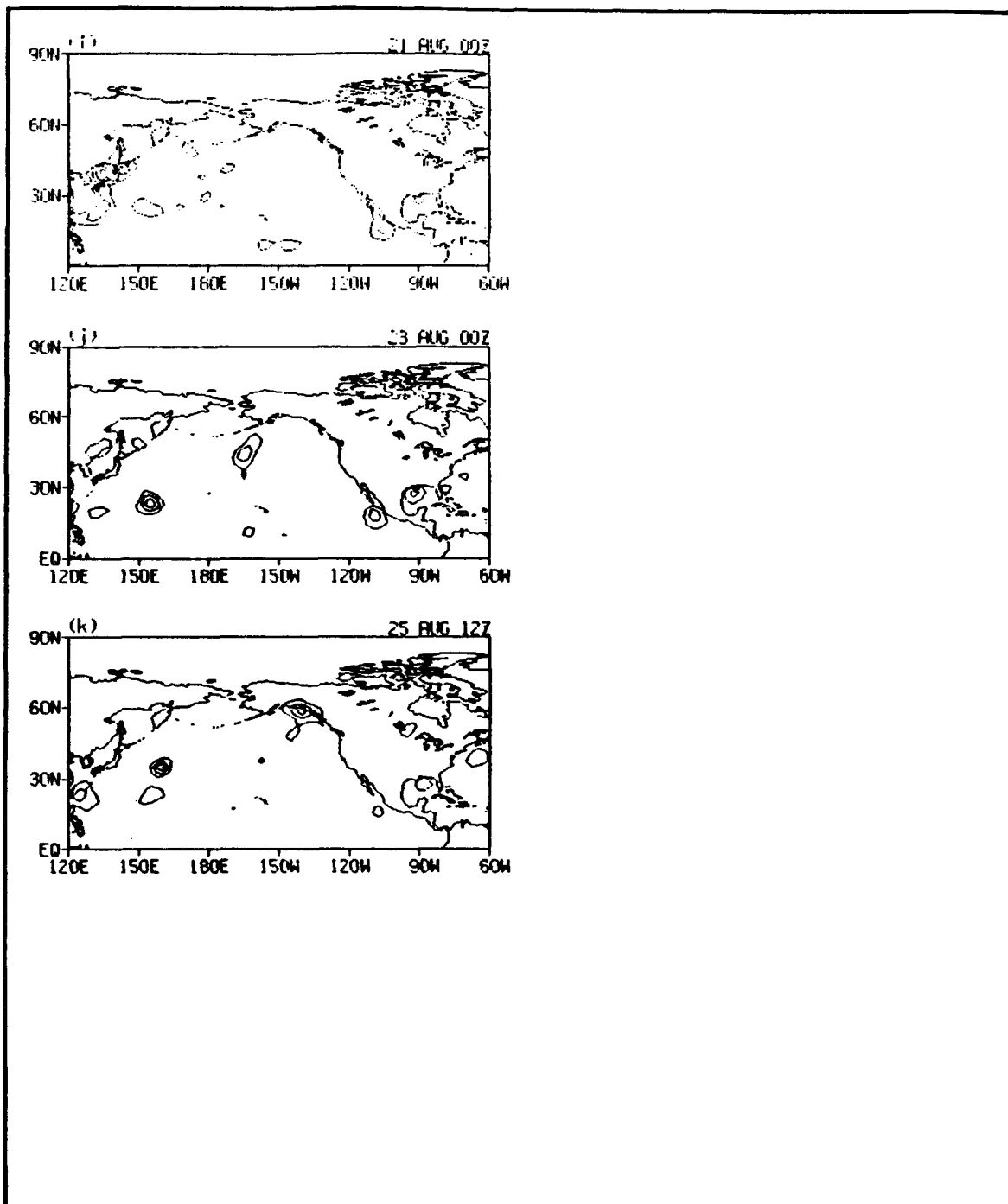


Figure 31. (Continued).

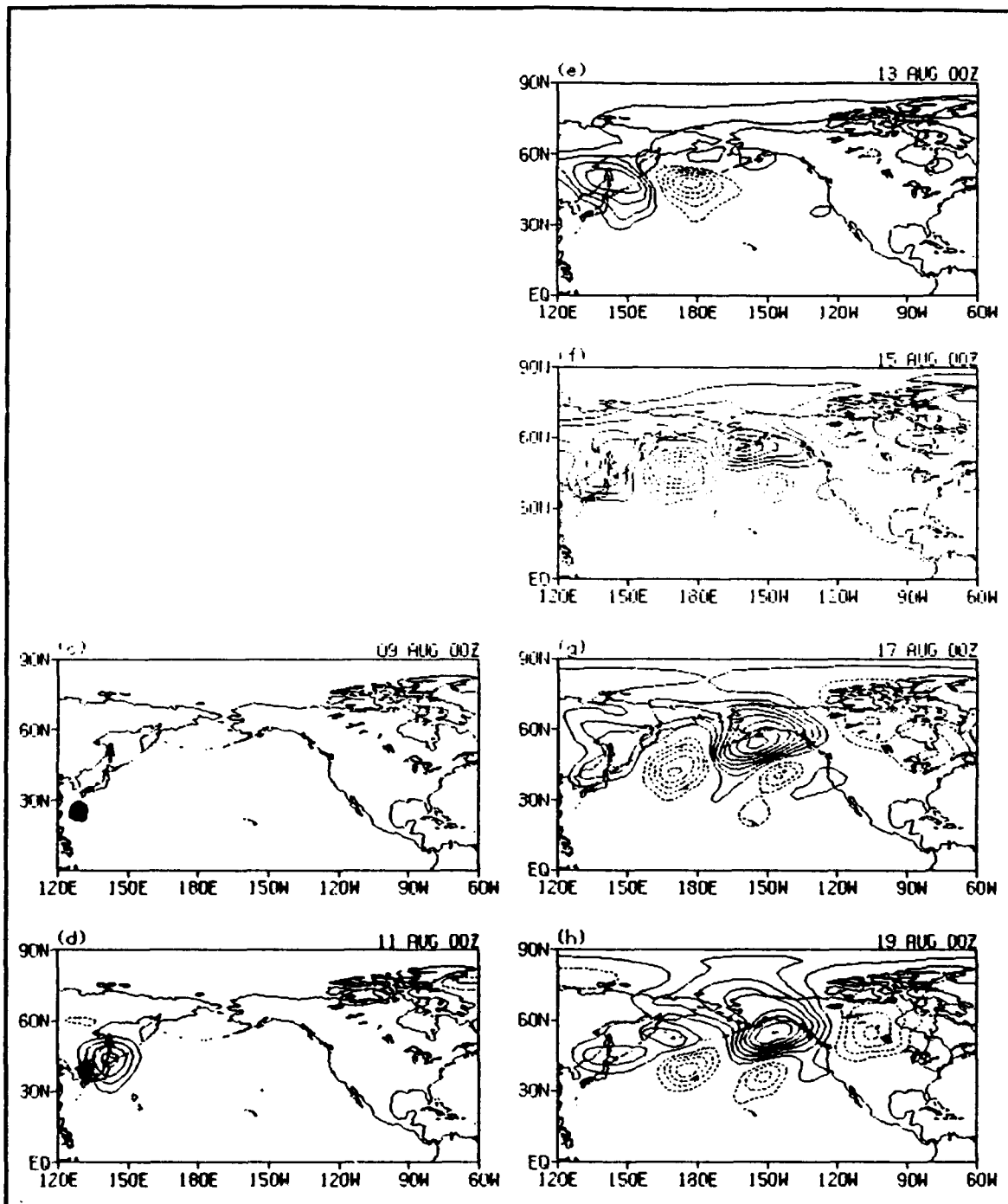


Figure 32. EA differences (POSITIVE-NEGATIVE) in heating and 200 mb heights at selected times. Solid (dashed) contours represent positive (negative) height differences; contour interval is 50 gpm. Zero contour omitted. Shaded areas shows heating differences $> 5^{\circ}\text{C}/\text{day}$. Panels (a) and (b) omitted to retain consistency between this and other figures.

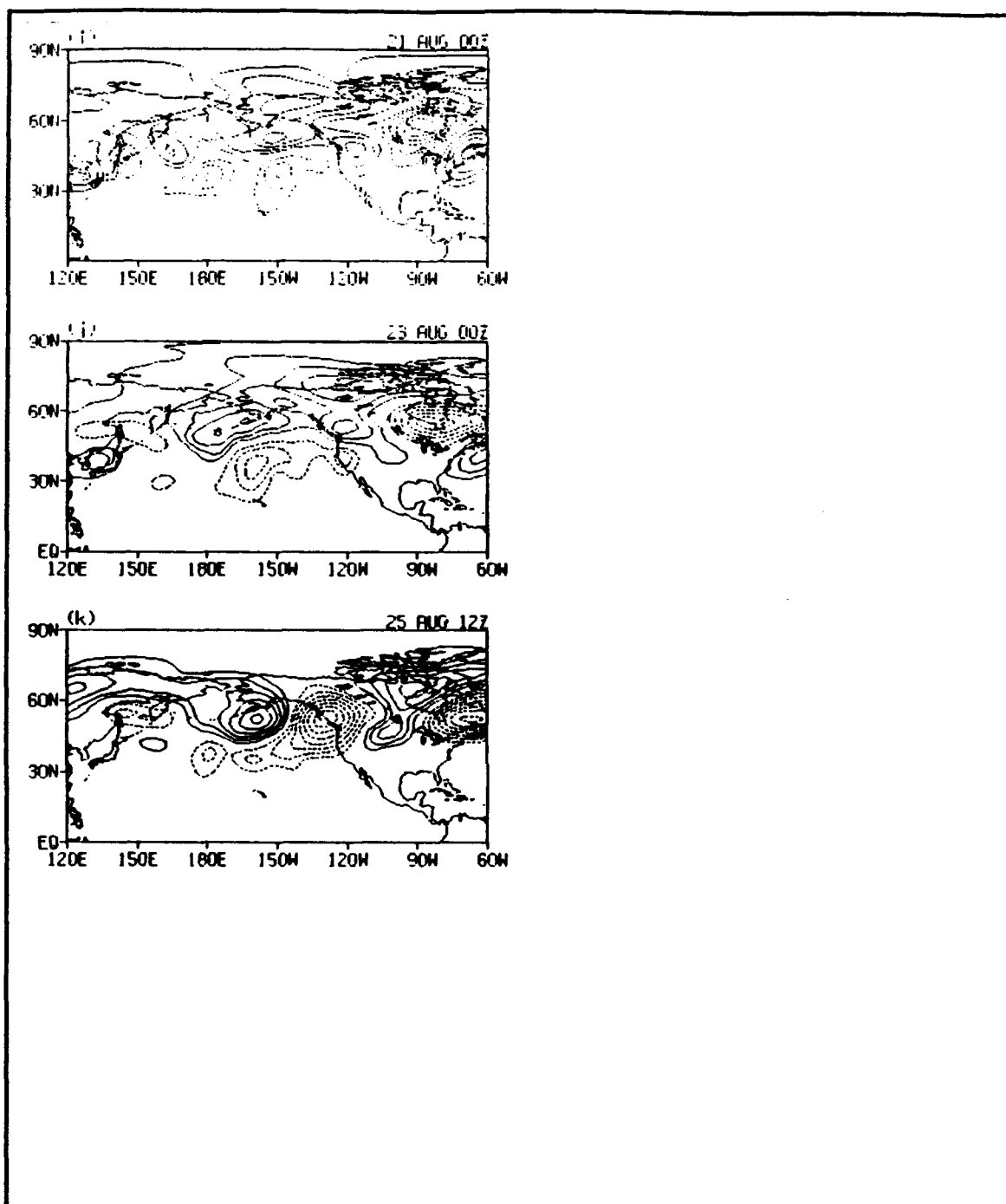


Figure 32. (Continued).

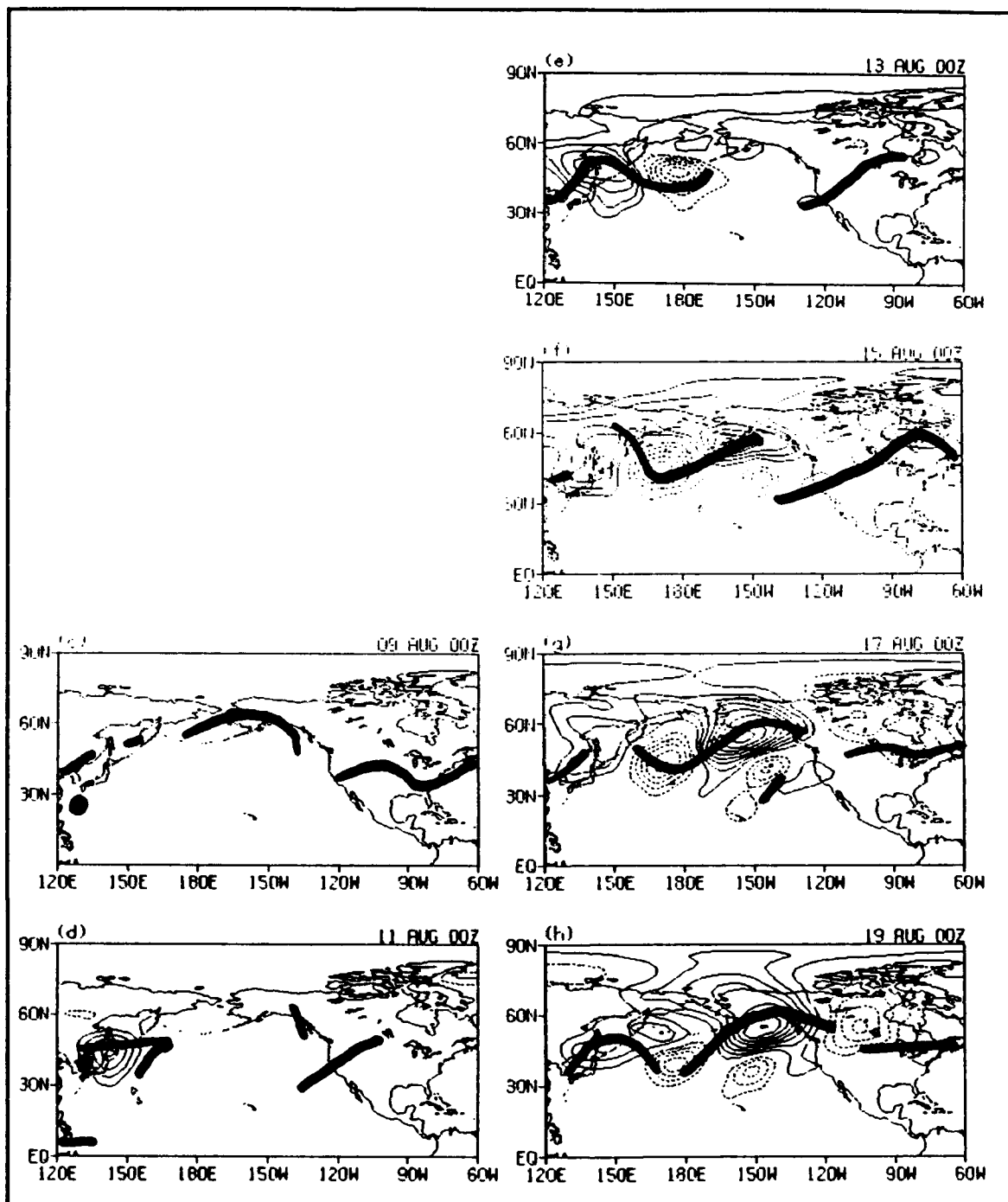


Figure 33. EA differences (POSITIVE-NEGATIVE) in heating and 200 mb heights at selected times. Solid (dashed) contours represent positive (negative) height differences; contour interval is 50 gpm. Zero contour omitted. Shaded areas shows heating differences > 5°C/day. Solid thick line shows axis of >30

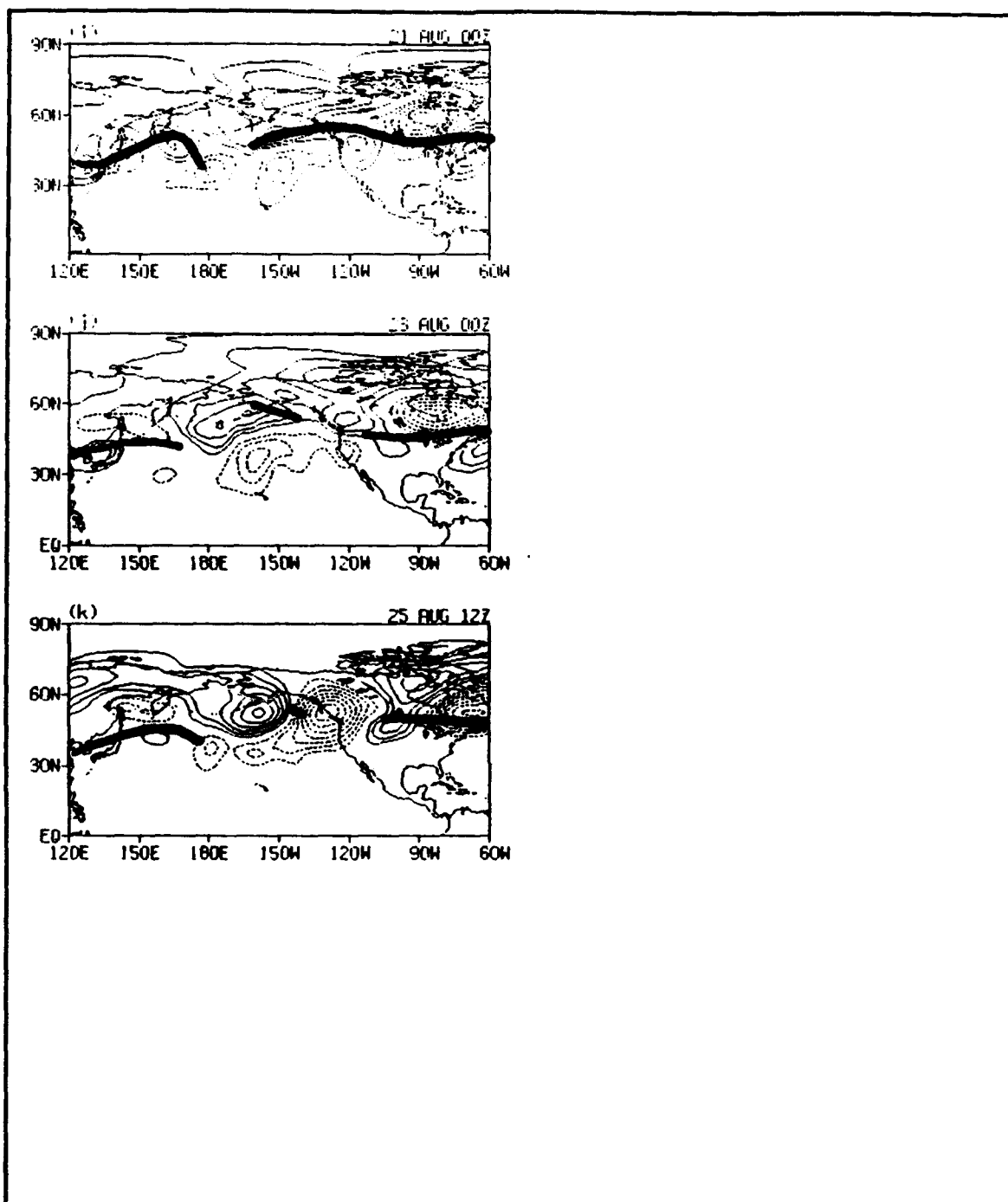


Figure 33. (Continued) m/s jet axis. Panels (a) and (b) omitted to retain consistency between this and other figures.

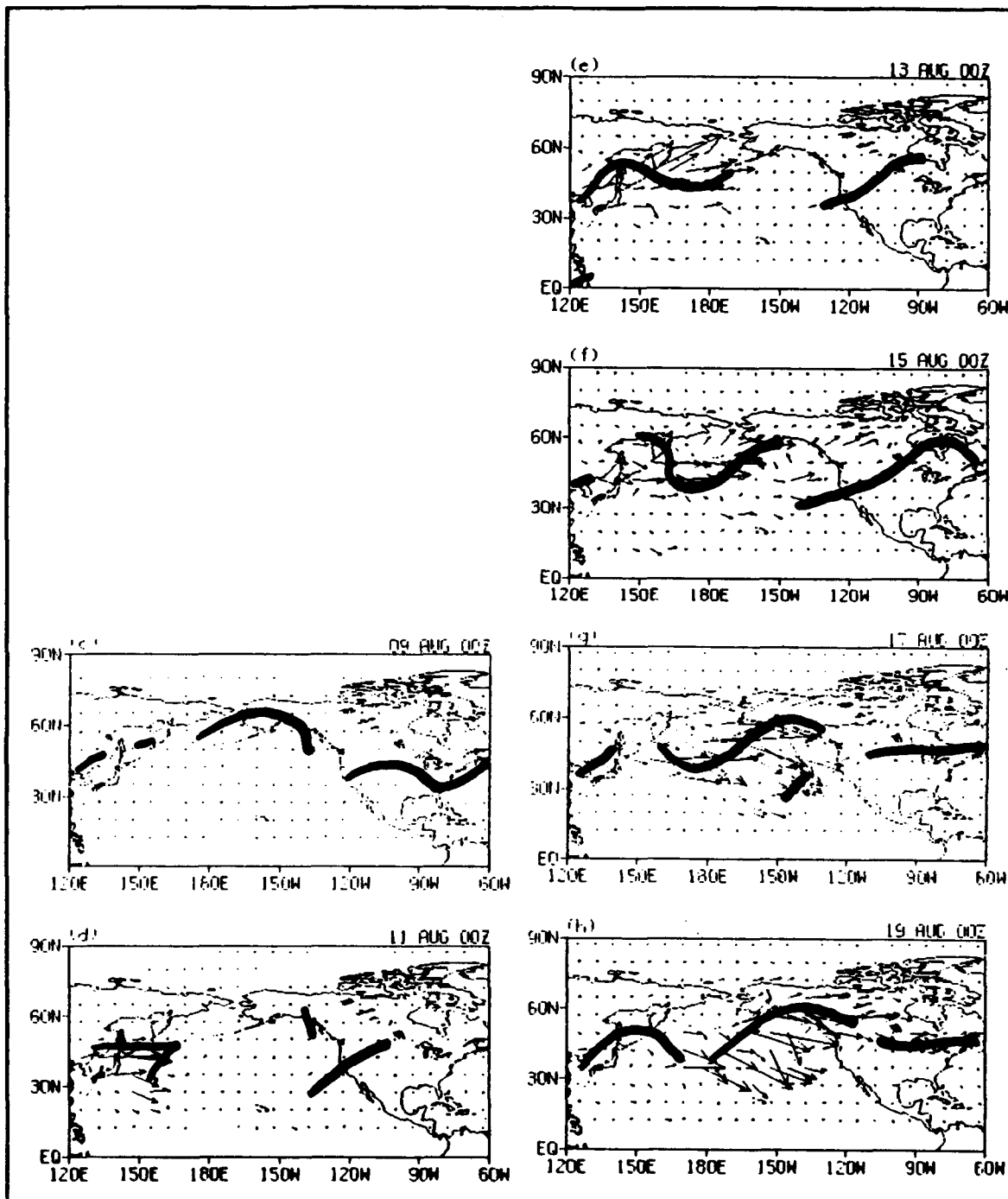


Figure 34. EA differences (POSITIVE-NEGATIVE) in QG wave activity fluxes at selected times. Solid thick line shows axis of >30 m/s jet axis. Panels (a) and (b) omitted to retain consistency between this and other figures. Vector scale in

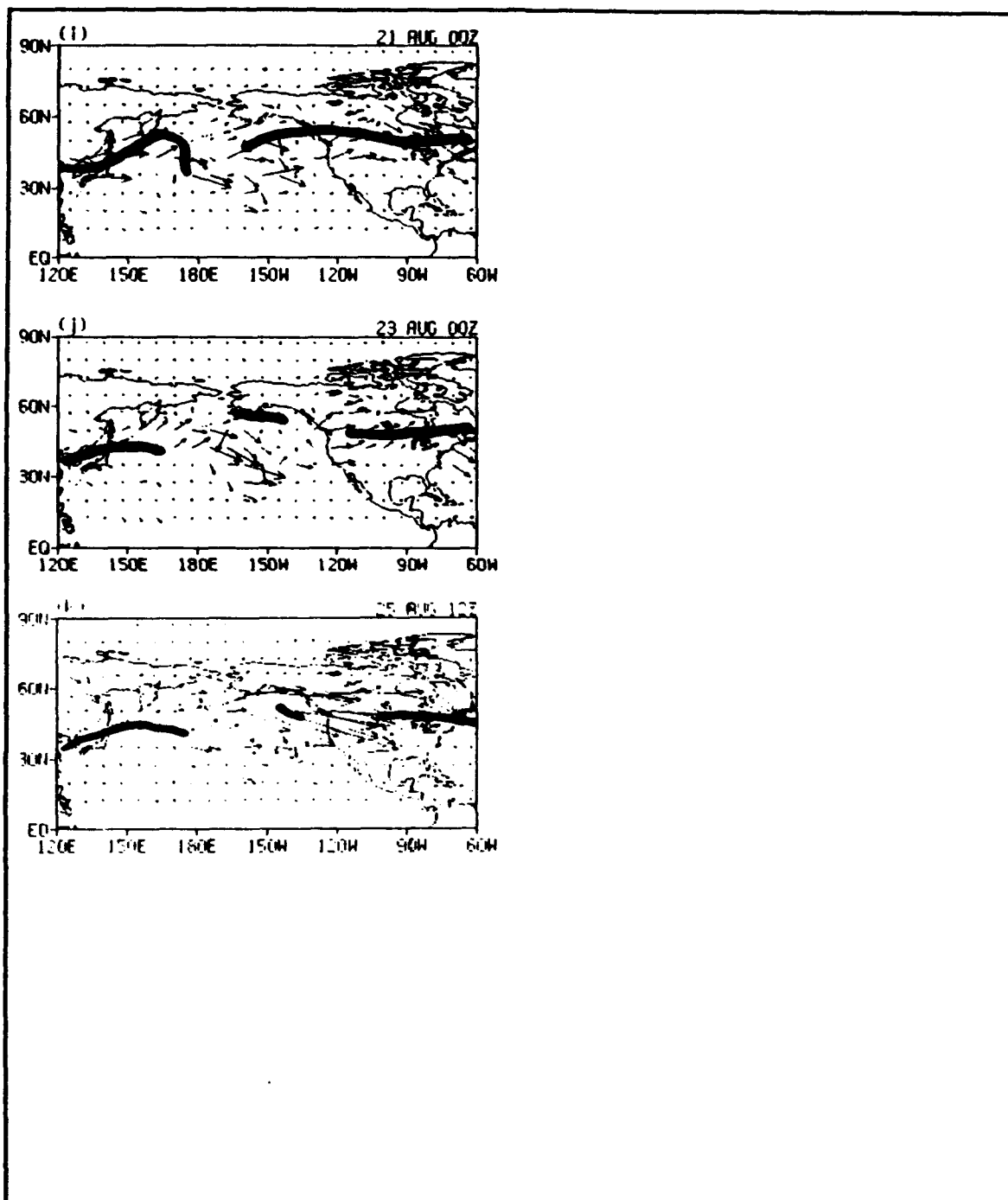


Figure 34. (Continued) m^2/s^2 as shown:

0.100E+09
MAXIMUM VECTOR

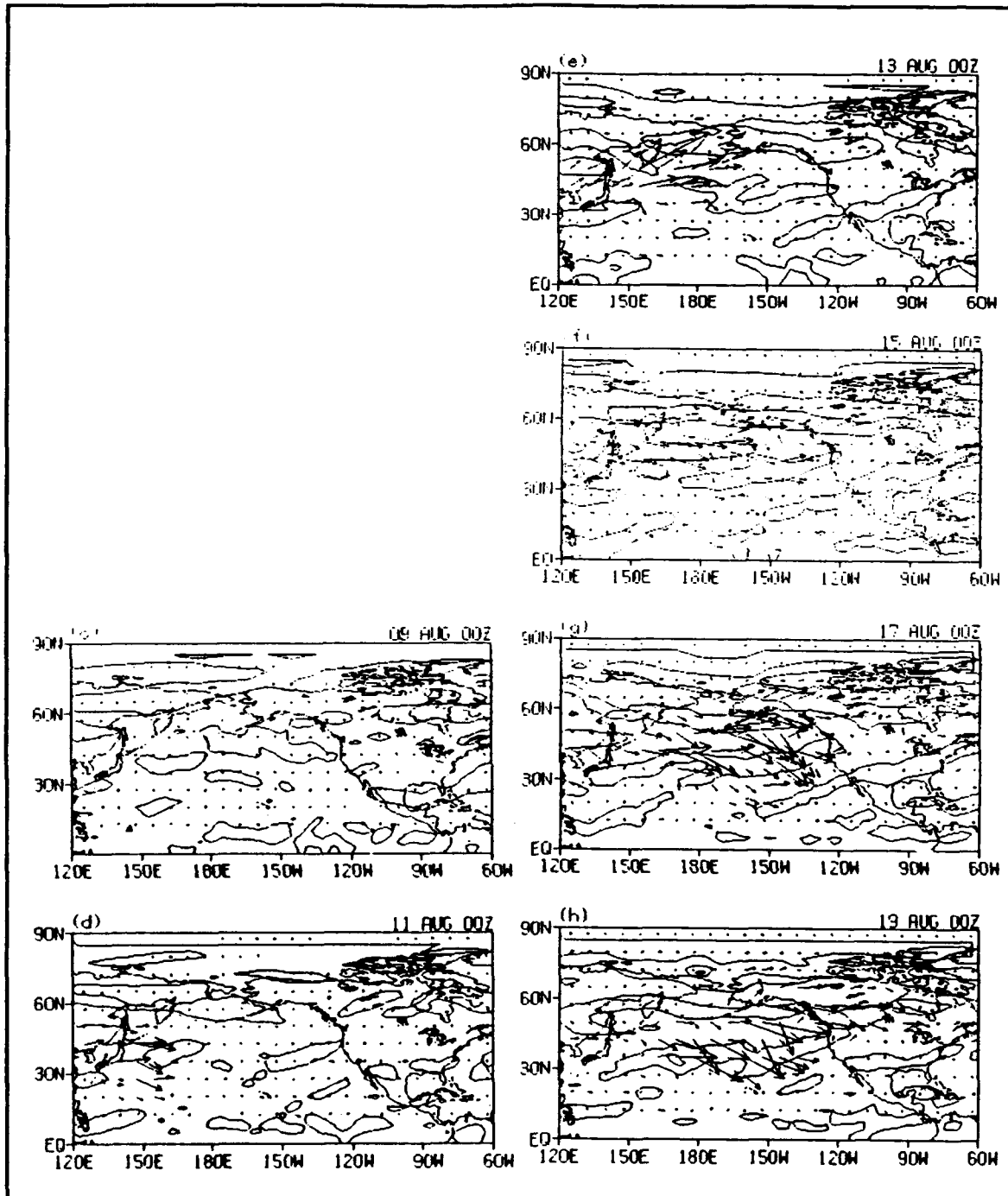


Figure 35. EA differences (POSITIVE-NEGATIVE) in QG wave activity fluxes at selected times. Solid medium lines indicate areas of potential BTI ($\beta - U_y = 0$). Panels (a) and (b) omitted to retain consistency between this and

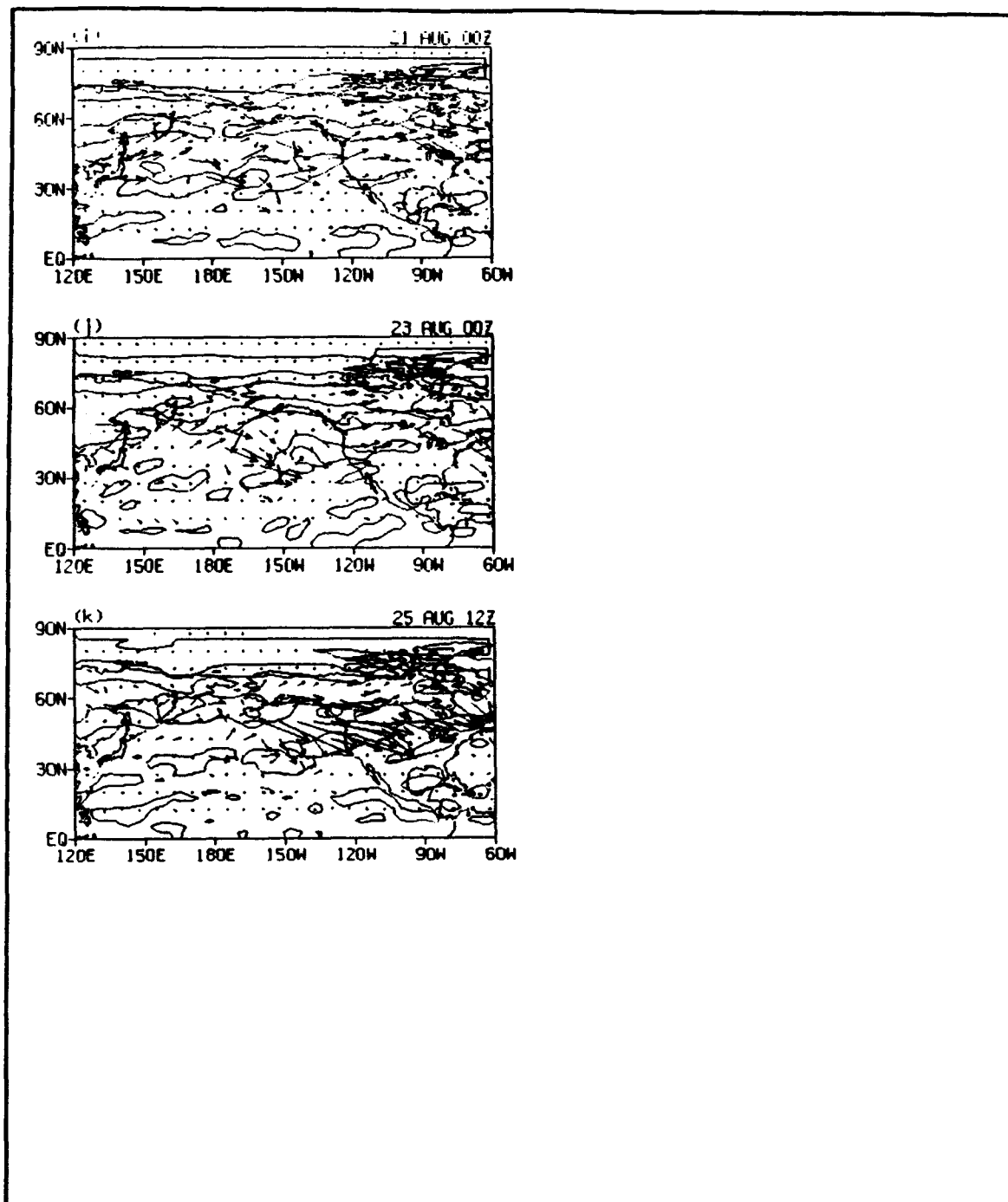
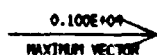


Figure 35. (Continued) other figures. Vector scale in m^2/s^2 as shown:



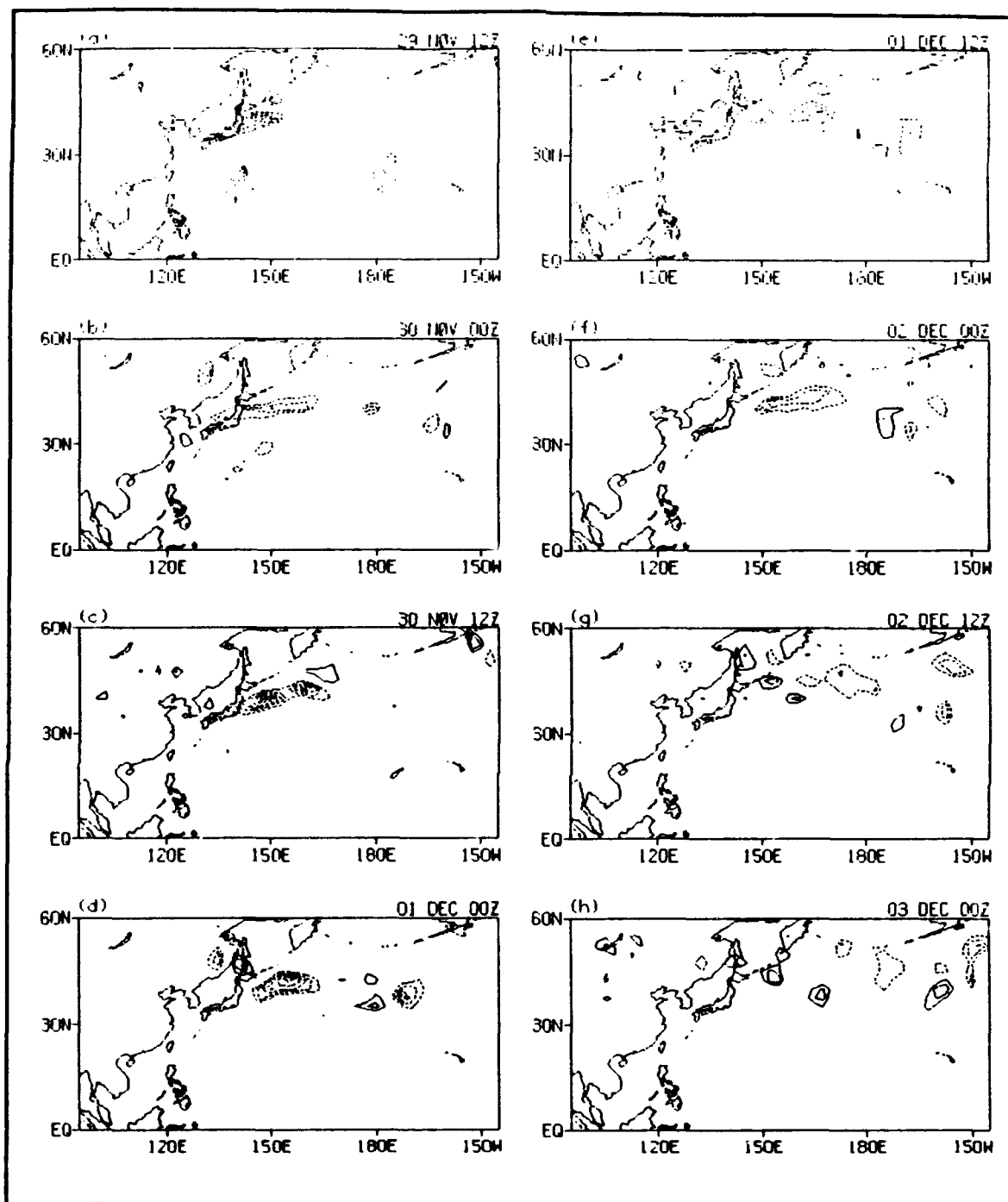


Figure 36. EA differences (POSITIVE-NEGATIVE) in 200 mb Rossby wave sources for Yuri. Solid (dashed) contours represent positive (negative) differences; minimum contour is $0.1\text{E-}08 / \text{s}^2$; contour interval is $0.05\text{E-}08 / \text{s}^2$. Zero contour omitted.

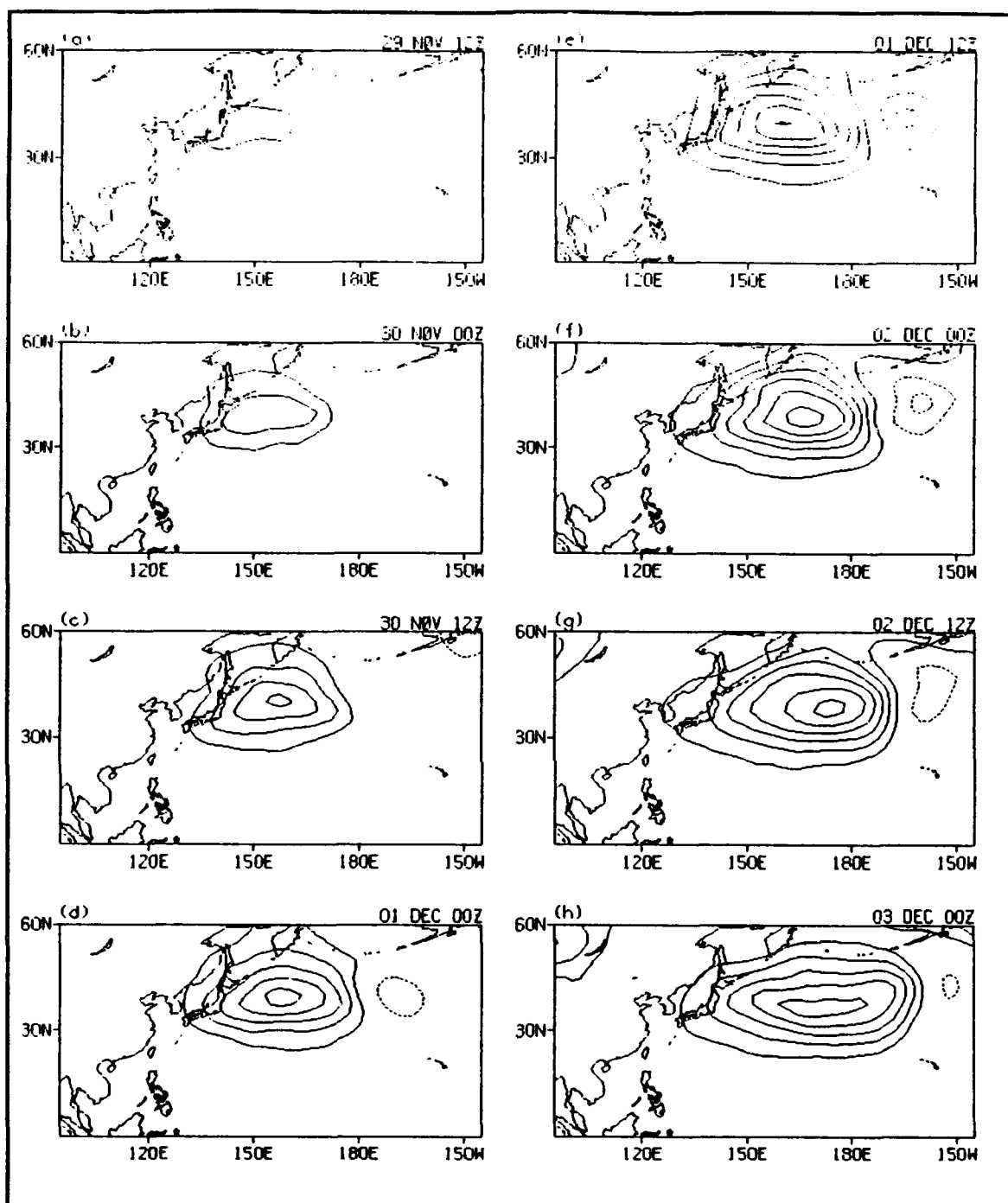


Figure 37. EA differences (POSITIVE-NEGATIVE) in 200 mb heights for Yuri. Solid (dashed) contours represent positive (negative) height differences; contour interval is 50 gpm. Zero contour omitted.

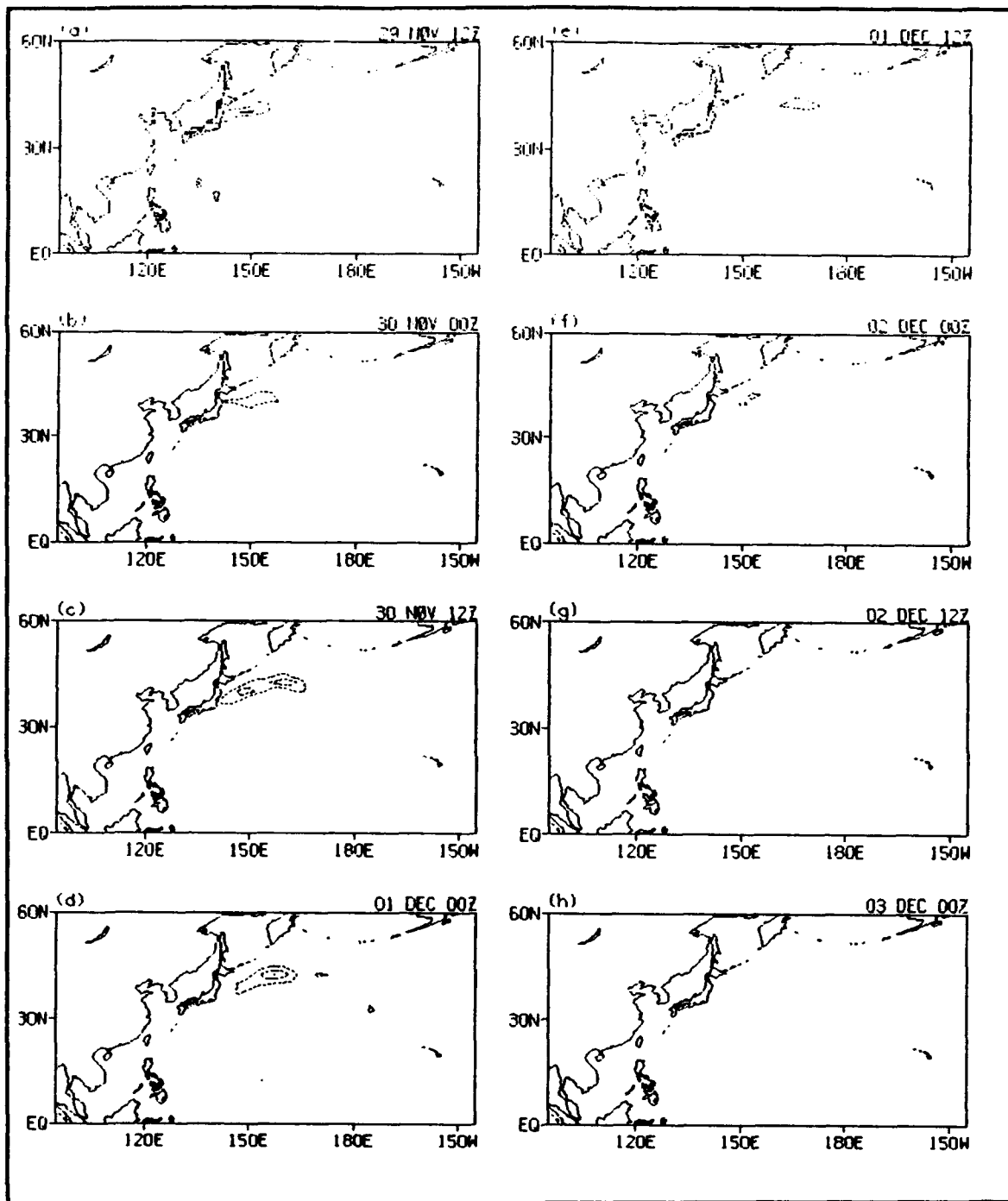


Figure 38. EA differences (POSITIVE-NEGATIVE) in 200 mb ADV DIV for Yuri. Solid (dashed) contours represent positive (negative) differences; minimum contour is $0.1\text{E-}08 /s^2$; contour interval is $0.05\text{E-}08 /s^2$. Zero contour omitted.

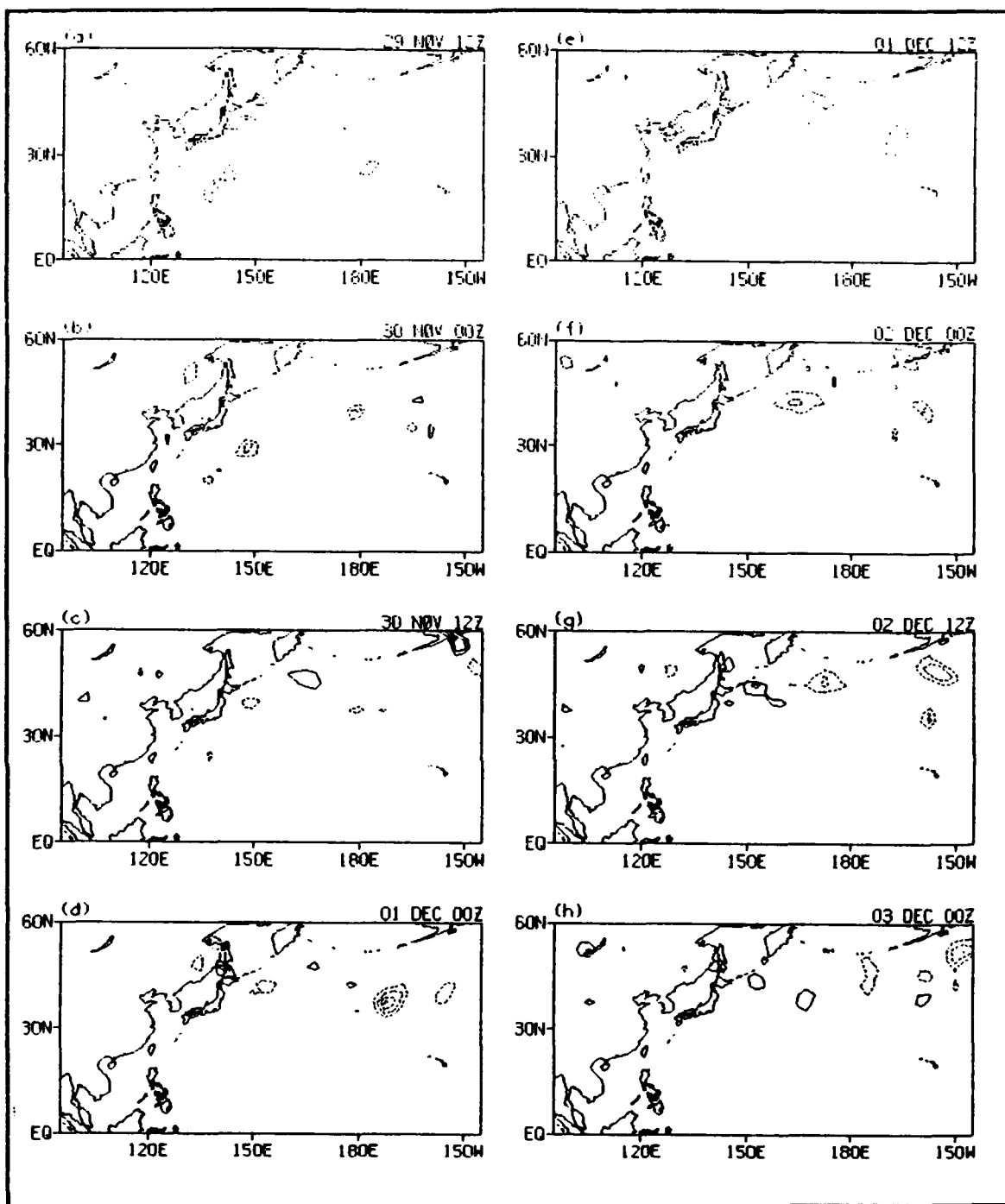


Figure 39. EA differences (POSITIVE-NEGATIVE) in 200 mb vortex stretching for Yuri. Solid (dashed) contours represent positive (negative) differences; minimum contour is $0.1\text{E-}08 \text{ /s}^2$; contour interval is $0.05\text{E-}08 \text{ /s}^2$. Zero contour omitted.

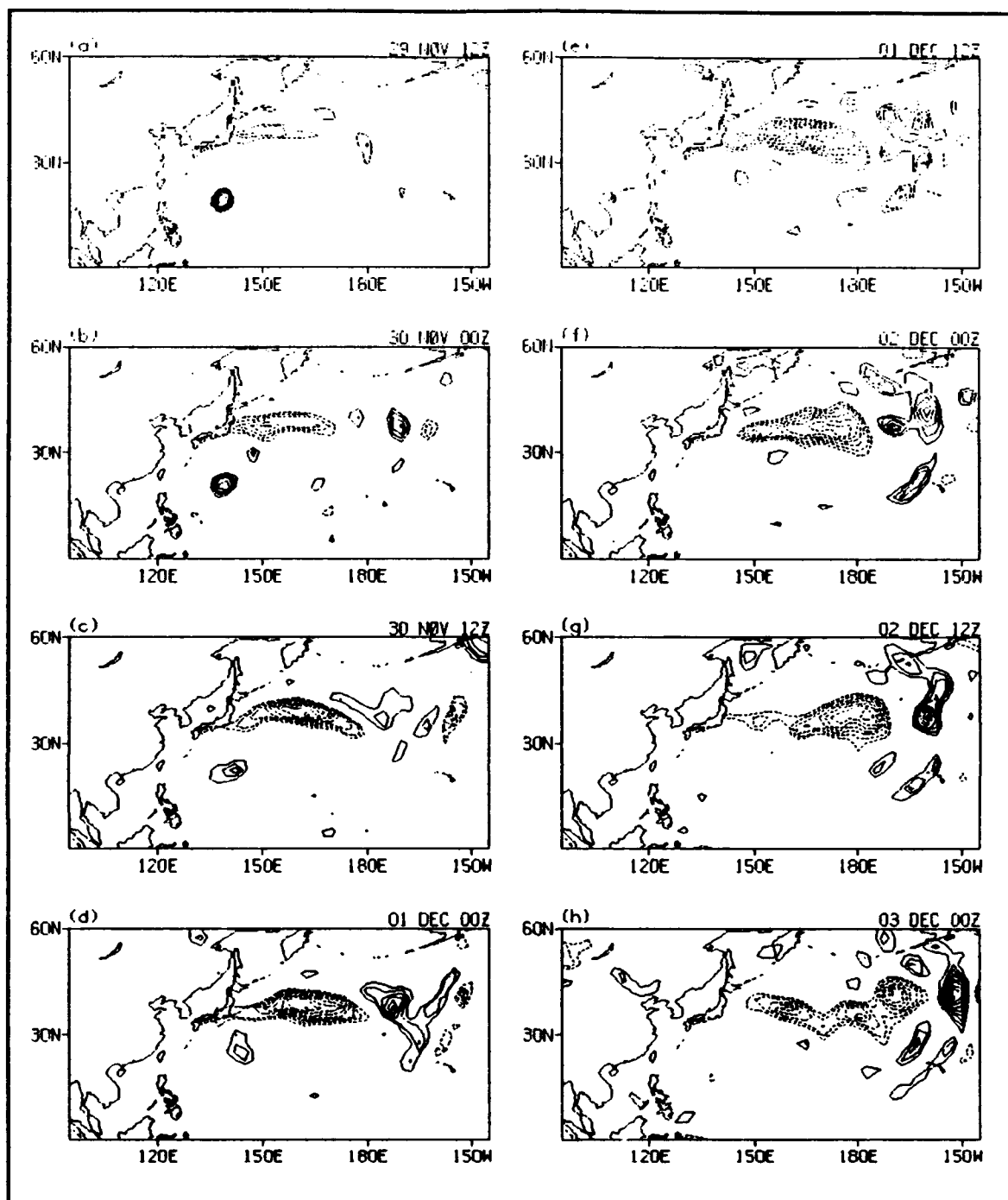


Figure 40. EA differences (POSITIVE-NEGATIVE) in 200 mb relative vorticity for Yuri. Solid (dashed) contours represent positive (negative) differences; minimum contour is $0.25\text{E-}04 /s$; contour interval is $0.10\text{E-}04 /s$. Zero contour omitted.

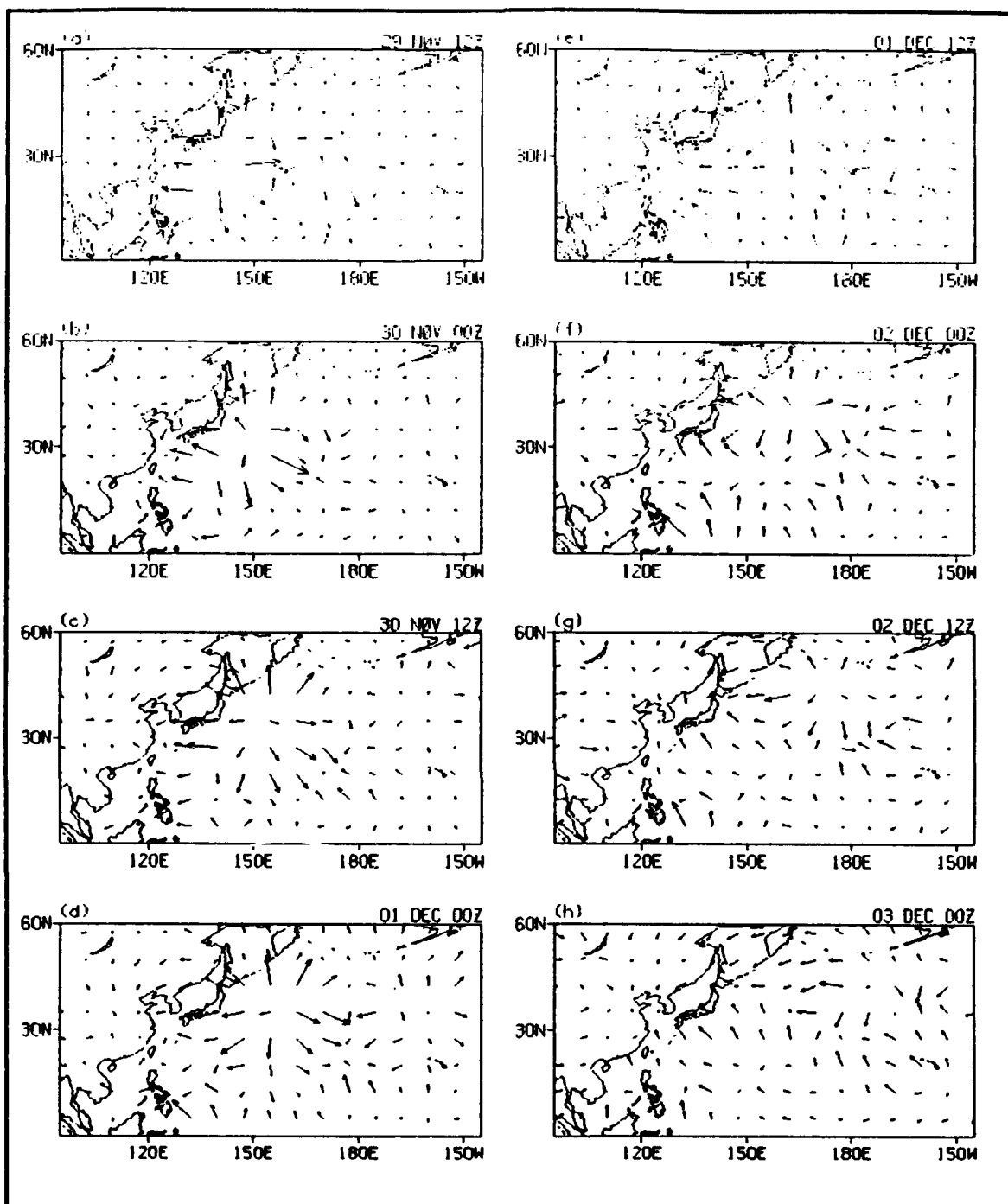


Figure 41. EA differences (POSITIVE-NEGATIVE) in 200 mb divergent winds for Yuri. Vector scale in m/s as shown:

$0.300E+02$
MAXIMUM VECTOR

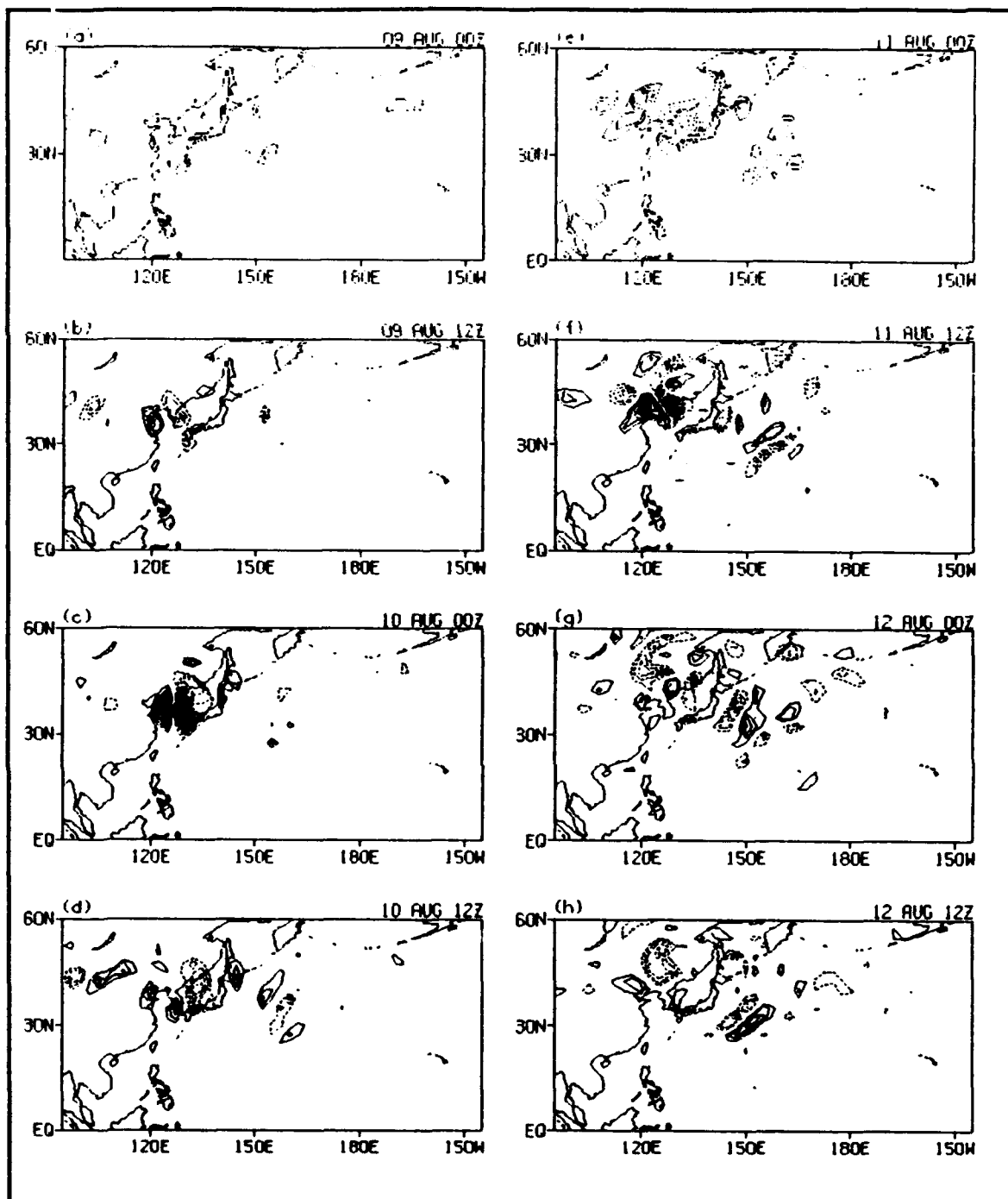


Figure 42. EA differences (POSITIVE-NEGATIVE) in 200 mb Rossby wave sources for Robyn. Solid (dashed) contours represent positive (negative) differences; minimum contour is $0.1\text{E-}08 / \text{s}^2$; contour interval is $0.05\text{E-}08 / \text{s}^2$. Zero contour omitted.

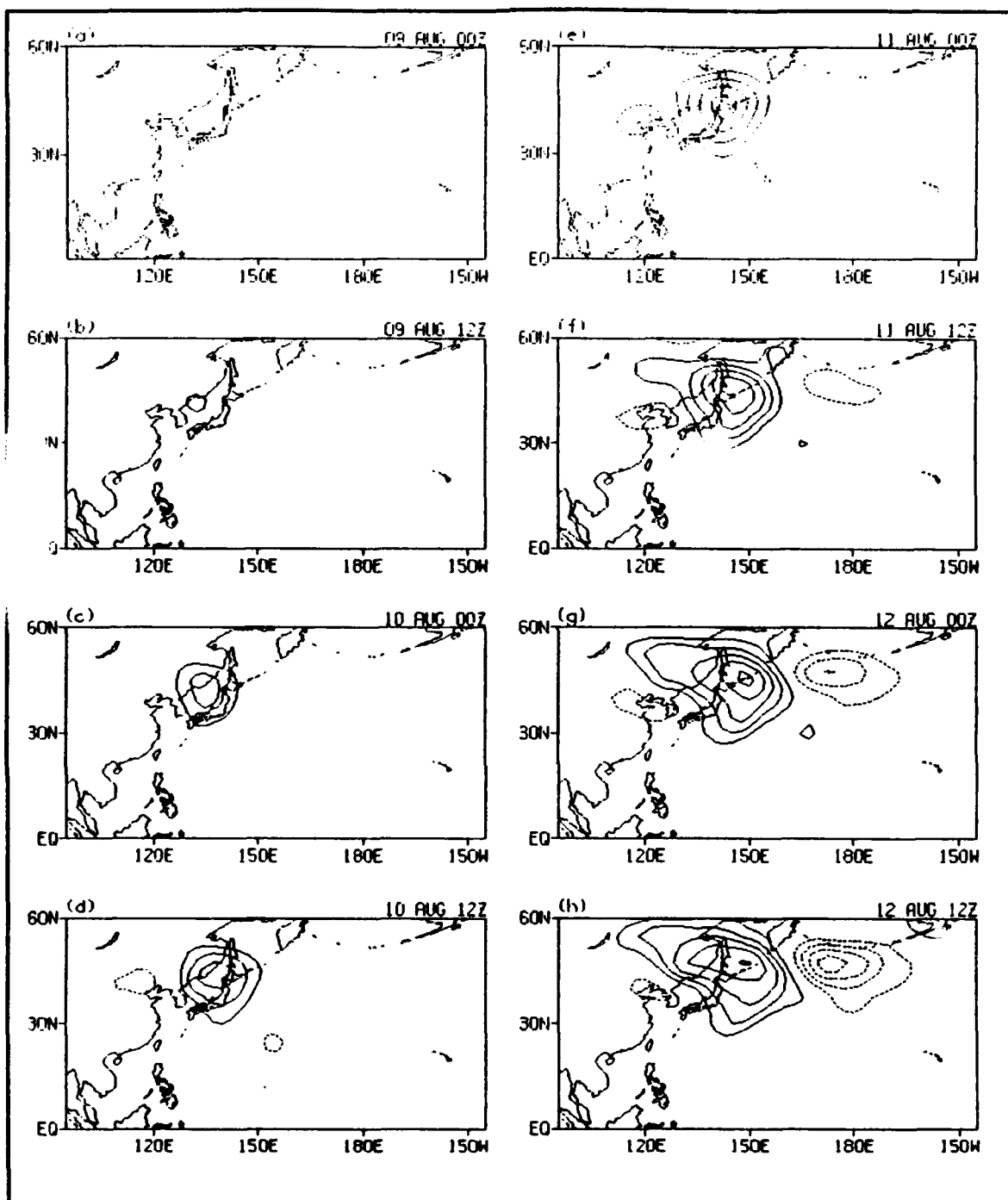


Figure 43. EA differences (POSITIVE-NEGATIVE) in 200 mb heights for Robyn. Solid (dashed) contours represent positive (negative) height differences; contour interval is 50 gpm. Zero contour omitted.

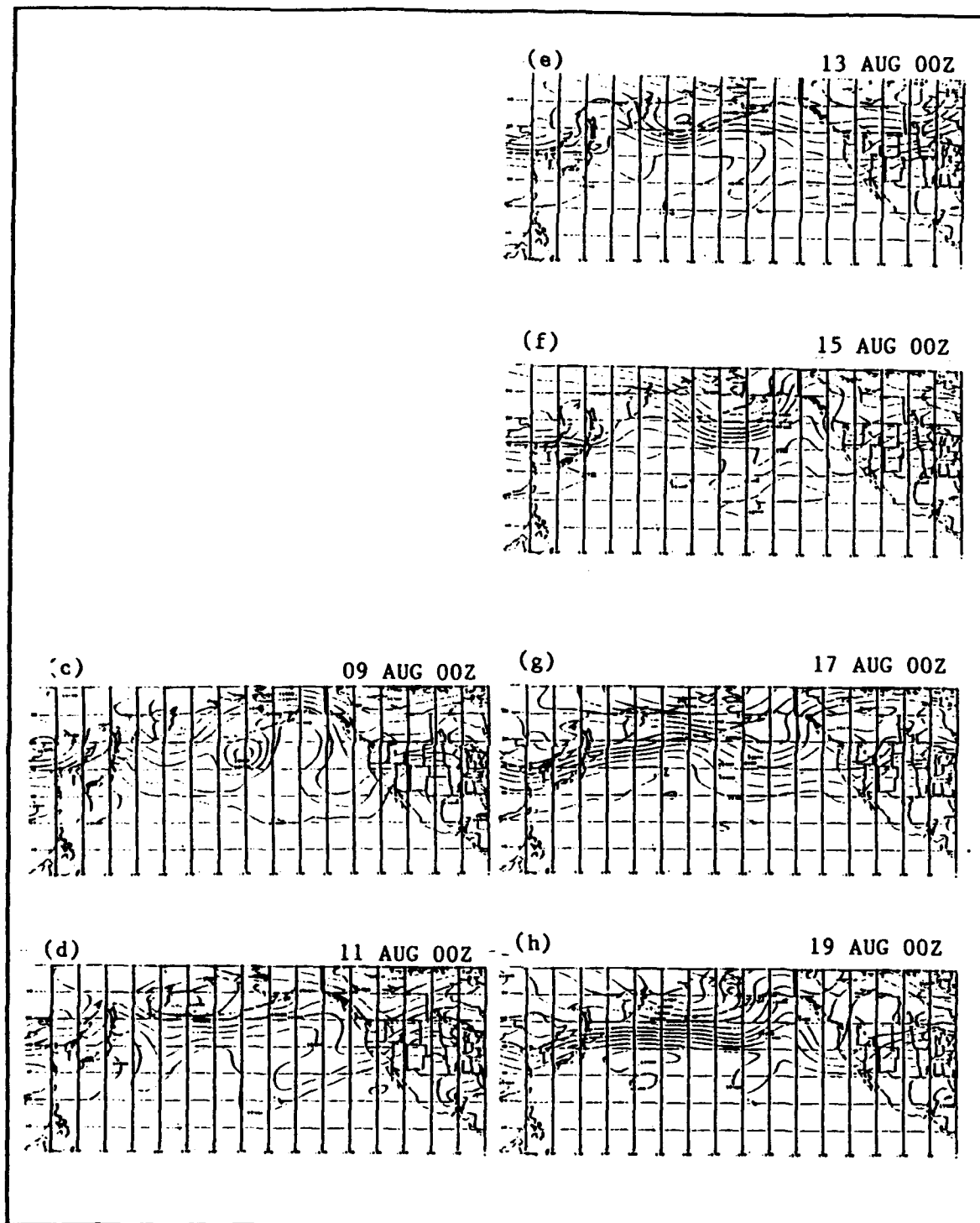
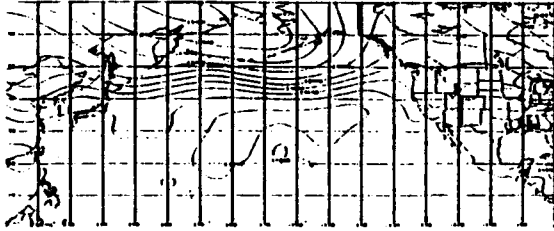


Figure 44. NMC 200 mb geopotential height analyzes at selected times. Minimum contour is 10500 gpm. Contour interval is 100 gpm. Panels (a) and (b) omitted.

(i)

21 AUG 00Z



(j)

23 AUG 00Z

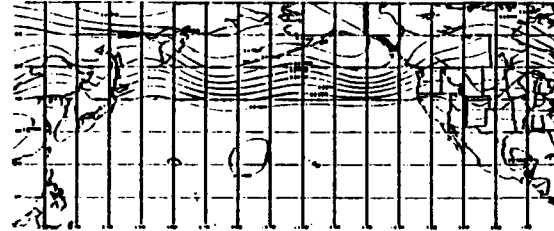
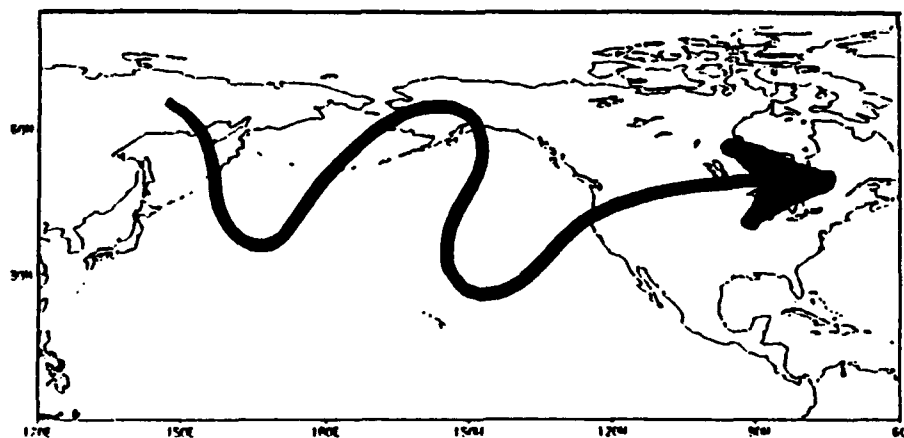
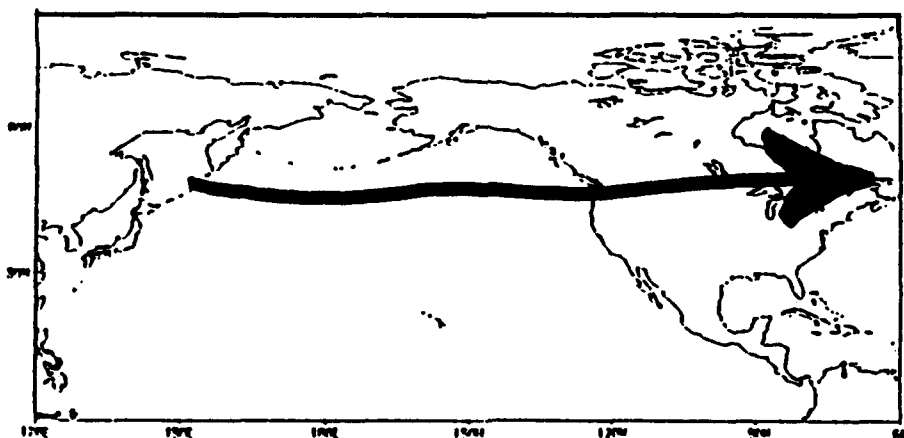


Figure 44. (Continued).



(a) 200 mb Jet With Typhoon Robyn



(b) 200 mb Jet Without Typhoon Robyn

Figure 45. Schematic of forecast 200 mb jet during the second week of: (a) POSITIVE run, (b) NEGATIVE run.

LIST OF REFERENCES

- Atkinson, G.D. and C.R. Holliday, 1977: Tropical cyclone minimum sea-level pressure and maximum sustained wind relationship for the western North Pacific. *Mon. Wea. Rev.*, **105**, 421-427.
- Bjerknes, J., 1966: A possible response of the atmospheric Hadley circulation to equatorial anomalies of ocean temperature. *Tellus*, **18**, 820-829.
- , 1969: Atmospheric teleconnections from the equatorial Pacific. *Mon. Wea. Rev.*, **97**, 163-172.
- , 1972: Large-scale atmospheric response to the 1964-1965 Pacific equatorial warming. *J. Phys. Oceanogr.*, **2**, 212-217.
- Gelaro, R., and T. Murphree, 1994: Intraseasonal variations in tropical-extratropical teleconnection mechanisms. Submitted to *J. Atmos. Sci.*
- Goerss, J., and R. Jeffries, 1994: Assimilation of tropical cyclone observations into the Navy Operational Global Atmospheric Prediction System. Submitted to *Mon. Wea. Rev.*
- Harr, P., and R. Elsberry, 1991: Tropical cyclone track characteristics as a function of large-scale circulation anomalies. *Mon. Wea. Rev.*, **119**, 1448-1468.
- Hogan, T., and T. Rosmond, 1991: The description of the Navy Operational Global Atmospheric Prediction System's Spectral Forecast Model. *Mon. Wea. Rev.*, **119**, 1786-1815.
- Horel, J., and J. Wallace, 1981: Planetary-scale atmospheric phenomena associated with the Southern Oscillation. *Mon. Wea. Rev.*, **109**, 813-829.
- Hoskins, B., and D. Karoly, 1981: The steady linear response of a spherical atmosphere to thermal and orographic forcing. *J. Atmos. Sci.*, **38**, 1179-1196.
- Kousky, V., 1993: *Climate Diagnostics Bulletin, August 1993*. Climate Analysis Center, Washington, D.C., 77 pp.
- Kuo, H.-L., 1949: Dynamic instability of two-dimensional nondivergent flow in a barotropic atmosphere. *J. Meteor.*, **6**, 105-122.
- Kurihara, K. and T. Tsuyuki, 1987: Development of the barotropic high around Japan and its association with Rossby wave-like propagations over the North Pacific: Analysis of August 1984. *J. Meteor. Soc. Japan*, **65**, 237-246.

- Madden, R. A., and P. R. Julian, 1971: Detection of a 40-50 day oscillation in the zonal wind in the tropical Pacific. *J. Atmos. Sci.*, **28**, 702-708.
- Miller, E., 1993: *The Impact of a Typhoon on the Global Atmosphere*. Master's Thesis, Naval Postgraduate School, Monterey, California, April 1993.
- Murphree, T., 1994: Subtropical mechanisms influencing Pacific-North American teleconnections. Submitted to *J. Climate*.
- Neith, M., 1992: *Intraseasonal relationships between tropical heating and extratropical jets*. Master's Thesis, Naval Postgraduate School, Monterey, California, December 1992
- Nitta, T., 1987: Convective activities in the tropical western pacific and their impact on the northern hemisphere summer circulation. *J. Meteor. Soc. Japan*, **65**, 373-390.
- Plumb, R., 1985: On the three-dimensional propagation of stationary waves. *J. Atmos. Sci.*, **42**, 217-229.
- Sardeshmukh, P., and B. Hoskins, 1988: The generation of global rotational flow by idealized tropical divergence. *J. Atmos. Sci.*, **45**, 1228-1251.
- Tribbia, J. J., 1991: The rudimentary theory of atmospheric teleconnections associated with ENSO. *Teleconnections linking worldwide climate anomalies 'scientific basis and societal impact'*. Glantz, M. H., R. W. Katz and N. Nicholls, editors. Cambridge Univ. Press. 535 pp.
- Walker, G., 1924: Correlation in seasonal variations of weather IX: a further study of world weather. *Memoirs of the Royal Meteorological Society*, **24**, 275-322.
- , and E. Bliss, 1932: World Weather V. *Memoirs of the Royal Meteorological Society*, **4**, 53-84.
- Woll, S., 1993: *Short Term Teleconnections Associated with an Individual Tropical Cyclone*. Master's Thesis, Naval Postgraduate School, Monterey, California, December 1993.

INITIAL DISTRIBUTION LIST

		No. Copies
1.	Defense Technical Information Center Cameron Station Alexandria, VA 22304-6145	2
2.	Librarian, Code 52 Naval Postgraduate School 411 Dyer Road Room 104 Monterey, CA 93943-5101	2
3.	Oceanography Department Code OC/CO Naval Postgraduate School 833 Dyer Road Room 331 Monterey, CA 93943-5122	1
4.	Meteorology Department Code MR/HY Naval Postgraduate School 589 Dyer Road Room 252 Monterey, CA 93943-5114	1
5.	Dr. Tom Murphree Code MR/ME Naval Postgraduate School 589 Dyer Road Room 231 Monterey, CA 93943-5114	6
6.	Dr. Ronald Gelaro Naval Research Laboratory 7 Grace Hopper Way Stop 2 Monterey, CA 93943-5502	2
7.	Lt. Cory A. Springer, USN 114 Poplar Road New Cumberland, PA 17070	1
8.	Director Naval Meteorology and Oceanography Division Naval Observatory 34th and Massachusetts Avenue NW Washington, DC 20390	1

- | | | |
|-----|---|---|
| 9. | Commander
Naval Meteorology and Oceanography Command
Stennis Space Center
MS 39529-5000 | 1 |
| 10. | Commanding Officer
Naval Oceanographic Office
Stennis space Center
MS 39529-5001 | 1 |
| 11. | Commanding Officer
Fleet Numerical Meteorology and Oceanography Center
7 Grace Hopper Avenue Stop 4
Monterey, CA 93943-0001-0120 | 1 |
| 12. | Dr. James Goerss
Naval Research Laboratory
7 Grace Hopper Way Stop 2
Monterey, CA 93943-5502 | 1 |
| 13. | Dr. Carolyn Reynolds
Naval Research Laboratory
7 Grace Hopper Way Stop 2
Monterey, CA 93943-5502 | 1 |
| 14. | Mr. Robin Brody
Naval Research Laboratory
7 Grace Hopper Way Stop 2
Monterey, CA 93943-5502 | 1 |
| 15. | Mr. Steve Payne
Naval Research Laboratory
7 Grace Hopper Way Stop 2
Monterey, CA 93943-5502 | 1 |
| 16. | Dr. Simon Chang
Naval Research Laboratory
7 Grace Hopper Way Stop 2
Monterey, CA 93943-5502 | 1 |
| 17. | Dr. Patrick Harr
Code MR/HR
Naval Postgraduate School
589 Dyer Road Room 244
Monterey, CA 93943-5114 | 1 |

- | | | |
|-----|--|---|
| 18. | Lt. Stephen Woll, USN
Naval Eastern Meteorology and Oceanography Center
Naval Air Station
Norfolk, VA 23511 | 1 |
| | | |
| 19 | Dr. Huug M. van den Dool
Chief, Prediction Branch
Climate Analysis Center
National Meteorological Center
W/NMC51
5200 Auth Road
Washington, DC 20233 | 1 |